Klinikum der Universität München, Campus Innenstadt
Medizinische Klinik und Poliklinik IV
Fachabteilung für Angiologie
Ziemssenstraße 5
80336 München

Vorstand: Prof. Dr. med. Ulrich Hoffmann

sowie

Medizinische Universität Wien
Universitätsklinik für Chirurgie
Anna Spiegel Center of Translational Research 25.05.031
Lazarettgasse 14, A-1090 Wien
Telefon: +43-1-40400 73524

Vorstand: Univ. Prof. Dr. Oliver Strobel

The Potential Role of "Neutrophil Extracellular Traps" (NETs) as Biomarker and Therapeutic Target in Abdominal Aortic Aneurysms

A thesis submitted for the degree of Doctor of Medicine

at the Faculty of Medicine

Ludwig-Maximilians-University Munich

submitted by

Marie Therese Grasl

from Vienna, Austria

2021

Mit Genehmigung der Medizinischen Fakultät

der Universität München

Berichterstatter: Prof. Dr. Ulrich Hoffmann

Mitberichterstatter: Prof. Dr. Dirk-André Clevert

PD Dr. Maximilian Pichlmaier

Prof. Dr. Christoph Schmitz

Prof. Dr. Christian Schulz

Mitbetreuung durch die promovierte Mitarbeiterin: Ao. Univ. Prof. Dr. Christine Brostjan

Dekan: Prof. Dr. med. Thomas Gudermann

Tag der mündlichen Prüfung: 14.10.2021

Die Rolle von „Neutrophilen Extrazellulären Traps“ (NETs) als potentielle Biomarker und therapeutischer Angriffspunkt im abdominellen Aortenaneurysma

Dissertation

zum Erwerb des Doktorgrades der Humanmedizin

an der Medizinischen Fakultät der

Ludwig-Maximilians-Universität zu München

vorgelegt von

Marie Therese Grasl

aus Wien, Österreich

Jahr

2021

Dedicated to all laboratory ApoE KO mice of this work

Table of contents

1. Abstracts

1.1. English Abstract

Background: The abdominal aortic aneurysm (AAA) is a pathological dilatation of the aorta. Due to frequent lack of symptoms AAA often is not diagnosed in time which may lead to life-threatening rupture. To date, screening is based largely on ultrasound and computed tomography. There is need for diagnostic and prognostic markers in order to predict progression and risk of rupture. Furthermore, pharmaceutical treatment is required to develop alternatives to surgical intervention.

Aim: Mouse models of AAA demonstrated that neutrophil extracellular traps (NETs) take part in the pathogenesis of AAA. Therefore, the aim of this study was to evaluate the prognostic marker potential of parameters indicating NETosis in patients with AAA throughout a monitoring period as well as pre- and post-surgical repair. In a second step, the therapeutic potential of inhibiting NETosis was tested in an experimental AAA mouse model.

Methods: 7 AAA patients undergoing an elective aneurysm repair and 5 AAA patients still in the pre-surgical monitoring process were evaluated. Peripheral blood was drawn and analyzed by ELISA for plasma levels of DNA-histone-complexes, myeloperoxidase, myeloperoxidase-histone complexes and citrullinated histone 3. Regarding the mouse model, the in vivo toxicity and optimal dosage of the selective NET inhibitor, GSK484, was evaluated in male ApoE KO mice. On day 0 an angiotensin II-loaded osmotic pump was implanted to induce AAA. From day 14 onwards either 200 µl buffered saline (5 controls) or 2.0 µg GSK484 in 200 µl saline/g body weight (n=5) were applied daily via an intravenous port for a period of 2 weeks. Aneurysm progression was controlled by ultrasound. Confocal microscopy images of blood smears, stained for DNA, a neutrophil surface marker and citrullinated histone 4, were analyzed for the frequency of NETs.

Results and Conclusion: In AAA patients in the monitoring phase plasma levels of citrullinated histone H3 correlated negatively with progression, i.e., low levels predicted fast progression over the next 6 months. However, NET parameters in blood decreased significantly after surgery. These findings support the notion that NETs are involved in the pathogenesis of AAA but may have limited potential as clinical AAA markers. In the experimental AAA model the NET inhibitor GSK484 was administered in established disease and reduced the NETosis reactivity significantly. Nevertheless, GSK484 had no impact on disease progression. Further studies on the pharmaceutical potential of NETosis inhibitors seem to be warranted.

1.2. Deutsche Zusammenfassung

Hintergrund: Das abdominelle Aortenaneurysma (AAA) ist eine pathologische Erweiterung der Aorta. Die Erkrankung verläuft in den meisten Fällen asymptomatisch, wird folglich oft nicht rechtzeitig diagnostiziert und kann im Fall einer Ruptur zu lebensbedrohlichen inneren Blutungen führen. Momentan basieren die einzigen Detektionsverfahren auf Ultraschall oder Computertomographie. Für die Evaluation der Progression und des Rupturrisikos sind bis jetzt noch keine Blutparameter etabliert. Die einzige effektive Behandlungsmöglichkeit ist die chirurgische Sanierung. Da diese Eingriffe ebenfalls ein Risiko darstellen, ist es wichtig eine medikamentöse Behandlung zu entwickeln.

Zielsetzung: In Tiermodellen für AAA konnte gezeigt werden, dass „neutrophile extrazelluläre Traps" (NETs) eine Rolle in der Pathogenese dieser Erkrankung spielen. Das Ziel dieser Studie war es daher, Laborparameter, die die Bildung von NETs anzeigen, in AAA Patienten unter Progression zu messen sowie vor und nach der Operation zu analysieren. In einem experimentellen AAA Tiermodell wurde untersucht, ob durch Hemmung der NETose auch die Progression des AAA vermindert werden kann.

Methoden: Von 5 AAA Patienten in der Monitoring (präoperativen) Phase und 7 AAA Patienten nach einer elektiven Aneurysma-Operation wurde peripheres Vollblut abgenommen und mehrere NETose Parameter wie DNA-Histon Komplexe, Myeloperoxidase-Histon Komplexe, Myeloperoxidase und citrulliniertes Histon 3 mittels ELISA im Plasma bestimmt. In einem AAA Tiermodell wurde das therapeutische Potential des selektiven NET Inhibitors GSK484 getestet. Männlichen ApoE KO Mäusen wurde Angiotensin II via osmotischer Pumpe verabreicht, was die AAA Bildung auslöste. Ab Tag 14 wurde für weitere 14 Tage die tägliche Behandlung mit entweder 200 µl gepufferter Saline (Kontrollen; n=5) oder 2.0 µg GSK484 in 200 µl Saline/g Körpergewicht (n=5) über einen intravenösen Port durchgeführt. Die Aorta wurde mittels Ultraschall vermessen. Von jedem Tier wurde am Ende der Behandlung ein Blutausstrich angefertigt. Dieser wurde auf DNA, einen neutrophilen Oberflächenmarker und citrulliniertes Histon 4 angefärbt; NETs wurden in Konfokal-mikroskopieaufnahmen ausgezählt.

Ergebnisse und Schlussfolgerung: In der präoperativen Monitoring Phase zeigten die Blutwerte für citrulliniertes Histon H3 eine negative Korrelation mit dem Aneurysmawachstum, d.h. niedrige Werte konnten eine rasche Progression vorhersagen. Jedoch waren die NET Parameter im Patientenblut postoperativ signifikant reduziert. Somit untermauern diese Daten, dass NETs eine Rolle in der Pathogenese des AAA spielen, jedoch scheinen sie als klinische Marker begrenztes Potenzial zu haben. Im Tiermodell bewirkte die Applikation des NET Inhibitors, GSK484, eine signifikante Verminderung der NETose Kapazität, nicht aber der AAA Progression. Diese Ergebnisse lassen darauf schließen, dass weitere Untersuchungen an größeren Kollektiven hilfreich wären.

2. Introduction

2.1. Definition

The abdominal aortic aneurysm (AAA) is an arterial, focal dilation of the aortic wall. It is defined to have a diameter of ≥3.0 cm or a diameter being at least 1.5 times larger than an aorta from a healthy individual [1].

All three parts of the arterial wall - adventitia, media and intima - are involved in the pathogenesis of the so called “aneurysm verum”. With over 80% the main localization of the AAA is below the renal artery (infrarenal) [1]. The aneurysm is one of the main diseases of the aorta. Over time aneurysms tend to dilate, with larger ones progressing faster [2]. They are associated with a high morbidity and mortality due to life-threatening bleedings after rupture [3].

2.2. Epidemiology

The overall prevalence mainly among men for the AAA is about 4-6% at the age of 65-80 [4]. Therefore it is higher than the 0.5-1.3% prevalence in women of the same age group [5]. It is assumed that women may be protected by their sex hormones, but the underlying mechanism is still not fully understood [6]. However, women tend to have a worse prognosis due to an increased risk of rupture [7]. The annual new AAA diagnoses rate is approximately 0.4 to 0.67% in the Western populations, which is equivalent to 4 to 6.7 aneurysms per 1000 persons per year [8].

The formation of the AAA is highly dependent on the age. An incidence of acute events affecting the aorta, like rupture or acute severe pain in the abdomen and/or back, increased to 55 per 100.000 persons per year in the 65- to 74-years-old age group and up to 298 per 100.000 persons per year in the above 85-years-old age group. Thus the risk is increasing constantly with the years of life with 66.0% of all events occurring at age ≥75 years [9]. Ruptured AAAs are responsible for 1-2% of all deaths in men above 65 years. Half of the deaths are occurring before the patient reaches the hospital. Still 30-70% of patients die after being admitted for emergency treatment. Therefore, the overall mortality rate is 65% -85% [10].

2.3. Risk Factors

The “Southern Community Cohort Study” evaluated 18782 participants of ≥65 years of age living in the USA. After 4.94 years of observation, 281 cases of AAA were identified. It was shown that the major risk factors for development are male gender, age and (in both sexes) smoking [11]. Minor risk factors are a positive family history, Caucasian race, a previous myocardial infarction, hypertension, hypercholesterolemia, atherosclerosis, presence of additional vessel aneurysms, cerebrovascular insufficiency, peripheral arterial disease and coronary arterial disease [12-14]. Also genetic tissue conditions like Marfan syndrome and Ehlers-Danlos syndrome are associated with an increased risk for developing an AAA [15].

Tobacco smoking is one of the main risk factors for AAA development and progression [16]. Twentytwo percent of screened patients in the USA, diagnosed with AAA, are current smokers and 36.9% are former

smokers. Therefore, nearly two thirds of AAA patients are exposed to tobacco smoke [17]. The odds for developing an AAA are positively associated with the number of pack years [18]. Men consuming more than 25 cigarettes per day have a 15-fold risk of developing an AAA when compared to non-smokers. Even after quitting the risk remains elevated, which indicates that the adverse effects induced by tobacco smoking are irreversible [19]. Current tobacco smoking results in an increased AAA growth of 0.05 cm per year [20] and a two-fold elevated risk of rupture [12]. Tobacco promotes AAA formation through triggering inflammation, proteolysis and apoptosis of smooth muscle cells (SMCs) due to the ability of nicotine to stimulate matrix metalloproteinase (MMP) expression [21]. Furthermore, chronic nicotine exposure results in higher release of pro-inflammatory cytokines by macrophages [22], as discussed in detail in section 6.

An increase in diastolic blood pressure per 10 mm Hg is associated with an enhanced growth rate of 0.02 cm per year [20]. Another study did not confirm the association between hypertension and progression of the aortic diameter, but described a positive correlation between hypertension and the risk of rupture [23].

2.4. Protective Factors

Non-Caucasian race, female gender [24], moderate ethanol consumption [19] and diabetes type II [20] have been considered as factors reducing the risk of AAA formation.

The protective effect of diabetes seems to be paradox. The exact biological mechanisms still remain unclear [25]. Diabetes mellitus is reportedly associated with a reduced mean AAA growth rate of 0.11 cm per year (standard deviation of 0.02 cm/year) [20]. Recently, a study suggested that not diabetes itself, but the oral antidiabetic metformin protects against AAA formation [26].

In addition, a healthy lifestyle consisting of physical activity and frequent consumption of fruits, nuts and vegetables reduces the risk of developing an AAA [16].

2.5. Histology

The aortic wall is composed of the tunica intima, media and the adventitia. The intima is formed by a thin layer of endothelial cells, subendothelial connective tissue and the internal elastic lamina. The media is composed of layers of vascular smooth muscle cells (VSMCs) and extracellular matrix (ECM). The adventitia consists of connective tissue containing the vasa vasorum and nerves [27].

Collagen and elastin fibers are mainly responsible for the mechanical properties. Their main function is opposing the force of blood pressure to preserve the structural integrity. Elastin fibers occur more often in the tunica media. Collagen fibers, especially collagen type I and III, are more abundant in the tunica media and tunica adventitia [28].

The AAA is organized spatially. The lumen is often filled with a multilayered, hemoglobin-rich intraluminal thrombus (ILT), followed by a thinned and degraded media and an inflamed and/or fibrotic adventitia [29]. In the atherosclerotic AAA the intima is thickened due to necrotic, lipid-enriched plaque formation. It is also observed that inflammatory cells, like macrophages and lymphocytes, infiltrate the adventitia and media of the aorta [30]. During the progression of disease the media is thinning and the

number of SMCs is decreasing [31]. In addition, the amount of elastin is reduced and the configuration of the fibers is distorted [32].

In addition, hem- and lymphangiogenesis are increased in the aneurysm wall. The expression of vascular endothelial growth factor receptor in the microvessels is elevated. In this area degradation and infiltration of inflammatory cells are more prominent [33]. Furthermore, it has been observed that the number of capillaries and thick-walled vessels are increased in the adventitia. These vessels are often surrounded by inflammatory infiltrates, mostly macrophages and lymphocytes [34].

The thrombus structure was reported to be inhomogeneous. The luminal side is composed of densely packed fibrin. This side is being invaded by leukocytes and erythrocytes [35]. On the contrary, the medial and abluminal parts are being exposed to fibrinolysis resulting in decreased stiffness. These parts of the thrombus contain a network of interconnected canaliculi functioning as a transport system for macromolecular particles [36]. Recently, three subtypes of ILT were identified based on their morphology and mechanical properties. The first type, representing the majority of ILTs, showed a decrease in strength and stiffness from the luminal to abluminal side. However, all three layers of the ILT were mostly intact - a distinct luminal and thick medial and abluminal layer. In the second type a loss of mechanical resistance from the luminal to the medial/abluminal part was observed. A thinning and enhanced degradation of the outer vessel wall was described. In a few cases a third type of thrombus was reported, characterized by an almost fluid-like consistency [37]. However, it has not been documented whether these subtypes promote/interfere with the progression of the disease or influence the risk of rupture.

2.6. Pathogenesis

AAA formation is characterized by a loss of stability of the aortic wall due to defect smooth muscle cells, smooth muscle cell apoptosis, inflammation, upregulation of proteolytic pathways, matrix degradation, formation of an intraluminal thrombus and many other factors [30, 31, 38-42].

2.6.1. Smooth Muscle Cells

The media of the abdominal aorta contains vascular smooth muscle cells. This cell type has numerous functions like synthesis of matrix, the inhibition or activation of proteases and the recruitment of inflammatory cells. Thus, SMCs play an important part in keeping the homeostasis of the aortic matrix [40].

SMCs of the descending aorta derive from the embryonal paraxial mesoderm somites, while SMCs in the aortic root, ascending aorta and the aortic arch derive from the neural crest, a part of the ectoderm [39]. It is assumed that the different origins may influence the formation of certain vascular diseases [43].

The SMCs of AAA patients differ in their gene expression in comparison to the ones of healthy individuals [40]. It has been shown that they have an elevated proteolytic activity, i.e. in comparison to non-AAA SMCs these cells show increased MMP-9 expression due to post-transcriptional failure of MMP-9 synthesis control. These findings suggest that SMCs from AAA patients take part actively in the degradation of the matrix resulting in weakening of the media [40]. It has been observed that these alterations in gene expression occur even before the aneurysm has developed [44].

SMCs express low density lipoprotein receptor protein 1 (LRP1), which may be linked to the formation of AAA [45]. One of the functions of this protein is to maintain the integrity of the vessel through regulating protease activity and ECM deposition [46]. However, it has been reported recently that in mice, treated with angiotensin II, deficiency for LRP1 does not influence the AAA formation [47].

The AAA is characterized by a depletion of medial SMCs due to apoptosis [48]. However, it still remains unclear whether the cell death is an active pathological event or a result of tissue deterioration [47].

2.6.2. Hemodynamic Pressure

At the point of the aortic bifurcation hemodynamic turbulences may occur resulting in an inhomogeneous pressure on the endothelial layer of the vessel. In case of the infrarenal aorta, elevated hemodynamic pressure leads to the deregulation of proteins which take part in AAA formation, and in turn, due to the decrease of elastin in the media along the length of the aorta the stiffness of the wall becomes higher and therefore the amplitude of the pulse waves are increasing [49].

Due to hemodynamic turbulences the endothelial NO synthase may become uncoupled leading to an increased production of NO, which may give rise to the generation of peroxynitrite [50]. Peroxynitrite is turning pro-MMPs, the inactive zymogens, to the active state [51]. As a result of this endothelial dysfunction, the endothelial cells produce more MMP-2 and MMP-9, which contribute to the adaptive remodeling due to their ability to change the tissue architecture in the vessel wall [52, 53]. In addition, elevated shear stress results in the secretion of factors like transforming growth factor beta or fibroblast growth factor-2 by endothelial cells which may again induce the production of MMPs by SMCs [54, 55].

2.6.3. Inflammation

2.6.3.1. Role of Neutrophils

The luminal part of the ILT contains many neutrophilic granulocytes and other polymorphonuclear cells (PMNs). Neutrophils use nicotinamide adenine dinucleotide phosphate (NADPH) oxidase and myeloperoxidase (MPO) for pro-oxidant activities [56]. To be specific, NADPH oxidase catalyzes the production of superoxide free radicals, which may give rise to the secondary generation of different reactive oxygen (ROS) or nitrogen species (RNS). MPO is expressed also in 95% of PMNs [56, 57]. Compared to healthy individuals, the blood from AAA patients contains PMNs with less catalase activity indicating reduced anti-oxidative capacities. Furthermore, PMNs from AAA patients express significantly more hydrogen peroxide and MPO than healthy controls [58]. These observations lead to the conclusion that increased oxidative stress could be one of the main factors in AAA pathogenesis [58].

Neutrophilic granulocytes play a key role in the pathogenesis of AAA by contributing not only to a pro-oxidant state but also to the proteolytic degradation of the media in the aortic wall and to the inflammation of the adventitia [29]. Accordingly, PMN depletion inhibits significantly AAA formation in a rodent model [59]. Their recruitment to the luminal part of the ILT may be due to the release of interleukin-8 (IL-8), a neutrophil chemotactic factor, which is increased considerably in AAA patients [60]. One source of IL-8 may be neutrophil extracellular traps (NETs) [61]. The expression of leukotriene B4, another neutrophil chemotactic factor, is also elevated in the luminal layer of the ILT [62]. In addition, the alternative complement pathway is activated in AAA, as confirmed by a murine model in which the formation of AAA is reportedly depended on the activation of this system [63].

2.6.3.2. Role of Macrophages

Macrophages play an important role in the pathogenesis of AAA. These cells are able to polarize into various phenotypes, i.e. the classically activated or the alternatively activated phenotype. Classically activated macrophages produce pro-inflammatory cytokines promoting tissue degradation, while alternatively activated macrophages are associated with tissue repair. In AAA there is an imbalance between these two phenotypes in favor of the classically activated macrophages [38].

Macrophages can be found in every part of the aortic wall but tend to accumulate mostly in the adventitia and the ILT [64, 65]. They are attracted most probably by ECM degradation products and various chemokines. Accordingly, it has been shown that chemotactic proteins like IL-8, tumor necrosis factor alpha (TNF-α) and monocyte chemotactic protein-1 are co-localized with infiltrating macrophages [66, 67].

Macrophages promote the disease by the release of pro-inflammatory cytokines such as TNF-α, IL-6, IL-1β, and interferon gamma [68, 69]. Furthermore, macrophages produce chemokines like CXCL1 leading to the recruitment of neutrophils, which further express pro-inflammatory cytokines like IL-6 [70]. It has been shown that elevated levels of IL-6 promote differentiation into activated macrophages again leading to an increased recruitment of monocytes to the aortic wall and enhancing further disease progression [71]. Thus, the recruited macrophages trigger a positive feedback loop supporting the development of chronic inflammation [38].

2.6.4. Degradation of Extracellular Matrix

Within the aortic wall the extracellular matrix is produced by SMCs, endothelial cells and fibroblasts [72]. The matrix contains amongst other proteins collagen, glycoproteins and elastin [73]. The AAA is characterized by a progressive dilatation of the abdominal aorta triggered by the degradation of ECM by proteolysis [74]. In general three classes of proteases are mainly responsible for matrix degradation: cathepsins, elastases, and MMPs [41, 75].

Deficiency of cathepsin K may attenuate the development of AAA, as shown in an experimental model of elastase-induced AAA [76]. MMPs disrupt and fragment the elastin lamellae and collagen in the extracellular matrix of the aorta [77]. In AAA MMP activity is generally increased and their inhibition decreased, leading to an imbalance towards enhanced proteolytic activity [78]. Accordingly, in mice being deficient in tissue inhibitors of metalloproteinases accelerated AAA formation is observed [79].

2.6.5. Thrombus

In 70-80% of the cases an intraluminal thrombus (ILT) can be found in an AAA [37]. It has been observed that the thrombus may protect the aneurysm from rupturing due to the fact that peak wall stress induced by hypertension is being significantly reduced [80]. More recent studies show that the potentially protective mechanism depends on the kind of attachment of the thrombus to the aortic wall [81].

A large thrombus, however, results in hypoxia in the underlying vessel wall. This process initiates adventitial angiogenesis and increases infiltration of inflammatory cells from the outer layers of the aortic wall leading to weakening of the wall [82]. Now the vessel wall is exposed to high concentrations of proteases, cytokines and reactive oxygen species further enhancing aneurysm formation. At the site of ILT localization SMC dedifferentiation and apoptosis occurs. It has been observed that the diameter of the AAA, MMP levels, SMC apoptosis and elastin degradation correlate with each other [42, 83].

The development of an ILT does not only lead to the thinning of the arterial wall [82], reduction of SMC density in the media and inflammation in the adventitia but also to degradation of elastin fibers [83]. This shows that protease activity partly originates from the ILT. Within the ILT MMP-9 in pro- and active form [84] and MMP-9-lipocalin complexes can be found. These enzymes originate from neutrophils [85]. Especially in the luminal part of the ILT high levels of MMP-8, MMP-9 and elastase have been observed to co-localize with neutrophils [86]. Proteases secreted by neutrophils may degrade matrix fibrillary proteins over time leading to the progression and rupture of AAA. It has been shown that high levels of proteases [87], increased leukocyte infiltration and neovascularization [88] occur at the site of adventitial rupture.

At the site of ILT, hemostasis and fibrin destruction are occurring continuously, leading to increased levels of coagulation and fibrinolysis factors in the blood of AAA patients and the tissue of the ILT [89]. Circulating fibrinogen, the fibrin degradation product D-dimer, and thrombin-antithrombin III complex correlate with the size of the AAA and ILT and have prevailed as diagnostic markers [90-92]. It has been reported that fibrinogen levels are elevated years before an AAA is formed. This indicates that deregulated hemostasis and fibrinolysis may be causally involved in AAA pathogenesis from an early stage onwards [93].

2.7. Clinical Presentation

Due to the lack of symptoms AAAs often remain undetected until rupture. They are frequently diagnosed by chance via ultrasound or abdominal palpation during a regular check-up [24].

In cases of symptomatic AAAs the patients suffer from diffuse pain in the back or abdomen. It is also possible that the ILT can lead to embolization. These cases should be treated electively by surgery due to an increased risk of rupture [13].

2.8. Screening and Treatment Indications

In general, AAAs smaller than 5.5 cm expand about 2-3 mm per year. The expansion of larger AAAs is reported to be more rapid [13]. However, there are large interindividual variations. Most AAAs remain constant for quite some time and progress afterwards, some grow continuously and others remain stable [94].

Small AAAs with a diameter of 3.0-3.9 cm carry nearly no risk of rupture within the next 12 months. The chance of rupturing for an AAA with the diameter of 4.0-4.9 cm is only 1% [13]. In these cases a strict surveillance via ultrasound or computed tomography (CT) is recommended. Men with an aneurysm diameter of 3.0-4.0 cm should be examined at regular intervals. If the diameter reaches 4.0-4.9 cm the check-up should take place every year. When the diameter is about 5.0-5.4 cm the interval should be shortened to 6 months [95]. Exact surveillance intervals for woman have not been established yet but are usually conducted comparable as for men.

AAAs over 5.0 cm for women and 5.5 cm for men have an elevated risk of rupturing within the next 12 months and therefore surgical intervention is recommended [13]. In case of rapidly expanding aneurysms, i.e. about 1 cm per year, early intervention is urgently required [13].

Not only the diameter, but also the AAA morphology is important for choosing whether surgical intervention is needed. AAAs exposed to high hemodynamic pressure and/or showing an intraluminal thrombus are more prone to rupture [96]. It has been reported that symptomatic and ruptured AAAs are under more peak wall stress compared to asymptomatic ones. As a result earlier intervention is recommended for symptomatic AAAs [96].

2.8.1. Treatment

2.8.1.1. Surgical Intervention

In general there are two options for surgical treatment, i.e., open surgical repair (OSR) and endovascular repair (EVAR). The latter one is based on the placement of an expandable stent graft in the aorta through the femoral artery. Prior to the intervention computed tomography angiography (CTA) or magnetic resonance imaging (MRI) are conducted in order to obtain information about the morphology of the AAA in case of OSR or for choosing the right stent graft in case of EVAR [13].

EVAR is the less invasive option and the intraoperative risk is lower. On the other hand it is only possible to conduct EVAR if the aorta and the iliac arteries are not kinked [13]. In up to 25% of the patients the implanted stent is leaking [13] and therefore re-intervention occurs more often in EVAR (18.9%) [97]. In cases of high age and/or comorbidities, EVAR is the preferred method due to its lower intraoperative risk and better initial outcome [98, 99]. Complications include perioperative disseminated intravascular coagulation [100] and venous thrombosis despite heparin prophylaxis [101]. Meta-analyses have shown that OSR performed in elective AAAs had a significantly higher 30-day mortality (3.2-4.2%) than EVAR (1.2-1.4%) [102]. Long-term mortality, however, did not differ between EVAR (37.3%) and OSR (37.8%) [102].

2.8.1.2. Pharmacological Treatment

Despite the fact that surgery is the only curative treatment, medical intervention is recommended in order to control comorbidities and slow down disease progression [56]. The guidelines of the "European Society for Vascular Surgery" recommend that AAA patients should be treated with statins to lower blood lipid levels and with low doses of acetylsalicylic acid, an inhibitor of cyclooxygenase 1 and 2, to prevent platelet aggregation [13]. The patients should start the treatment with statins one month prior to the intervention in order to minimize cardiovascular morbidity. The intake should be continued during the perioperative period. In addition, low-dose acetylsalicylic acid administration should be started at the point of diagnosis and should be continued throughout the perioperative period [13].

It needs to be mentioned that only statins have been reported to reduce cardiovascular mortality and to slow down the progression of the disease. Other drugs like beta-blockers, angiotensin-converting enzyme inhibitors and angiotensin 1- receptor antagonists, which may be prescribed in order to treat comorbidities, do not reduce the growth of the AAA [103]. According to a clinical study a 50% reduction of the AAA expansion rate has been observed under statin treatment [104], an observation confirmed by a large meta-analysis [105, 106]. However, Golledge et al. observed similar growth rates in subjects prescribed (median 1.2 mm) and not prescribed statins (1.0mm) (p=0.226) [92]. With regard to the mode of action, the statin simvastatin reduces free radical formation and inflammatory molecules in the AAA wall by suppressing the NF-κB signaling pathway [107]. As a consequence, infiltrating T helper lymphocytes, SMCs and monocytes [108] release less of pro-inflammatory cytokines, like IL-6 and IL-8, and MMPs [109]. In fact, the reduction of experimental AAA development by 25% and the reduced incidence of AAA by 30% under statin therapy [110] are associated with a lower MMP-9 expression in the vessel wall [111].

Animal models of cholesterol-fed rabbits suffering from atherosclerosis have demonstrated that aortic plaque size and thrombus formation may decrease significantly under therapy with acetylsalicylic acid [112]. A meta-analysis of randomized trials on primary and secondary prevention of vascular disease has shown that immediately after AAA diagnosis low-dose therapy with acetylsalicylic acid should be started due to potential reduction of vascular deaths [113]. It was recommended to proceed with the treatment lifelong in order to prevent cardiovascular complications like stroke, myocardial infarction or death [114]. On the other side, a retrospective aneurysm study on data from the National Health Insurance Research Database did not find any correlation between low-dose treatment with acetylsalicylic acid and mortality reduction [115].

Also neutrophilic granulocytes may serve as a therapeutic target. In a clinical trial the number of neutrophils in the aortic wall was reduced by preoperative doxycycline therapy resulting in an improved proteolytic balance [116]. In a further clinical study MMP-9 protein levels were 2.5-fold decreased under doxycycline treatment (100 mg orally twice a day for 7 days before surgery) indicating a potential pharmaceutical target [117]. In experimental animals - male Wistar rats whose abdominal aorta was perfused with porcine pancreatic elastase - the antibiotic doxycycline inhibited directly the activity of MMPs in neutrophils, suppressing elastase-induced AAA development [118]. In addition, a reduced number of cytotoxic T-cells in the aortic wall was observed as well [119]. However, clinical trials with antibiotic treatment largely failed in demonstrating a benefit for AAA patients [120].

2.9. Surrogate Markers

Up to date most AAAs are detected by chance. Therefore, current research aims to find predictors to detect early AAA, monitor the progression of this disease and to identify patients with high rupture risk. In general such disease markers could possibly be based on alterations in morphological features or parameters in blood.

2.9.1. Morphological markers

First, the determination of the maximal AAA diameter via ultrasound is the most common morphological surrogate marker for disease progression [121]. However, ultrasound results often vary in dependence of the observer [122] and the way the calipers are placed [121]. MRI and CTA show better reproducibility, are more accurate [123] but are not always available and entail higher costs.

Alternatively, the assessment of AAA volume may obtain more reproducible data and may be a more sensitive progression marker [124]. This approach takes into consideration that the morphology of aneurysms is highly variable and that the overall size rather than the diameter is of importance. The volume may be measured by MRI, CTA and ultrasound [125, 126]. Nonetheless, until now no exact volume (cut-off value) could be determined, serving as indication for surgical intervention [127].

Third, the formation, morphology and the size of an intraluminal thrombus (ILT) may be used as a marker. As outlined in section 2.6.5. the ILT is composed of many cell types, interacting with each other and leading to a progressive weakening of the aortic wall [102]. Accordingly, large ILTs lead to an accelerated formation and dilatation of AAA [124].

2.9.2. Functional markers

Currently positron emission tomography combined with CT imaging (PET/CT) is used for functional imaging of the AAA. Labeling with 18-fluorodeoxyglucose (FDG) reveals that the glucose metabolism is elevated in areas of inflammation and cell proliferation. It has been reported that in AAA patients suffering from symptoms the FDG-uptake is increased [128]. On the other hand, asymptotic AAA patients do not show an increased FDG-uptake in the aortic wall [129].

Functional imaging via MRI enables to assess the composition of the aortic wall and the cellular activity. For example, the phagocytic activity of macrophages may be determined by applying the contrast agent superparamagnetic iron oxide. This technique has been established for patients suffering from AAA [130]. It was reported that the extent of iron oxide uptake in the aortic wall is dependent on the activity of macrophages and correlates with an increased AAA expansion rate [131]. This method has the benefit of not utilizing ionizing radiation and therefore enables repeated examination of AAA patients.

2.9.3. Markers in blood

Several blood parameters have been associated with the formation and progression of AAA, e.g., elevated D-dimer levels may indicate the remodeling of ILT and expansion of AAA [91], increased concentrations of MMP-9 are a surrogate for an enhanced proteolytic activity, high serum levels of the

type-III procollagen peptide may be a sign of collagen-turnover and AAA expansion [132] and elevations in IL-6 indicate inflammation [133].
To be specific, based on elevations in plasma D-dimer concentration it was possible to identify different progression rates in patients with an AAA. In men D-dimer levels lower than 150 ng/ml were associated with a median expansion rate of 0.7 mm per year whereas D-dimer levels over 900 ng/ml were associated with a median expansion rate of 1.7 mm per year [92]. In the last few years, the formation and progression of AAA was monitored with circulating micro-RNAs, such as miR-155, miR-191-3p, miR-455-3p, miR-1281, and miR-411 [134]. Recent research indicates that factors released by neutrophilic granulocytes may serve as AAA markers, e.g., elevated levels of gelatinase-associated lipocalin were found in patient plasma and indicated activation of neutrophils and expansion of AAA [135]. Also elevated MPO and cell-free DNA levels correlated significantly with the diagnosis of AAA [135].

Hitherto, however, no blood-borne marker has been introduced into the clinical practice due to the limited sensitivity, specificity and prognostic value.

2.10. Neutrophilic Granulocytes

Neutrophilic granulocytes, also known as polymorphonuclear cells, are the most common white blood cells in the human blood [136, 137]. They take part in the first line of immune defense against various pathogens.

Mature neutrophils leave the bone marrow and enter the circulation. Cytokines recruit PMNs to the site of inflammation by inducing the expression of E- or P- selectin on the surface of endothelial cells [138]. After interacting with these selectins, the neutrophils start to roll on the endothelium. PMNs may be chemotactically attracted and activated through IL-8, complement factors (C5a) or *N*-formyl-peptides from bacteria. This stimulation leads to the activation of integrins, which bind to cell adhesion molecules of the immunoglobulin superfamily (intercellular adhesion molecules) on the surface of the endothelium and keep neutrophils at this site. In case of a gradient of chemotactic cytokines, PMNs migrate through gaps in the endothelium into the inflamed tissue [137, 139]. The hypothesis that neutrophils are unable to return to the peripheral blood has been challenged by many studies demonstrating that the cells move back and reach different sites of the body, including secondary lymphoid tissues [140, 141].

Neutrophils are known to play an important role in AAA development. Accordingly, neutrophil depletion in mouse models inhibits AAA formation [59, 142]. In recent years, it has been shown that neutrophils can undergo a form of cell death called “NETosis” [139, 143]. This phenomenon has also been linked to the pathogenesis of AAA [144].

2.11. Neutrophil Extracellular Traps

In 2004 so called neutrophil extracellular traps (NETs) were first mentioned by Brinkmann et al. [143]. It was shown that NETs are derived from neutrophil granulocytes and are able to trap bacteria and degrade virulence factors locally by their enzymatic activity before the pathogens are engulfed by neutrophils or macrophages [143]. This process prevents dissemination of pathogens. This discovery offered new insight into the role of neutrophils in the innate immune response.

2.11.1. Formation of NETs

NETs are web-like structures composed of discharged chromatin, histones, neutrophil elastase, myeloperoxidase, MMP-9, cathepsin G, gelatinase and several other proteins [143]. Scanning electron microscopy has shown that NETs contain smooth fibers with a diameter of 15 to 17 nm and globular domains with a diameter of about 25 nm. Through aggregation a larger thread is formed with a diameter of 50 nm [143]. Further research revealed that these threads are composed of thin and parallel fibers of a diameter smaller than 2 nm [145]. DNase can destroy NETs which is indirect evidence that DNA in chromatin is building the backbone of NETs [139]. About 70% of all proteins within NETs are the histones H2A, H2B, H3 and H4 [146]. The molecular mass of histones in NETs is larger than the ones in the nucleus due to posttranslational modification [146]. It was suggested that the modification is involved in the regulation of NET formation [147].
The formation of NETs is triggered when neutrophils are overly activated [148] by a wide spectrum of stimuli, like lipopolysaccharides, bacteria, fungi, viruses, and parasites [143, 149, 150]. In addition, also endogenous, noninfectious stimuli like C5a, an important complement factor, lead to the release of NETs, after neutrophils have been primed with GM-CSF [151]. Depending on the dose of the activator more or less NETs are formed [143].

Within the first hour after being stimulated most neutrophilic granulocytes are involved in phagocytosis. Then about one third of the neutrophils changes the morphology and prepares for NET formation [139, 150]. In this phase less phagocytosis is observed. A few hours later NETs are formed and from this point onwards most of the antimicrobial activity is NET-associated. In sum phagocytosis and NETs show similar effectiveness with regard to defense [150].

During the formation of NETs, the nucleus loses its lobules followed by decondensation of the chromatin and swelling [150]. The inner and outer nuclear membranes separate from each other. The nuclear envelope disintegrates into vesicles after about 2 hours; the nucleoplasm and cytoplasm are no longer separated. After a few hours neutrophils round up and contract until the cell membrane ruptures. Then neutrophils eject intracellular components into the extracellular space and NETs are formed. It appears that NETs are flexible structures surrounding the dying neutrophils. It is reported that the release does not occur due to apoptosis or necrosis. Therefore, NETosis marks a new form of cell death [150].

It has been shown that macrophages are able to clear NETs after they have finished executing their function. This path is initiated when DNase I degrades the extracellular structures and the debris is opsonized with the complement factor C1q. As a result NETs are internalized by macrophages through endocytosis and are degraded in lysosomes [152].

2.11.2. Molecular Pathways

The formation of NETs is called NETosis [150, 153, 154]. Despite intense research the molecular pathways involved in this process are not fully understood and seem to be diverse.
NETosis is promoted through the activation of protein kinase C (PKC) [155]. Research has shown that PKC plays a major role in regulating the citrullination of histones during NETosis, i.e., PKCζ may activate PAD4, an enzyme important for citrullination of arginine residues in histones. The resulting change in the charge of the histones enables chromatin decondensation [155, 156]. Also ROS production is important for NET formation. It is believed that ROS plays a role in the translocation of neutrophil elastase and MPO from the granules to the nucleus where they induce chromatin decondensation and histone degradation [150]. The role of ROS is confirmed by observations that inhibition of the NADPH oxidase (NOX) complex by diphenyleneiodonium (DPI) inhibits NETosis. Phorbol-12-myristate-13-acetate (PMA), an activator for PKC and the Raf/MEK/ERK pathway, leads to increased ROS production and NET formation [156-158]. The Raf-MEK-ERK pathway has also been observed triggering NETosis and preventing apoptosis by regulating the expression of the anti-apoptotic protein Mcl-1 [158].

Another study observed that immobilized immune complexes (iICs) can trigger NETosis [159]. This mechanism is ROS dependent. Following iICs stimulation, FcγIIIB and Mac-1 receptors on the surface of neutrophils are activated, which leads to a Syk-, PI3K/Akt-, and p38 MAPK-mediated signaling, causing NET formation and release [159].

Autophagy plays also an important part in NET generation. In most cells, including neutrophils, mTOR (mammalian Target of Rapamycin) kinase is the key autophagy regulator [160]. The mTOR pathway is able to coordinate intracellular cascades that lead to the activation of neutrophils and NET release. Accordingly, rapamycin, an antibiotic, used to inhibit mTOR kinase, leads to decreased NET formation [161]. These finding were confirmed by the PI3K inhibitor Wortmannin, a non-specific autophagy inhibitor, which was able to impair NETosis [162]. In addition, Wortmannin seems to be able to inhibit histone protein deimination, preventing neutrophils from forming NETs [160].

Furthermore, it has been demonstrated that calcium-activated potassium channels are able to induce ROS-independent NETosis based on histone citrullination [163].

In general, three different kinds of NETosis have been observed.

Suicidal NETosis

After about 2-3 hours of stimulation with PMA suicidal NETosis can be observed. NADPH oxidase (NOX2) is activated through protein kinase C, ROS are released and enzymes like the neutrophil elastase and MPO translocate into the nucleus to promote nuclear remodeling and NET release [155, 163]. Alternatively, neutrophil treatment with calcium ionophores such as A23187 triggers the NOX2-independent activation of peptidyl arginine deiminase 4 (PAD4) leading to decondensation of the chromatin. The nuclear membrane disrupts. Now the chromatin is being released into the cytosol. Here the granule and cytosolic proteins decorate the chromatin. In the end, the plasma membrane ruptures, the nuclear DNA is released, NETs are formed and the neutrophils die [164].

Vital NETosis, not depending on ROS

It has been shown that vital NETosis may be induced within 5 to 60 minutes after contact with bacteria via toll like receptors. It is assumed that PAD4 is activated without any oxidants. The chromatin

decondensates. Neutrophil elastase translocates to the nucleus to further enhance chromatin unfolding and disruption of the nuclear membrane. During vital NETosis the neutrophil stays alive due to the fact that the chromatin is expelled in form of vesicles. The neutrophil is still able to function partly afterwards [164, 165].

Vital NETosis, depending on ROS

In 2009 Yousefi described a third form of NETosis [151]. Here neutrophils are able to release their mitochondrial DNA. It has been shown that this pathway is ROS dependent. When DPI is added, no mitochondrial NETosis is observed. This form of NETosis does not lead to cell death [151] and has been observed in patients with systemic lupus erythematosus [166]. Immune complexes activate neutrophils leading to mitochondrial ROS production. The mitochondria are extruded to the surface of the cells where they release their DNA. They can also be detected together with expelled nuclear NETs [166].

2.11.3. NETosis in disease

NET formation is not only observed in pathogen defense but is also associated with various diseases like systemic lupus erythematosus [167], chronic granulomatous disease [168] and vasculitis [169]. NETs are also able to recruit platelets and neutrophils to the endothelium, supporting the pathogenesis of venous thrombosis [170, 171].

As mentioned in section 2.11.1. NETosis plays an important role in the immune response [172]. About 5% of the proteins in NETs is neutrophil elastase [146] which degrades virulence factors and pathogens [173]. On the other hand, bacteria expressing DNase are more pathogenic since they avoid being trapped by NETs [174]. It has been speculated that chronic bacterial infections sustain a basal NETosis activity in the body which may trigger AAA formation, e.g., NETs may contribute to AAA development in conjunction with periodontitis [144]. In this study it has been observed that markers for NETs, like citrullinated histones and cell-free DNA (cfDNA), are elevated in the luminal part of the ILT and the adventitia of the abdominal aortic aneurysm wall. In addition, in the plasma of AAA patients levels of cfDNA and DNA-myeloperoxidase complexes were increased in comparison to a healthy control group. NETs were also detected in the aortic aneurysm tissue. Likewise, in an animal model of AAA formation, plasma levels of cfDNA and DNA-MPO complexes were elevated [144].

2.11.4. Inhibition of NETosis

In an experimental animal model for AAA the aorta of mice was perfused with elastase to trigger aneurysm formation and DNase1 was applied to destroy NETs [175]. It was found that AAA formation was decreased when DNase1 was administered on days 0-5 post elastase treatment, but DNase1 injections on days 4-9 were not able to suppress AAA development. In the study it has been noted that the effect of delayed DNase1 application should be evaluated in an animal model that more closely mimics the pathogenesis of human aneurysm formation [175].

Treatment with DNase1 enzymatically degrades DNA molecules of already formed NETs. Other treatments focus on the inhibition of early steps in NETosis to prevent NET formation. The transformation of arginine to citrulline residues is modulated through the enzymes protein arginine deiminases 1, 2, 3, 4 and 6 [176, 177]. Especially high levels of PAD4 have been detected in neutrophil granulocytes. For the activation of PAD4 calcium is needed [178]. PAD4 is able to citrullinate the arginine

of histones leading to a weakening of the electrostatic binding between histones and DNA [179]. It has been observed that PAD4 deficient mice are unable to form NETs [180].

GSK484, a selective and reversible PAD4 inhibitor, has been developed [177]. The compound binds to the non-activated form of PAD4. GSK484 has a half maximal inhibitory concentration of 50 nM. In human and in murine neutrophils histone H3 citrullination and NET formation has been reduced through GSK484 in vitro [177]. GSK484 has not been tested in AAA animal models to date.

3. Study Hypotheses and Aims

Considering the importance of recruitment and activation of neutrophils for the development of AAA, the working hypothesis is raised that increased NETosis may accelerate the growth of AAA. To date, the therapeutic and marker potential of NETs in AAA has not been fully examined. Therefore, the aims of this study are

1. to analyze different parameters which reflect neutrophil activation and NETosis (DNA-histone complexes, MPO-histone complexes, MPO and citrullinated histone H3) in plasma of AAA patients being monitored in the pre- and post-surgery phase. Furthermore, the NETosis parameters are to be evaluated for their potential to predict disease progression.

2. to test the therapeutic impact of anti-NET therapy in established disease with a recently developed, highly selective and reversible PAD4 inhibitor (GSK484) which inhibits histone citrullination by PAD4 and therefore reduces neutrophil extracellular trap formation in human and mouse neutrophils. This work aims to determine the optimal in vivo application and dosage of GSK484 in an experimental model of AAA based on ApoE deficient mice exposed to angiotensin II (AngII).

Based on the proposed study, we expect to gain more scientific knowledge on the therapeutic and marker potential of NETs in AAA disease.

4. Materials and Methods

4.1. Human Study

4.1.1. Human Study Design

The protocol was approved by the Ethics Committee of the Medical University of Vienna as part of the clinical study "Predictive Potential of Neutrophil and NET Biomarkers in Patients with Abdominal Aortic Aneurysm" (no. 1729/2014).

All patients gave written, informed consent to participate in this clinical study. Patients diagnosed with an abdominal aortic aneurysm were recruited through the Vascular Surgery outpatient clinic of the Medical University of Vienna.

Every six months visits were being scheduled to withdraw blood for biomarker analysis and to conduct a CTA scan in order to asses AAA growth. In case of surgical repair, blood was collected immediately prior to the intervention and at 3-6 months thereafter.

Patients with following diseases were excluded:

- Rare types of AAA with special genesis such as in Ehlers-Danlos syndrome and Marfan syndrome
- Oncological disease: present carcinoma or chemotherapy during the last year
- Hematological disorders
- Organ transplantation or immunosuppression
- Autoimmune diseases

Patients did not suffer from any current or recent infection at the time of blood withdrawal.

A total of 100 long-term follow-up patients were scheduled for a monitoring period of three years. In this thesis only a part of this collective was analyzed.

4.1.2. Blood Sampling

Per patient following samples were taken: one serum tube with a gel plug and one hirudinized tube (Roche, Basel, Switzerland) at room temperature and three CTAD plasma tubes at 4°C (Greiner Bio-One, Kremsmünster, Austria) containing a mixture of citrate, theophylline, adenosine and dipyridamole (CTAD).

The total number of neutrophils was determined in hirudinized whole blood using a hemocytometer (Sysmex XN-350 Europe GmbH Europe, Norderstedt, Germany).

4.1.2.1. Preparation of Plasma

For the plasma preparation the CTAD tubes were kept on ice for at least 10 minutes before being centrifuged. Then the blood was centrifuged at 1000 x g (2500 rpm) at 4°C for 10 minutes using the Rotanta 460 RC centrifuge (Hettich, Kirchlengern, Germany). The supernatant was collected, briefly mixed with an IKA Vortex Genius 3 (IKA-Werke GmbH & Co. KG, Staufen, Germany) and again centrifuged at 10000 x g (10000 rpm) at 4°C for 10 minutes with the Microfuge 22R centrifuge (Beckman Coulter, Brea, California, USA). The samples were stored in aliquots at –80°C.

4.1.2.2. Routine Laboratory Blood Analysis

In addition to the determination of NET markers in plasma by enzyme-linked immunosorbent assay (ELISA), a routine hospital laboratory analysis was conducted for each patient. This enabled to compare the explorative parameters to established blood markers of cardiovascular disease such as total cholesterol, high density lipoprotein (HDL) cholesterol, low density lipoprotein (LDL) cholesterol, lipoprotein a, C-reactive protein (CRP), creatinine, urea, free hemoglobin, fibrinogen and D-dimer.

4.1.3. Enzyme-Linked Immunosorbent Assay

4.1.3.1. Cell Death Detection ELISA

The Cell Death Detection ELISA (Roche, Mannheim, Germany, no. 11 544 675 001) measured complexes of DNA with histones (H1, H2, H3, H4) released upon cell death. The sandwich antibodies were directed against DNA and histones.

Plate coating: The plate was coated one day before assay performance. The anti-histone solution was reconstituted by adding 1 ml sterile water. Then 1 ml of the 10 x coating buffer was diluted in 9 ml sterile water (1:10). The coating solution was prepared by mixing 1 ml anti-histone solution and 9.5 ml coating buffer. 100 µl coating solution were added to each well. The plate was incubated at 4°C for 19 hours at 600 rpm (shaker IKA MS3 digital, IKA-Werke, Staufen, Germany).
Plate blocking: The next day the plate was emptied and 200 µl incubation buffer were added. The plate was placed at room temperature (RT) for 30 minutes onto the shaker.
Preparation of plasma samples and standards: In the meantime plasma samples from -80°C were thawed at RT. Afterwards they were mixed with the vortex and briefly centrifuged.
The self-made standard stock was thawed. The stock was composed of culture supernatant from isolated human neutrophils, stimulated for 3 hours by PMA for NETosis induction and stored at -80°C. The standard was of unknown concentration of free DNA-histone complexes and could hence only be applied as a relative reference. The standard dilution series was prepared as follows: 1:9, 1:27, 1:81, 1:243, 1:729 and blank, resulting in relative reference values of 81, 27, 9, 3, 1 and 0.
Washing buffer was diluted (1:10) in deionized water. After blocking, the plate was washed three times; 95 µl of standards were added into each well of the first row. Then 95 µl of sample (CTAD plasma) were added to each well in duplicates. The plate was coved with an adhesive strip and incubated with agitation at RT for 1.5 hours.
Addition of detection antibody: Anti-DNA solution was reconstituted by adding 1 ml of sterile water. Conjugate solution was prepared by mixing 1 ml anti-DNA solution with 9.5 ml incubation buffer. The plate was washed three times. Then, 100 µl conjugate solution were added to each well. The plate was covered with an adhesive strip and incubated/agitated at RT for 1.5 hours. Subsequently, the plate was washed three times.
Addition of substrate: 3 ABTS tablets were dissolved in 15 ml substrate buffer; 100 µl of substrate were added to each well.
Measurement: The plate was incubated for 10-20 min protected from light. Measurements were conducted after 10, 16, 23 minutes. The optical density was measured at 405 nm wavelength and 490 nm for correction.

4.1.3.2. Human Myeloperoxidase ELISA

Preparation of MPO ELISA (R&D Systems, Minneapolis, Minnesota, USA, no. DMYE00B) components: Wash buffer was diluted (1:25) with deionized water. Standard was diluted by simply adding water (to a final concentration of 100 ng/ml after reconstitution). CTAD plasma samples from -80°C were thawed at RT and afterwards mixed with the Vortex instrument.
Preparation of plasma samples and standards: Plasma samples were diluted with RD6-58 calibrator diluent (1:10). The standard was diluted with RD6-58 buffer to the following concentrations: 10.00 ng/ml, 3.33 ng/ml, 1.11 ng/ml, 0.37 ng/ml, 0.12 ng/ml and blank**.**
Distribution of plasma samples and standards: 100 µl of RD1-27 buffer were added to each well and 50 µl of standard were distributed into the first row. 50 µl of diluted plasma samples of patients were added per well (in duplicates). The plate was covered with an adhesive strip and incubated at RT for 2 hours at 500 rpm.
Addition of detection antibody: The plate was washed 4 times with wash buffer. 200 µl MPO conjugate were added to each well. The plate was covered by adhesive strip and incubated at RT for 2 hours at 500 rpm.
Addition of substrate: The plate was washed 4 times with wash buffer. Equal volumes of color reagents A and B were mixed together in order to prepare the substrate solution. 200 µl of substrate solution were added to each well. The plate was incubated for 30 min without agitation and protected from light. The incubation time was 30 minutes.
Measurement: 50 µl stop solution were added to each well. The content in each well was pipetted up and down 8-10 times until the color completely changed to yellow. Optical density was measured at 450 nm and for correction, at 540 nm wavelength.

4.1.3.3. Histone-CitH3 ELISA

The histone-citH3 ELISA was partly based on the Cell Death Detection Kit (Roche, Basel, Switzerland, no. 11 544 675 001) but modified to measure citrullinated histone H3 (citH3) released upon NETosis [181].

Preparation of standard: 1 µg of recombinant human PAD4 (Cayman Chemicals, Ann Arbor, Michigan, USA) was mixed with 2 µg of recombinant human histone H3.1 (New England Biolabs, Ipswich, Massachusetts, USA) in a total of 20 µl of the following buffer: 50 mM Tris-HCl at pH 7.6, 4 mM $CaCl_2$ (calcium chloride), 1 mM phenylmethylsulfonyl fluoride and 4 mM dithiothreitol. The solution was incubated for 2 h at 37°C. The mix was diluted in phosphate-buffered saline deficient of Ca2+ und Mg2+ (PBS-/-) for a final concentration of 1 µg/ml of citrullinated histone H3 and stored at -20°C.
Plate coating: Anti-histone solution was prepared by adding 1 ml sterile water. Coating buffer was diluted 1:10 with sterile water. Coating solution was prepared by mixing 1 ml anti-histone solution with 9.5 ml coating buffer; 100 µl of coating solution was added to each well. The plate was covered by adhesive strip and incubated (generally under agitation) at 4°C overnight.
Preparation of plasma samples and standards: Washing buffer was prepared by adding 0.05% Tween20 in PBS-/-. 200 µl of incubation buffer was added to each well. The plate was covered with adhesive strip and incubated at RT for 1 h. Plasma samples from -80°C were thawed at RT and mixed. The prepared

standard was diluted with incubation buffer to following concentrations: 500 ng/ml, 166.7 ng/ml, 55.6 ng/ml, 18.5 ng/ml 6.17 ng/ml and blank.

Distribution of samples and standards: The plate was washed 3 times with wash buffer. Afterwards 50 µl of standards were added into each well of the first row. 50 µl of patient plasma sample were added per well (in duplicates). The plate was covered with an adhesive strip and incubated at RT for 1.5 hours.

In the meantime bovine serum albumin (BSA) was dissolved in PBS-/- (at a final concentration of 1% BSA; Sigma-Aldrich, St. Louis, Missouri, USA, no. A7030, stored at 4°C). Anti-citH3 antibody (Abcam, Cambridge, United Kingdom, no. ab5103) was diluted 1:1000 in PBS-BSA 1%.

Addition of detection antibody: The plate was washed three times with washing buffer. 100 µl of anti-citH3 antibody were added to each well. The plate was covered with an adhesive strip and kept at RT for 1.5 hours.

In the meantime anti-rabbit horseradish peroxidase conjugate (Cell Signaling, Danvers, Massachusettes, USA, no. 7074S) was diluted 1:2000 in PBS-BSA 1%.

Addition of conjugated secondary antibody: The plate was washed three times with washing buffer. 100 µl of anti-rabbit horseradish peroxidase antibody was added to each well. The plate was covered by adhesive strip and incubated at RT for 1 hour.

In the meantime stop solution, consisting of 2% sulfuric acid, was prepared.

Addition of substrate: The plate was washed three times with washing buffer. 100 µl substrate were added to each well. The plate was incubated for 30 minutes protected from light. Afterwards 50 µl stop solution were added to each well. Optical density was measured at 450 nm and 540 nm wavelength, for correction.

4.1.3.4. MPO-Histone ELISA

A combination of the Cell Death Detection ELISA (Roche no. 11 544 675 001) and the myeloperoxidase ELISA (R&D Systems, Minneapolis, Minnesota, USA, no. DMYE00B) was applied to measure complexes of MPO with histones (H1, H2, H3, H4) released upon neutrophil cell death. The sandwich antibodies were directed against MPO and histones.

Plate coating: Anti-histone solution was reconstituted by adding 1 ml sterile water. Coating buffer was diluted 1:10 with sterile water. Coating solution was prepared by mixing 1 ml anti-histone solution and 9.5 ml coating buffer. 100 µl of coating solution were added to each well. The plate was covered by adhesive strip and incubated at 4°C overnight at 600 rpm (on the IKA MS3 digital plate shaker).

Plate blocking: Washing buffer was diluted 1:10 with deionized water. 200 µl of incubation buffer were added to each well. The plate was covered with an adhesive strip and kept at RT for 30 min with agitation. In the meantime CTAD plasma samples were retrieved from -80°C, thawed at RT and vortexed.

Preparation of plasma samples and standards: A self-made standard was prepared from supernatant of isolated human neutrophils, stimulated for 3 h by PMA for NETosis induction and stored at -80°C. The standard had an unknown concentration of free histone-MPO complexes and was hence applied as a relative reference. The standard was thawed and diluted with incubation buffer at 1:2, 1:6, 1:18, 1:54, 1:162 and blank, resulting in relative reference values of 81, 27, 9, 3, 1 and 0.

Distribution of plasma samples and standards: The plate was washed three times with washing buffer. Afterwards 95 µl of standard were added to the wells in the first row. 95 µl of sample were added to the rest of the wells in duplicates. The plate was covered by adhesive strip and incubated with agitation at RT for 1.5 hours.

Subsequently, the ELISA procedure was switched to the MPO ELISA components.

Addition of detection antibody: MPO ELISA wash buffer was diluted 1:25 with deionized water. The plate was washed four times with washing buffer. 150 µl MPO conjugate were added to each well. The plate was covered with an adhesive strip and incubated at RT for 2 hours at 500 rpm.

Addition of substrate: Equal volumes of color reagents A and B were mixed. The plate was washed four times with washing buffer. 150 µl of substrate were added to each well. The plate was incubated for 30 minutes without agitation and protected from light.

Measurement: 50 µl stop solution were added to each well and pipetted up and down for 8-10 times until the color was completely changed to yellow. Optical density was measured using 450 nm and 540 nm as correction wavelength.

4.2. Animal Study

4.2.1. Mouse Model of AAA Formation

The study protocol "The Therapeutic Potential of Neutrophil Extracellular Traps (NETs) in Abdominal Aortic Aneurysms" was approved by the Ethic
s Committee for Animal Experimentation of the Medical University of Vienna and by the Austrian Ministry of Science (GZ 66.009/0355-WF/V/3b/2016).

There are a number of different AAA animal models, like the elastase perfused rat model, the elastase perfused mouse model and the angiotensin II infused mouse model. However, not all of them mimic the risk factors of the human disease and some do not even develop a thrombus [182-185]. For this study the angiotensin II infused mouse model was used due to the fact that it mimics several essential human risk factors. Mice homozygous for the ApoE mutation develop hyperlipidemia. The treatment with angiotensin II leads to hypertension. The mice are of male gender. All these risk factors in combination play an important part during the pathogenesis of AAA. It also has been observed that angiotensin II infusion leads to an increased infiltration of macrophages resulting in a dilatation of the wall [186, 187]. In addition, this model generates an atherosclerotic lesion, luminal dilatation, medial degeneration, inflammation and intramural thrombus development. However, it has to be noted that the aneurysm forms suprarenal and the thrombus develops intramural, whereas in humans most aneurysm are located infrarenal and the thrombus forms in the luminal part of the aorta [188].

4.2.2. Animal Study Design

B6.129P2-ApoEtm1Unc/J mice, homozygous for the ApoE mutation, were obtained from the Department of Biomedical Research at the Medical University of Vienna (Ass.-Prof. Dr. Harald Höger). All mice were fed a normal chow diet with fresh, clean water ad libitum. After pump implantation they were kept in individual cages. Mice were aged between 8-12 weeks and were of male gender for the experiment. The animals weight between 25-30 g.

The first part of the study focused on determining an appropriate in vivo dosing of GSK484, due to the fact that until this time the PAD4 inhibitor, GSK484, had only been tested in vitro. Therefore, GSK484 was injected into the vena jugularis externa at the following concentrations: 0.2 µg, 2 µg or 20 µg/g body weight. Mice were closely observed for toxicity or aberrant behavior within the next day. After 24 hours the blood was harvested from the vena cava inferior. Neutrophils were isolated, blood smears were performed and DNA release was measured upon in vitro NET induction.

The second part of the study was conducted after the appropriate in vivo dosage of GSK484 had been determined. Mice were implanted with an osmotic angiotensin II (Ang II) pump. After 14 days a catheter was inserted into the vena jugularis externa and mice were treated with GSK484 or PBS-/- for negative control daily via the intravenous port. At day 28 mice were sacrificed and blood samples were taken for NET detection. The maximum diameter of the suprarenal abdominal aorta was assessed by ultrasound at baseline, day 14 and day 28 to monitor AAA development.

4.2.3. Injection into the Vena Jugularis Externa

Mice were anesthetized with isoflurane at a flow rate of 1-2%. Buprenorphine (0.01 ml/g body weight) was injected subcutaneously in order to prevent pain sensation. Animals were kept on heating pads to

avoid hypothermia. Eyes were protected by an ocular gel. After hair removal, the skin was disinfected with betaisodona (povidone-iodine). The vena jugularis externa was prepared under the microscope (Leica, Wetzlar, Germany, M651). The distal part of the vena was ligated (Fig. 1).

The GSK484 (PAD4 inhibitor) stock was dissolved in ethanol at 20 mg/ml. Afterwards GSK484 was diluted with PBS -/- in order to apply either 0.2, 2.0 or 20 µg per g mouse weight into the vena jugularis externa with a bent 30G needle.

Then the proximal part of the vessel was immediately ligated. In the end mice were sutured. During the whole procedure the general condition of the animals was monitored by checking posture, breathing frequency and activity.

Materials: suture (B. Braun, Maria Enzersdorf, Austria, Silkam 7/0, , no. 0766038), skin suture (Covidien, Dublin, Ireland, Polysorb 4-0 CV-23,), 30 G needle (B.Braun, Sterican), GSK484 (Cayman ChemicalsAnn Arbor, Michigan, USA , no. 17488) stock solution of 20 mg/ml (39.22 mM) in ethanol, stored at -20°C

A B C

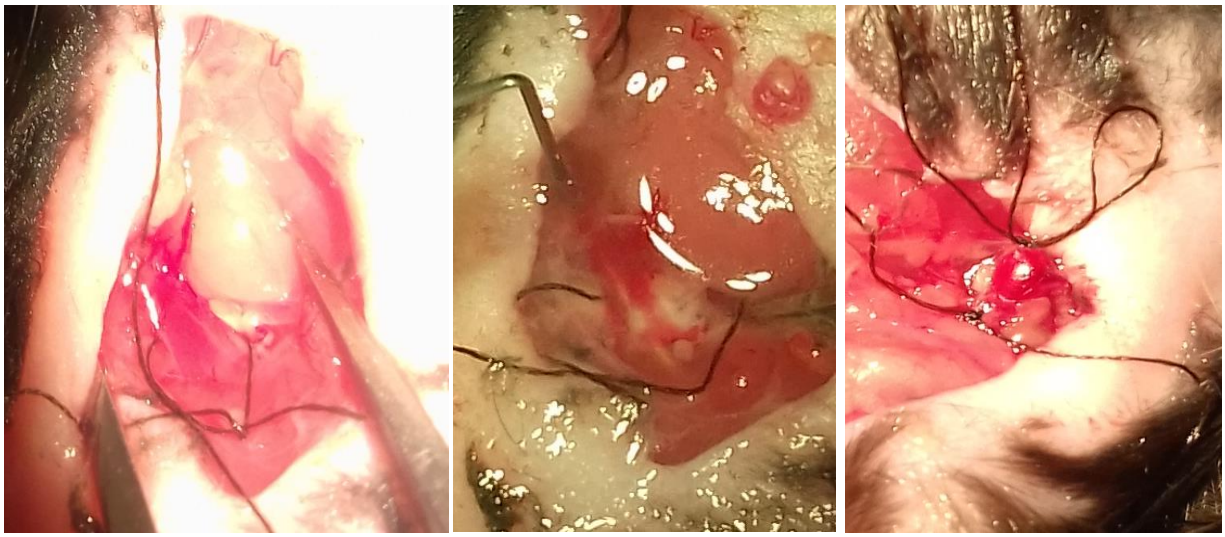

Figure 1: Injection into the vena jugularis externa.
A) Preparation of the vena jugularis externa and preparation of the ligations B) Injection into vena jugularis externa C) Complete ligation of vena jugularis externa

4.2.4. Blood Collection

At first the animals were anesthetized with 100 mg/kg ketamine and 5 mg/kg xylazine. Afterwards the abdomen was opened via laparotomy. The vena cava inferior was prepared (Fig. 2). Before the blood was taken each syringe was coated with EDTA solution. On an average about 0.5-1 ml blood was drawn from each mouse. Then this blood sample was transferred into the mini EDTA blood collection tubes.

Material needed per mouse: 2 × 1 ml syringe, 27¾ G needle (Microlance 3, Dublin, Ireland, no. 302200), 9× EDTA solution in PBS-/- (EDTA contained in one 9 ml EDTA blood collection tube was dissolved in 1 ml PBS-/-), 1 ml EDTA blood collection tubes (e.g. Greiner Bio-one, Kremsmünster, Austria, MiniCollect EDTA tubes 1.0 ml no. 450474), ketamine for anesthesia, operation instruments

A B

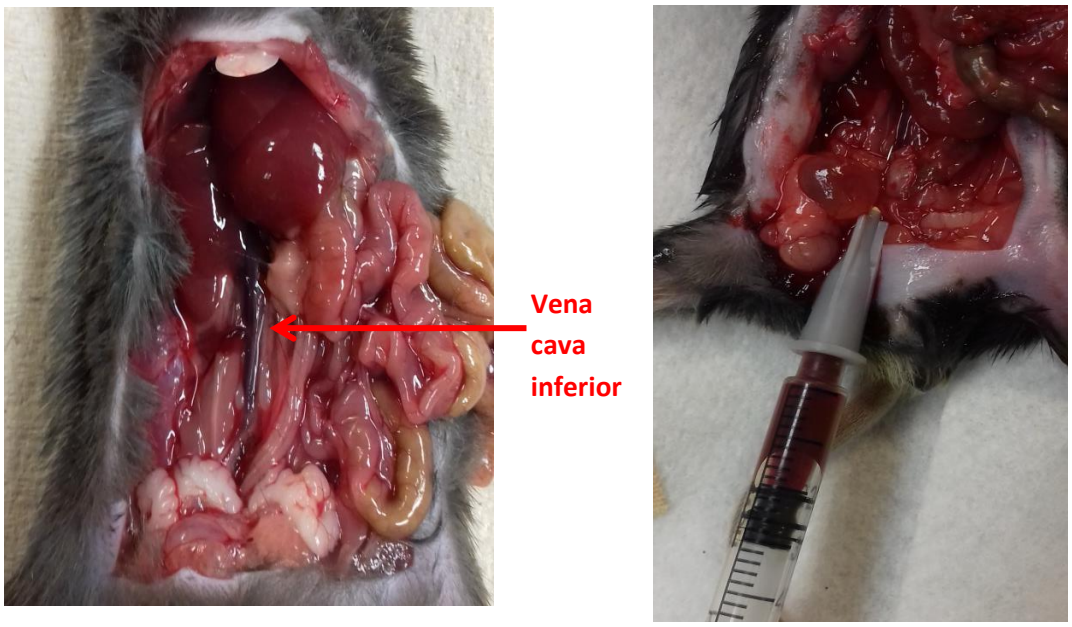

Figure 2: Blood withdrawal from vena cava inferior.
A) Preparation of vena cava inferior, B) Blood withdrawal from vena cava inferior

4.2.5. Isolation of Neutrophil Granulocytes

The isolation was performed with the Easy Step Mouse Neutrophil Enrichment Kit (Stemcell Technologies, Vancouver, Canada, no. 19762A) based on negative selection, i.e. removal of non-granulocytes from whole blood by antibody labeling and magnetic particles. All steps were performed on ice. To lyse erythrocytes 1 ml of EDTA-anticoagulated blood was mixed with 9 ml of precooled ammonium chloride solution. The suspension was mixed by gently inverting the tube a few times and was then incubated on ice for 15 minutes. The tube was centrifuged at 300 × g for 6 minutes at 4°C: The supernatant was discarded. The cell pellet was gently resuspended in recommended medium at 3 ml of medium per 1 ml of original blood.

Then, 110 µl were used to count the white blood cells. First, 10 µl were mixed with 10 µl trypan blue solution and evaluated in the manual counting chamber. The remaining 100 µl were used to count the cells via Sysmex XN-350 device using the body fluid program.

Thereafter, medium was added to the cells at 10 ml per 1 ml original blood volume. The suspension was again centrifuged at 300 × g for 6 minutes at 4°C. The supernatant was discarded. The cell pellet was resuspended and diluted to obtain 1×10^8 cells/ml medium. Mostly, a yield of 50×10^6 cells in 500 µl medium was reached. The suspension was transferred into a 5 ml polystyrene round bottom tube.

50 µl rat serum were added per ml of medium. Comparably, 50 µl enrichment cocktail were added to each ml of the sample. The cell suspension was gently mixed with a 1000 µl pipette and incubated for 15 minutes on ice. Then medium was added to each sample (final volume 4.5 ml). The cells were centrifuged at 300 × g for 10 minutes at 4°C. Supernatant was discarded and the cell pellet was resuspended with the original volume (mostly 500 µl) of medium. 50 µl of Biotin Selection Cocktail were

added per ml of sample. The suspension was gently mixed with a 1000 µl pipette and incubated for 15 minutes on ice.

Prior to adding 150 µl magnetic particles per sample, the particles were vortexed for 30 seconds. The cell suspension was supplied with the particles, gently mixed with a 1000 µl pipette and incubated for 10 minutes on ice. The samples were topped up with medium to a final volume of 2.5 ml. The suspension was again mixed with a 1000 µl pipette. The polystyrene tubes were placed onto the magnet and incubated for 5 minutes at room temperature. The labelled cells (non-neutrophils) accumulated at the magnet. The rest of the suspension was pipetted into a new polystyrene tube.

The neutrophils were counted manually and via Sysmex device in body fluid mode. For the manual count 10 µl cell suspension and 10 µl trypan blue were mixed. Cell numbers were determined via counting chamber under the microscope (Zeiss, Oberkochen, Germany, Axiovert 40 CFL).

In order to confirm that the isolated cells are actually neutrophils, 20 µl of cell suspension were incubated with 2 µl of Ly6G antibody directly conjugated to AlexaFluorA488 dye (BioLegend, San Diego, California, USA, no. 127626) for 10 minutes at room temperature. Then 480 µl PBS-/- were added. The neutrophil measurement was conducted by flow cytometry in a Gallios instrument (Beckman Coulter, Brea, California, USA).

Materials: Easy Step Mouse Neutrophil Enrichment Kit (Stemcell Technologies, no.19762A), Easy Eights Magnet (Stemcell Technologies, no. 18103), polystyrene tubes, trypan blue solution (0.4%) (Life Technologies, no. 15250-061), normal rat serum (Stemcell Technologies, no. 13551), ammonium chloride solution stored at -20°C (Stemcell Technologies, no. 07850), 50 mM EDTA stock solution: 18.6 mg EDTA dissolved in 1 ml PBS-/- and filtered at 0.22 µm, **"**recommended medium" was prepared and stored at +4°C: 500 ml PBS-/-, 10 ml fetal bovine serum (2%), 10 ml 50 mM EDTA stock for a final concentration of 1 mM EDTA

4.2.6. DNA Release Assay

First, a predilution of A23187 in Hank´s balanced salt solution with calcium and magnesium (HBSS+/+) was prepared at a ratio of 1:100 to reach a final concentration of 200 µM. If necessary, this solution was further diluted 1:2 to reach 100, 50, 25 µM and 12.5 µM of A23187. Second, 5 mM SYTOX Green was added to HBSS+/+ at a 1:100 ratio to achieve 50 µM. Third, predilutions of GSK484 were conducted using the 20 mM stock in HBSS+/+: 20 µl GSK484 stock were added to 80 µl HBSS+/+ (1:5 dilution to 4 mM). Then, 20 µl thereof were combined with 80 µl HBSS+/+ (additional 1:5 dilution to 800 µM). Fourth, comparable predilutions were generated from the 40 mM GSK484 stock dissolved in ethanol: 10 µl 40 mM GSK484 stock were added to 90 µl HBSS+/+ (4 mM) and 20 µl thereof were combined with 80 µl HBSS+/+ (800 µM).

After the mouse neutrophils had been isolated with the Easy Step Mouse Neutrophil Enrichment Kit, in most experiments they were pooled from all mice due to a low yield of cells. Afterwards the neutrophils were brought to a concentration of 1×10^6/ml in HBSS+/+. The required amount of all components for the DNA release assay (performed in a 96-well plate) was calculated as listed in Table 1, resulting in 50000 neutrophils/well and a final volume of 150 µl per well. First, HBSS+/+ was pipetted into the wells. The indicated concentrations of GSK484 were added to the required wells. Then, 50 µl of cells (50000

neutrophils) were added per well, followed by incubation at 37°C for 30 minutes in the Heraeus incubator (Thermo Fisher Scientific, Waltham, Massachusetts,USA) in order to inhibit PAD4 activity. Afterwards the indicated volume of A23187 was added to the required wells to trigger NET formation. Finally, SYTOX Green (prediluted) was added to all wells to fluorescently label cell-free DNA released upon NETosis. The fluorescence measurement was conducted with the Varioskan Flash plate reader (Thermo Fisher Scientific).

Materials: HBSS+/+ (Lonza, Basel, Switzerland, no. BE10-527F), A23187 calcium ionophore (Sigma Aldrich, no. C7522) 20 mM stock in dimethyl sulfoxide, GSK484 (Cayman Chemicals, no. 17488) 20 mM stock in in HBSS+/+ and 40 mM stock in ethanol stored at -20°C, SYTOX Green (Thermo Fisher Scientific, no. S7020) supplied as 5 mM stock in dimethyl sulfoxide and stored at -20°C, black 96-well plates with white wells

Condition	HBSS++ [µl]	Neutros [µl]	GSK484 predilution [µl]	A23187 predilution [µl]	SYTOX 50 µM predilution [µl]	EtOH [µl]
Untreated	85	50	-	-	15	-
Untreated + EtOH	77.5	50	-	-	15	7.5
A23187 133 µM	84	50	-	1 (20 mM)	15	-
A23187 4 µM	82	50	-	3 (200 µM)	15	-
A23187 4 µM + EtOH	74.5	50	-	3 (200 µM)	15	7.5
A23187 2 µM + EtOH	74.5	50	-	3 (100 µM)	15	7.5
A23187 1 µM + EtOH	74.5	50	-	3 (50 µM)	15	7.5
A23187 0.5 µM + EtOH	74.5	50	-	3 (25 µM)	15	7.5
A23187 0.25 µM + EtOH	74.5	50	-	3 (12.5 µM)	15	7.5
GSK484 2 mM HBSS++	70	50	15 (20 mM) HBSS++	-	15	-
GSK484 80 µM HBSS++	70	50	15 (800 µM) HBSS++	-	15	-
GSK484 2 mM EtOH	77.5	50	7.5 (40 mM) EtOH	-	15	-
GSK484 80 µM EtOH	70	50	15 (800 µM) EtOH	-	15	-

A23187 4 µM + GSK484 2 mM HBSS++	67	50	15 (20 mM) HBSS++	3 (200 µM)	15	-
A23187 4 µM + GSK484 80 µM HBSS++	67	50	15 (800 µM) HBSS++	3 (200 µM)	15	-
A23187 4 µM + GSK484 2 mM EtOH	74.5	50	7.5 (40 mM) EtOH	3 (200 µM)	15	-
A23187 4 µM + GSK484 80 µM EtOH	67	50	15 (800 µM) EtOH	3 (200 µM)	15	-
A23187 2 µM + GSK484 2 mM EtOH	74.5	50	7.5 (40 mM) EtOH	3 (100 µM)	15	-

Table 1: Pipetting scheme for the DNA release assay.
Abbreviations. EtOH, ethanol. neutros, neutrophil granulocytes. HBSS++, hanks balanced salt solution with calcium and magnesium.

4.2.7. Ultrasound Analysis of Aneurysm Diameter

Ultrasound imaging was performed with a high-frequency ultrasound device (Vevo 2100, VisualSonics, Toronto, Canada). The linear array probe had a peak of 55 MHz. The whole procedure was performed under general anesthesia with isoflurane at a flow rate of 1-2%. Animals were fixed onto heating pads in a dorsal position, as illustrated in Figure 3. The abdominal skin was shaved. Eyes were protected by an ocular gel.

The baseline ultrasound was performed on the day of the implantation of the osmotic pumps for AngII administration. The follow-up ultrasound analyses were conducted on day 14 and 28 after the pump implantation. The abdominal aorta was measured from the outer vessel wall to the outer part of the opposite wall during systole in B-mode.

At first the diameter and the area of the aorta was measured in short axis view at the following locations: infrarenal region, at the level of the left and right renal artery, at the level of the renal vein and twice in the suprarenal region. A mean area and aortic diameter was calculated for the suprarenal region.

The diameter of the abdominal aorta was then measured in long axis view. The infrarenal aorta (from the iliac bifurcation to the arteria renalis) was measured at 4 different locations. The suprarenal region was measured at 6 different locations. A mean diameter was calculated for each region.

Figure 3: Ultrasound setting for short axis view of the abdominal aorta.
Mice were fixed in a dorsal position. Hair was removed from the abdominal skin.

4.2.8. Osmotic Pump Implantation

One day prior to the implantation the pumps were prepared (Fig. 4) [188]. First, the mice were weighed and the required amount of angiotensin II was calculated to be released at 1000 ng/kg/min over a time frame of 28 days. For example, for a mouse weighing 29 g the pump should dispense 29 ng AngII/min or 1740 ng/h. Since the osmotic pump releases 0.25 µl solution per hour, 168 µl are required for a total of 28 days with a loading concentration of 6960 ng/µl or 6.96 mg/ml. Therefore 2.08 mg Ang II were dissolved in 300 µl sterile saline and 250 µl of the solution were filled into the pump for a mouse weighing 29 g. The pump was closed with the flow moderator. Finally, the pumps were put into a 15 ml tube filled with saline for preconditioning overnight at room temperature

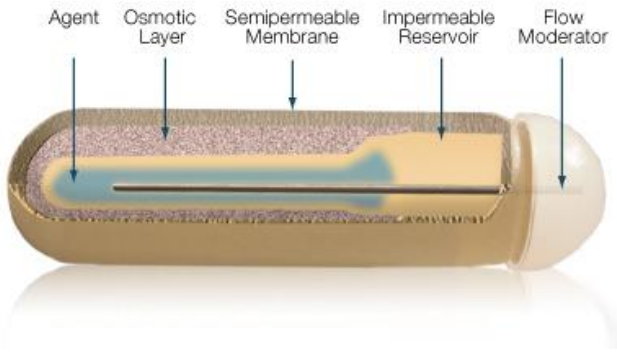

Figure 4: ALZET Mini-Osmotic Pump Model 2004.
Image by DURECT Corporation (Cupertino, California, USA)[189]

The next day the osmotic pumps were implanted into mice under general anesthesia with isoflurane at a flow rate of 1-2% (Fig. 5). Animals were kept on heating pads during the whole procedure in order to avoid hypothermia. Eyes were protected by an ocular gel. After disinfection a small cut was made on the back of the mouse. A subcutaneous pocket was prepared. Then the pump was inserted into the

mouse. Finally, the skin was sutured. The pumps remained for 28 days until sacrifice. Due to the semipermeable outer membrane interstitial fluid was entering the outer pump reservoir, gradually compressing the inner (impermeable) reservoir to slowly release Ang II into the mouse skin.

Materials:

ALZET Mini-Osmotic Pump, model 2004 (DURECT Corporation, Cupertino, California, USA), sutures (Covidien, Dublin, Ireland, Polysorb 4-0 CV-23,), angiotensin II (Bachem AG, Bubendorf, Switzerland, no. 4006473.0025), physiological saline (sodium chloride solution) (Fresenius Kabi, Bad Homburg von der Höhe, Germany, no. 19KB03GB)

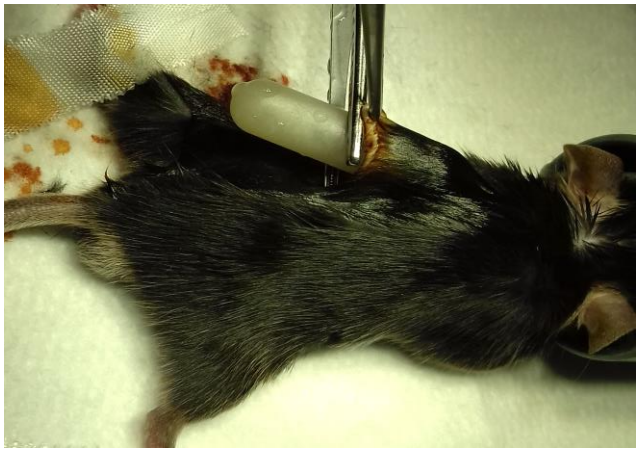

Figure 5: Implantation of the angiotensin II osmotic pump.

4.2.9. Intravenous Mouse Port Implantation

On day 14 of AngII treatment the port (Fig. 6) was implanted under general anesthesia, again using isoflurane at a flow rate of 1-2%. Animals were kept on heating pads during the whole procedure in order to avoid hypothermia. Eyes were protected by an ocular gel. Buprenorphine was injected at 0.01 ml/g body weight subcutaneously in order to avoid pain sensation. After hair removal the skin was disinfected with betaisodona (povidone-iodine).

The first incision was made ventrally and the vena jugularis externa was prepared. The distal part of the vein was ligated completely. The ligation of the proximal part of the vein was prepared. Before implantation the port chamber was filled with PBS-/- (avoiding any air bubbles in order to prevent gas emboli).

A B

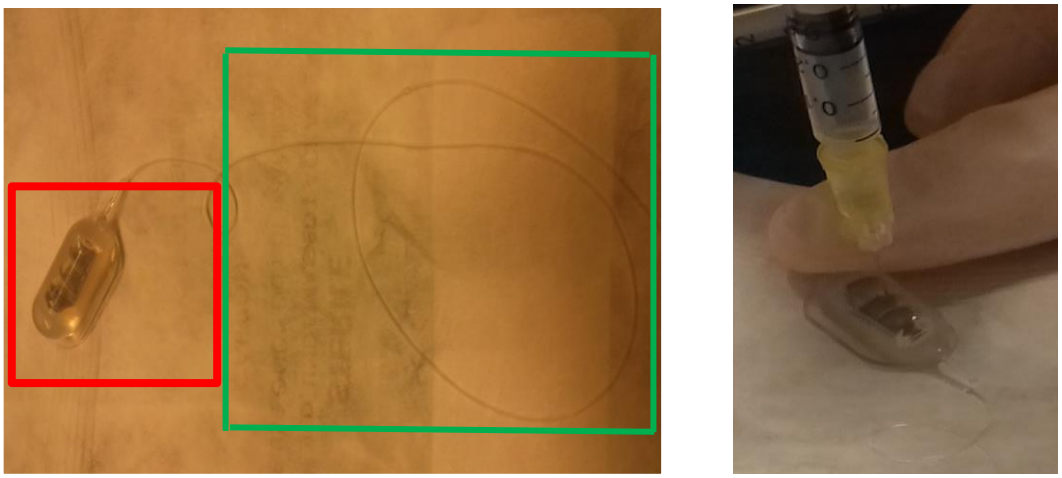

Figure 6: Mouse port system.

A) Mouse port MMP-1S and 30cm 1.2Fr catheter B) Injection of saline into the port chamber for preparation

After hair removal and disinfection with betaisodona a subcutaneous pocket was prepared. The port was implanted subcutaneously (Fig. 7 and 8). The port chamber was fixed to the skin with sutures in order to avoid any unwanted movement. With a pair of scissors a subcutaneous tunnel was prepared to connect the dorsal with the ventral incision (Fig. 9).

Figure 7: Dorsal subcutaneous implantation of the port.

Figure 8: Fixation of the port.

Figure 9: Preparing for implanting the catheter into the vena jugularis externa.

The catheter was pulled from the dorsal side of the tunnel to the ventral side. The mouse was turned around. Then the catheter could be implanted into the vena jugularis externa. A small incision was made in the vein with a 27G needle. The catheter was carefully placed into the vein under constant rinsing with saline. Once the catheter was correctly placed the proximal part of the vein was ligated in order to fix the catheter (Fig. 10). 100 µl of PBS-/- were injected into the port chamber to check if the catheter was functioning.

Figure 10: Fixation of the catheter in vena jugularis externa.

Due to the silicon nature of the port chamber, the mouse port is suited for serial intravenous injections (up to 100) without leakage from the chamber. The GSK484 treated mice received of 2.0 µg GSK484 in 200 µl PBS-/- per g body weight once a day under anesthesia using isoflurane at a flow rate of 6% for about 30 seconds. For control, 200 µl of PBS-/- were injected into the port once a day under the same conditions (Fig. 11).

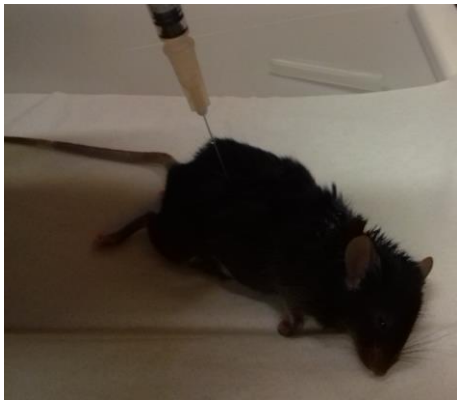

Figure 11: Injection into the port chamber.

Materials: Sutures (Covidien, Polysorb 4-0 CV-23), 7-0 Sikam silk, braided, coated, non-absorbable DMP7 (Braun Surgical, no. 0766038), UNO Mouse Port (UNO B.V., Zevenaar, Netherlands, no. MMP-1S-30CM), Posi-Grip Huber point needle (UNO B.V.)

4.2.10. NET Detection in Blood Smears

At first a protocol for NET detection in blood smears from healthy human blood was implemented. Therefore, the already established immunostaining protocol for neutrophil extracellular traps and citH3 was adapted [190]. After the blood - mixed with EDTA for anticoagulation purposes - was withdrawn it was incubated with A23187 at a final concentration of 10 or 50 µM for two hours at 37°C in order to induce NETosis. To this end, the 20 mM stock solution of A23187 in DMSO had to be prediluted to 250 µM (1 µl A23187 stock + 79 µl PBS-/-) and 1.25 mM (5 µl A23187 stock + 75 µl PBS-/-), respectively and 1 µl of the dilutions was added to 25 µl of whole blood. At the same time control samples were treated with DMSO dilutions, as a solvent control. After incubation in reaction tubes, the 25 µl blood were pipetted on an object slide and immediately spread by carefully moving the slide. After the smear had fully dried it was stored at -80°C.

When ready to perform staining, object slides were transferred into a humid chamber. All procedures were performed at room temperature.

The blood smear was fixed with 4% paraformaldehyde for 30 minutes. Afterwards the sample was washed with PBS -/- (pH 7.4) three times. Then the permeabilization buffer (0.2% Tween-PBS) was added onto the object slide for 15 min at RT. Thereafter, the slide was washed with PBS for three times. The smears were incubated with blocking buffer (containing 1.5% bovine serum albumin, 0.1% sodium azide in PBS) for one hour. The sample was washed with PBS three times. The primary rabbit antibody against citrullinated histone H4 (citH4) was diluted 1:1000 in the blocking buffer. 300 µl of this solution were pipetted onto the slide. The slide was incubated for one hour at 37°C. Then the sample was washed

with PBS-/- three times. The secondary anti-rabbit IgG antibody with AlexaFluor555 conjugate, the Hoechst 33342 stain and Ly6G-AlexaFluor488 conjugate were diluted 1:1000 in the blocking buffer. Again, 300 µl of this solution were pipetted onto the slide. The slide was incubated for one hour at 37°C. In the end the coverslip was washed twice with PBS-/-, was carefully dried and mounted with a drop of Fluoromount-G reagent on the object slide. Slides were stored at 4°C until microscopy.

Five pictures were taken randomly per slide with the LSM 700 confocal microscope (Zeiss) and objective 20x / 0.8 Plan-Apochromat. Pictures were taken of blue (Hoechst), green (Ly6G) and red (citH4) fluorescent signals.

Hoechst positive nuclei were counted in the defined region (frame size 173.68 µm x 173.68 µm). In a second step neutrophils were identified by Ly6G staining (green fluorescence). In addition, NETs were identified by the occurrence of Hoechst positive fragmented nuclei (early stages of NETosis) or DNA strings (late stages of NETosis). To confirm that the Hoechst positive strings or fragmented cells were NETs, citH4 antibody (red fluorescence) was used.

The percentage of NETs in relation to white blood cells and neutrophils was determined.

Counting protocol:

- total cells: all Hoechst positive nuclei
- neutrophils: Hoechst positive nuclei and Ly6G antibody positive
- NETs: Hoechst positive cells, also positive for Ly6G and citH4 antibody; additionally, Ly6G antibody positive string- like structures

Materials: Object slides (LaborChemie GmbH, Vienna, Austria, Star Frost 76×26mm, no. E5501-CW), Fluoromount-G (Southern Biotech, Birmingham, Alabama, USA, no. 0100-01), cover slips (Thermo Fisher Scientific, Waltham, Massachusetts, USA, Menzel-Gläser 24×50mm), blocking buffer with 1.5% bovine serum albumin (Sigma-Aldrich, St.Louis, Missouri, USA, no. A7030-50G) and 0.1% sodium azide in PBS-/-), permeabilization buffer with 0.2% Tween20 (Sigma-Aldrich, no. 9005-64-5) in PBS-/-

DNA dye: Hoechst 33342 trihydrochloride, trihydrate (Thermo Fisher Scientific, no. H3570)

Antibodies:
Primary: anti-histone H4 (citrulline 4) antibody (Merck & Co., Kenilworth, New Jersey, USA, no.07-596) and AlexaFluor488 conjugated anti-mouse Ly6G (BioLegend, San Diego, California, USA, no. 127626)
Secondary: Alexa-Fluor555 conjugated donkey anti-rabbit IgG (H+L) (Thermo Fisher Scientific, no. A32572)

4.3. Statistical Analysis

Statistical analysis was carried out with SPSS 23.0 Software (SPSS Inc., Chicago, IL, USA) and was based on non-parametric tests, since a study collective of only 5 pre and post-operative patients, 7 monitoring patients, 5 control mice and 5 GSK484 treated mice rarely follows normal distribution. This study was defined as an explorative study. Therefore, no corrections/adjustments for multiple testing were conducted.

During the course of this evaluation several NETosis and routine laboratory parameters were analyzed. The Wilcoxon signed-rank test was applied to evaluate differences between the pre- and post-operative data as well as changes from monitoring time point one to time point two. The Mann Whitney U test was used to analyze the difference between AAA area/diameter progression and the percentage of NETs in blood smears of control mice and GSK484 treated mice. The results were displayed by boxplots.

Furthermore, the correlation between parameters was assessed by Spearman´s coefficient in order to investigate a possible association with NETosis (NET parameters). The data are visualized by scattergrams.

Data of DNA release assays were analyzed with the 2013 version of Microsoft Excel.

A p-value below 0.05 was regarded as significant.

5. Results

5.1. Patient Study

5.1.1. Pre- and Post-Surgery Analysis

5.1.1.1. Patient Demographics

The baseline characteristics of the patients are presented in Table 2. All of the 7 investigated AAA patients were men, which reflects the elevated risk of AAA development for male gender. This group showed an age range from 67 to 81 with a median of 71 years. The body mass index (BMI) ranged from 22.4-28.4 with a median of 24.5. All patients had a positive smoking status. The pack years varied from 5 to 60 (median of 30). Six men had smoked in their past and 1 person was a current smoker. As a likely result 42.9% suffered from chronic obstructive pulmonary disease.

Concerning comorbidities associated with cardiovascular disease, 85.7% patients suffered from hypertension, 100% from hyperlipidemia, 28.6% from diabetes mellitus type II and 28.6% of the patients had experienced coronary artery disease and myocardial infarction.

57.1% of patients underwent endovascular aneurysm repair and 42.9% underwent open surgical repair. The mean interval between blood withdrawal before and after surgery was 12 months (range: 6 – 16 months). Within this collective there were no inflammatory or mycotic aneurysms.

Parameter	N	(%)	Median	Min-Max
Age (years)	7		71	67-81
Body Mass Index	7		24.5	22.4-28.4
Pack years	7		30	5-60
Gender (male)	7	100		
Smoker Status				
Never	0	0		
Current	1	14.3		
Past	6	85.7		
Hypertension	6	85.7		
Hyperlipidemia	7	100		
Coronary artery disease	2	28.6		
Myocardial infarction	2	28.6		
Diabetes mellitus	2	28.6		
COPD	3	42.9		
Atherosclerotic aneurysm	7	100		
Type of surgery				
EVAR	4	57.1		
OSR	3	42.9		

Table 2: Demographics of patients analyzed before and after surgery.
Abbreviations: COPD, chronic obstructive pulmonary disease. EVAR, endovascular aortic repair. OSR, open surgical repair.

5.1.1.2. Explorative Parameters

As described in the methods, DNA-histone complexes, citrullinated histone 3 protein (citH3), myeloperoxidase protein and MPO-histone complexes were measured in plasma samples by ELISA. The data obtained were converted to ng/ml plasma or relative units (RU), as shown in Table 3.

DNA-histone complexes, citH3 protein and MPO protein were significantly increased in AAA patients before surgery when compared to data obtained from plasma samples in the post-surgery phase. There was no significant difference in the plasma concentrations of MPO-histone complexes between the two time points of investigation.

Parameter	preOP	postop	p-value	N
	Median (min-max)	Median (min-max)		
DNA–histone (RU)	34.62 (26.91-84.02)	16.66 (8.88-29.83)	**0.018**	7
CitH3 (ng/ml)	281.45 (174.91-406.41)	200.58 (75.27-272.86)	**0.043**	7
MPO-histone (RU)	7.77 (5.39-19.96)	10.02 (6.94-19.60)	0.612	7
MPO (ng/ml)	21.31 (8.72-52.60)	13.81 (6.72-24.64)	**0.028**	7

Table 3: Explorative parameters in AAA patients before (preOP) and after surgery (postOP).
Abbreviations: RU, relative units. citH3, citrullinated histone 3. MPO, myeloperoxidase.

In AAA patients DNA-histone complexes were significantly higher (p=0.018) before surgery when compared to the postoperative time point of investigation (Fig. 12A). Accordingly, the median of the preoperative samples was 34.62 RU (range: 26.91 - 84.02 RU) and in the postoperative samples less than half with 16.66 RU (range: 8.88 - 29.83 RU) (Table 3).

In contrast to DNA histone complexes, MPO-histone complexes remained unchanged (Fig. 12B), i.e., the median of the preoperative samples was 7.77 RU (range 5.39 - 19.96 RU) and 10.02 RU (range: 6.94 - 19.60 RU) after surgery (Table 3).

The plasma concentration of MPO protein was elevated in the AAA patients before surgery and dropped significantly (p=0.028) after the surgical intervention (Fig. 12C); the median of the preoperative measurements was 21.31 ng/ml (range: 8.72 -52.60 ng/ml) and decreased to 13.81 ng/ml (range: 6.72 - 24.64 ng/ml) after aneurysm repair (Table 3).

The concentration of citH3 protein was found to be significantly higher (p=0.043) at the preoperative compared to the postoperative time point (Fig. 12D) with a median of 281.45 ng/ml (range: 174.91 - 406.41 ng/ml) before surgery and of 200.58 ng/ml (range: 75.27 -272.86 ng/ml) after the intervention (Table 3).

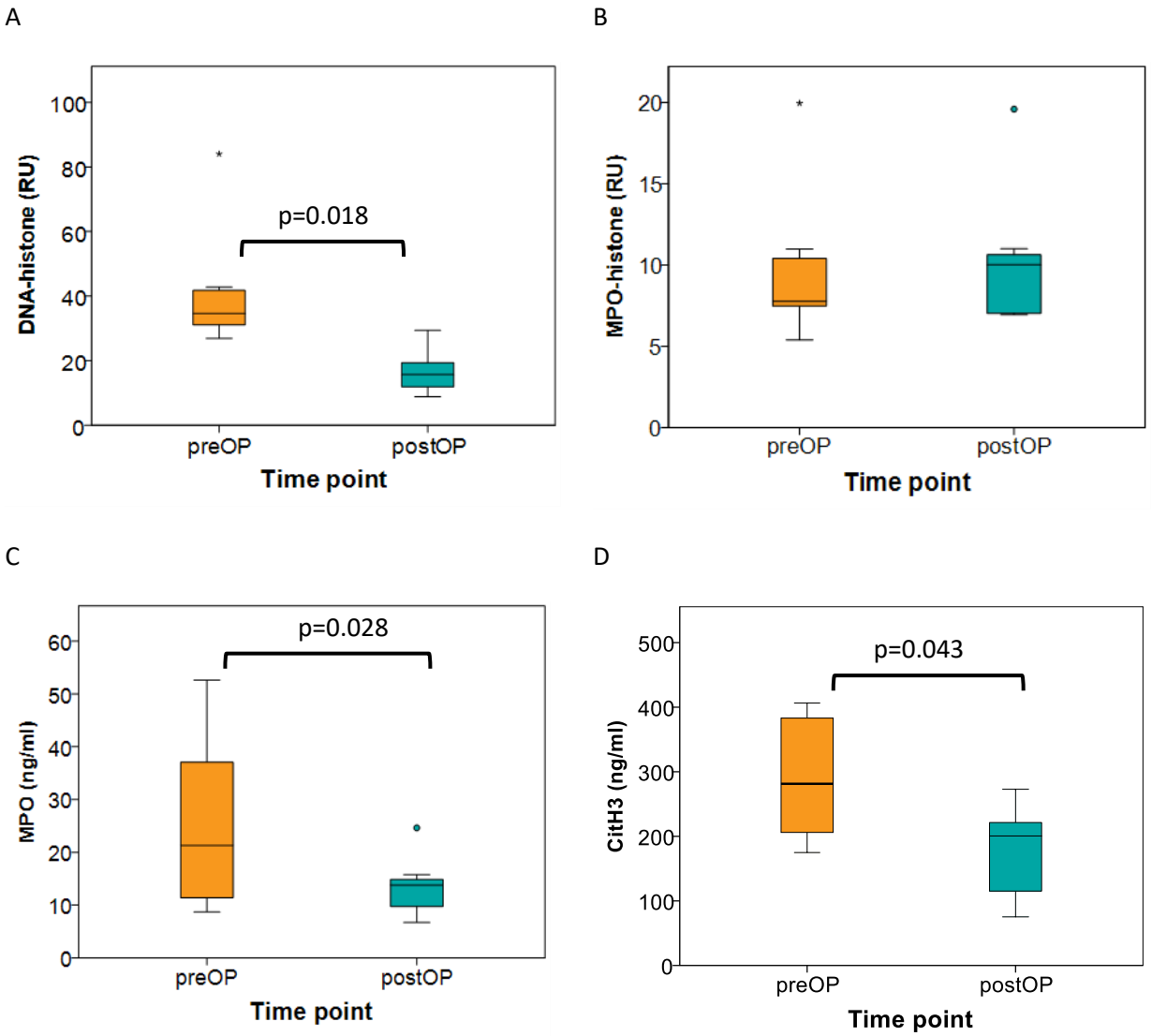

Figure 12: Explorative parameters in plasma of AAA patients before (preOP) and after (postOP) surgery.

Boxplots illustrate the different concentrations of A) RU of DNA-histone complexes B) RU of MPO-histone complexes C) MPO protein (ng/ml) and D) citH3 protein (ng/ml) in plasma of AAA patients before and after surgical aneurysm repair. Data are shown as boxplots with whiskers at minimum and maximum, box at 25th percentile and 75th percentile and a line at the 50th percentile. Outliers and extreme values are indicated by circles and asterisks, respectively.
Abbreviations. RU, relative unites. MPO, myeloperoxidase. citH3, citrullinated histone 3.

5.1.1.3. Laboratory parameters

Common laboratory parameters were determined in AAA patients in order to characterize potential co-morbidities. When comparing pre- and postoperative levels there were no significant differences with regard to mean thrombocyte volume, alpha amylase, 24-hydroxyvitamin D, C-reactive protein, low density lipoprotein, high density lipoprotein, total cholesterol, cholesterol/high density lipoprotein ratio, triglycerides, albumin, urea, creatinine, fibrinogen, activated partial thromboplastin time, monocytes, neutrophils, leukocytes and platelets (Table 4).

On the other hand, concentrations of lipoprotein (a) (p=0.034) (Fig. 13A) and free hemoglobin (p=0.028) (Fig. 13 B) were elevated significantly in the preoperative blood analyses; the preoperative blood lipoprotein (a) levels displayed a median of 13.0 nmol/l (range: 9.0 - 303.0 nmol/l) as opposed to 11.0 nmol/l (range: 7.0 - 254.0 nmol/l) after the surgical intervention. Free hemoglobin showed a median of 3.70 mg/dl (range: 2.48 - 6.31 mg/dl) in the preoperative samples while in postoperative measurements the median had dropped to 2.22 mg/dl (range: 1.10 - 4.13 mg/dl) (Table 4).

Also the percentage of lymphocytes was significantly higher (p=0.028) in the preoperative samples (Fig. 13C) with a median of 31.5 (range: 18.3 - 40.4) before surgery and 24.1 (range: 12.0 - 31.8) after the intervention. In contrast to lymphocytes, the number of erythrocytes was significantly lower (p=0.018) in the pre-surgery phase (Fig. 13D) with a median of 4.68 x 10^6/µl (range: 4.43 - 5.39 x 10^6/µl) versus a median of 4.92 x 10^6/µl (range: 4.62 - 5.77 x 10^6/µl) after surgical treatment (Table 4).

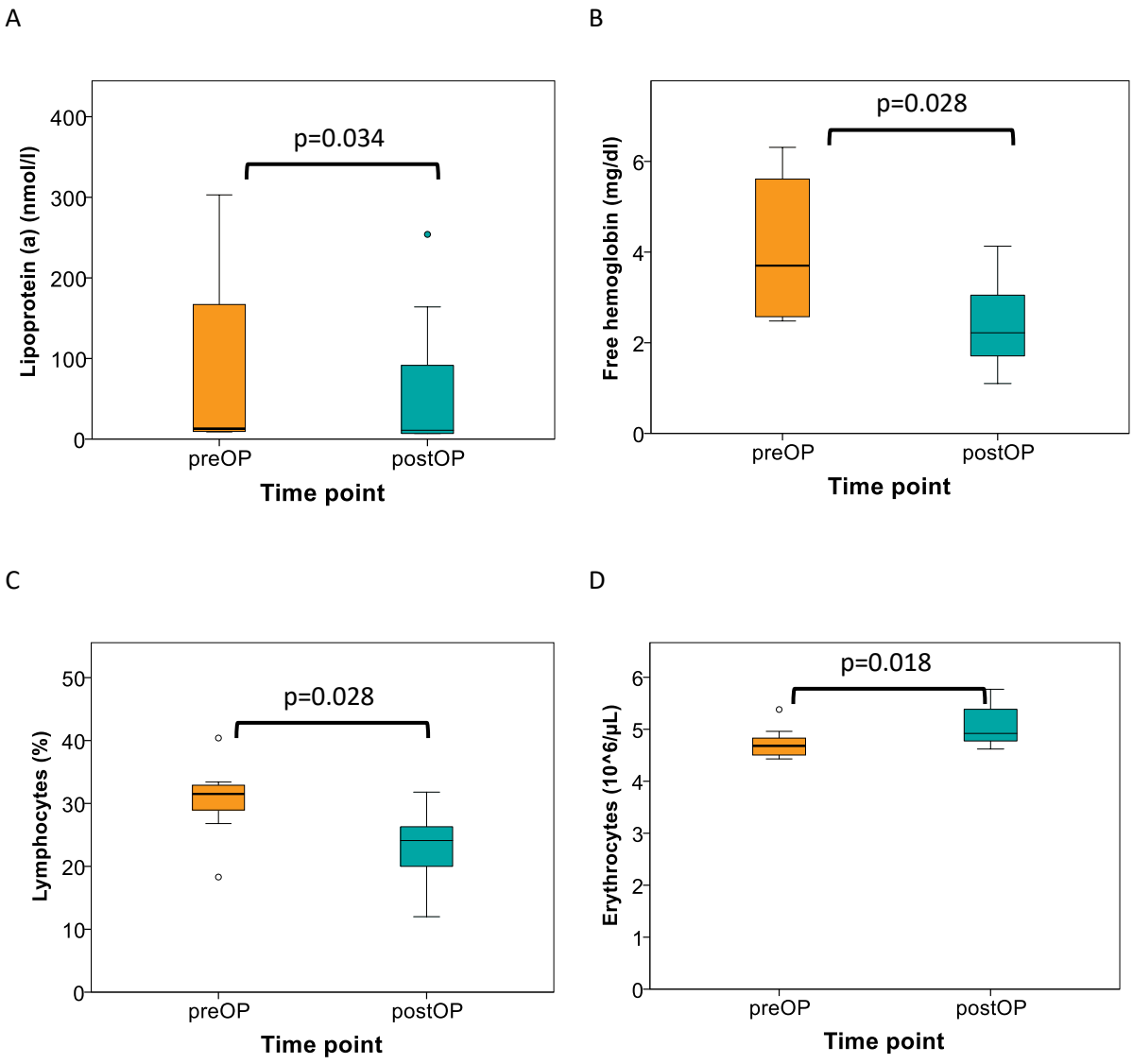

Figure 13: Parameters determined by routine laboratory blood analysis in AAA patients pre (preOP) and post-surgery (postOP).

The boxplots illustrate the distribution of A) lipoprotein (a) levels, B) free hemoglobin levels, C) the percentage of lymphocytes and D) number of erythrocytes in pre and postoperative blood samples of aneurysm patients.

Parameter	preOP	postOP	p-value	N
	Median (min-max)	Median (min-max)		
Lipoprotein (a) (nmol/l)	13.0 (9.0-303.0)	11.0 (7.0-254.0)	**0.034**	7
Free hemoglobin (mg/dl)	3.70 (2.48-6.31)	2.22 (1.10-4.13)	**0.028**	7
Lymphocytes (%)	31.5 (18.3-40.4)	24.1 (12.0-31.8)	**0.028**	7
Erythrocytes (10^6/µl)	4.68 (4.43-5.38)	4.92 (4.62-5.77)	**0.018**	7
Platelets (10^3/µl)	170.0 (71.0-252.0)	215.0 (142.0-287.0)	0.091	7
Leukocytes (10^3/µl)	6.2 (4.1-9.9)	6.0 (4.3-11.8)	0.735	7
Monocytes (%)	11.2 (6.4-13.6)	9.5 (6.1-13.9)	0.463	7
Neutrophils (%)	57.85 (53.00-69.20)	65.30 (56.30-76.90)	0.172	7
Mean thrombocyte volume	10.3 (8.5-11.3)	10.5 (8.8-11.4)	0.497	7
Activated partial thromboplastin time (s)	37.8 (30.5-45.0)	36.8 (32.1-39.2)	0.237	7
Fibrinogen (mg/dl)	279.0 (248.0-560.0)	336.0 (248.0-519.0)	0.917	7
D-dimer (µg/ml)	1.095 (0.390-2.950)	1.420 (0.680-3.220)	0.753	7
Albumin (g/l)	44.7 (39.7-47.5)	44.1 (43.0-48.2)	1.000	7
C-reactive protein (mg/dl)	0.16 (0.03-1.12)	0.18 (0.03-1.83)	0.400	7
Cholesterol total (mg/dl)	152.0 (110.0-197.0)	159.0 (108.0-194.0)	0.735	7
Low density lipoprotein (mg/dl)	74.8 (32.2-117.4)	55.6 (40.2-138.4)	0.499	7
Cholesterol/High density lipoprotein ratio	3.5 (2.4-4.3)	3.0 (2.4-5.0)	0.753	7
High density lipoprotein (mg/dl)	43.0 (36.0-61.0)	45.0 (35.0-62.0)	0.865	7
Triglycerides (mg/dl)	99.0 (63.0-399.0)	120.0 (77.0-237.0)	0.735	7
Urea (mg/dl)	20.8 (15.5-24.9)	24.7 (16.2-28.4)	0.091	7
Creatinine (mg/dl)	1.00 (0.82-1.74)	1.29 (0.79-1.61)	1.000	7
Alpha amylase (u/l)	91.0 (43.0-146.0)	106.0 (63.0-134.0)	0.735	7
25-Hydroxyvitamin D (nmol/l)	42.1 (13.9-90.1)	76.0 (22.5-89.1)	0.176	7

Table 4: Routine laboratory parameters in AAA patients before (preOP) and after surgery (postOP).

5.1.1.4. Correlation of parameters

The pre- and postoperative data sets of the explorative and routine laboratory parameters were investigated for positive or negative correlations.

Plasma levels of DNA-histone complexes, MPO and citH3 concentrations correlated positively and significantly (Table 5). To be specific, the most notable positive and significant correlations were obtained between DNA-histone complexes and citH3 protein (R=0.732, p=0.003) (Fig. 14A), DNA-histone complexes and MPO protein (R=0.626, p=0.017) (Fig. 14B), as well as between citH3 protein and MPO protein (R=0.868, p<0.001) (Fig. 14C, Table 5).

Parameter 1	Parameter 2	Rho	p-value	N
DNA–histone (RU)	CitH3 (ng/ml)	0.732	**0.003**	14
DNA–histone (RU)	MPO (ng/ml)	0.626	**0.017**	14
CitH3 (ng/ml)	MPO (ng/ml)	0.868	**<0.001**	14

Table 5: Correlation of explorative parameters in AAA patients.

Abbreviations. MPO, myeloperoxidase. citH3, citrullinated histone 3. RU, relative unites.

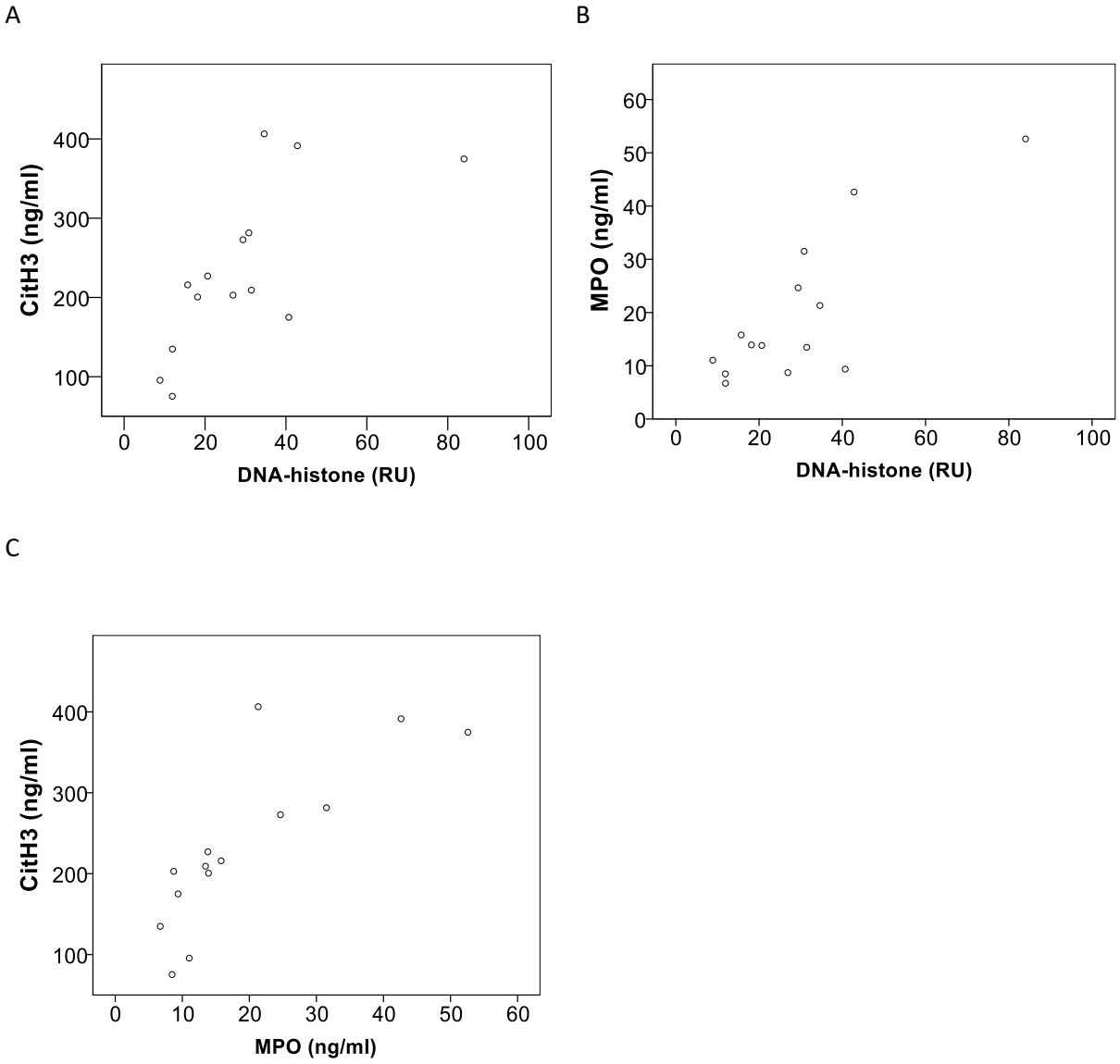

Figure 14: Correlations of explorative parameters in AAA patients.

The scatter grams illustrate the correlation of A) DNA-histone complexes and citH3 protein, B) DNA-histone complexes and MPO protein and C) MPO protein and citH3 protein in pre- and post-surgery plasma samples of AAA patients. Abbreviations. MPO, myeloperoxidase. citH3, citrullinated histone 3.

As outlined in section 4.1.2.2., the analysis of common laboratory parameters, used to evaluate AAA patient comorbidities, showed that lipoprotein (a) and free hemoglobin blood levels were significantly higher pre than post-surgical aneurysm repair. It was tested whether lipoprotein (a) or free hemoglobin correlate with the explorative parameters, determined in this study (Table 6). In fact, a positive and significant correlation was found between lipoprotein (a) and MPO protein (R=0.572, p=0.032) (Fig. 15A) and a trend between the percentage of lymphocytes and DNA-histone complexes (R=0.521, p=0.056) (Fig. 15B). There were no correlations between lipoprotein (a) blood concentration, level of free hemoglobin, percentage of lymphocytes or number of erythrocytes per µl blood with other explorative parameters (Table 6).

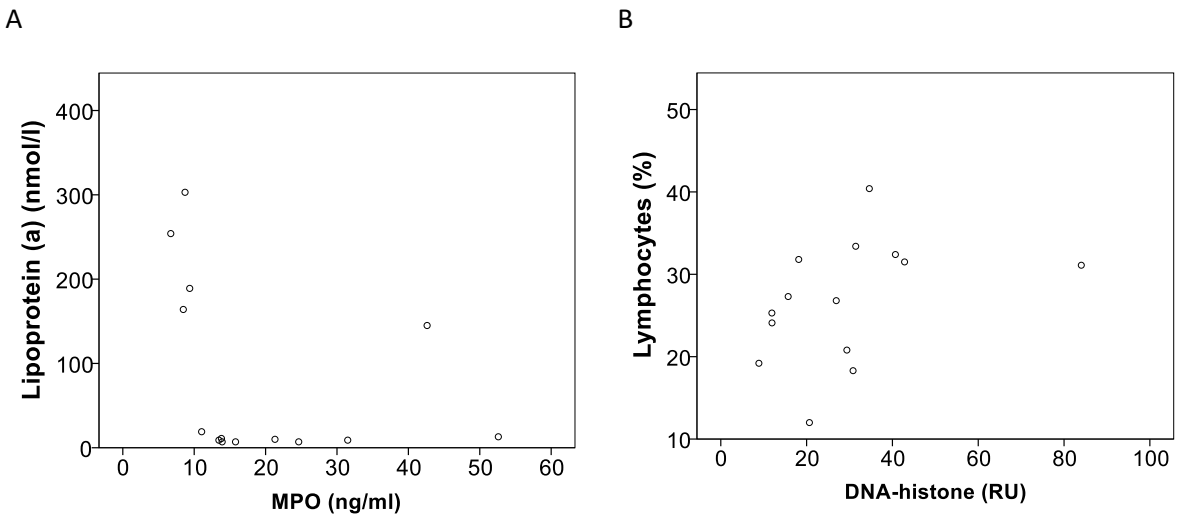

Figure 14: Correlations of explorative and routine laboratory parameters in AAA patients. The scatter diagrams illustrate the correlation of A) MPO protein and lipoprotein (a), B) DNA-histone complexes and percentage of lymphocytes in blood of AAA patients collected before and after surgical repair. Abbreviations. MPO, myeloperoxidase. RU, relative units.

Parameter 1	Parameter 2	Rho	p-value	N
DNA–histone (RU)	Lipoprotein (a) (nmol/l)	-0.027	0.928	14
DNA–histone (RU)	Free hemoglobin (mg/dl)	0.030	0.296	14
DNA–histone (RU)	Lymphocytes (%)	0.521	**0.056**	14
DNA–histone (RU)	Erythrocytes (10^6/µl)	-0.323	0.260	14
CitH3 (ng/ml)	Lipoprotein (a) (nmol/l)	-0.387	0.172	14
CitH3 (ng/ml)	Free hemoglobin (mg/dl)	0.301	0.296	14
CitH3 (ng/ml)	Lymphocytes (%)	0.196	0.503	14
CitH3 (ng/ml)	Erythrocytes (10^6/µl)	-0.248	0.392	14
MPO (ng/ml)	Lipoprotein (a) (nmol/l)	-0.572	**0.032**	14
MPO (ng/ml)	Free hemoglobin (mg/dl)	0.051	0.864	14
MPO (ng/ml)	Lymphocytes (%)	0.099	0.737	14
MPO (ng/ml)	Erythrocytes (10^6/µl)	0.095	0.748	14

Table 6: Correlation of explorative and routine laboratory parameters which differed significantly in AAA patients pre/post surgery.
Abbreviations. MPO, myeloperoxidase. citH3, citrullinated histone 3. RU, relative unites.

5.1.2. Monitoring Analysis

5.1.2.1. Patient Demographics

The baseline characteristics of 5 AAA patients who were monitored with serial blood analyses are presented in Table 7.

All AAA patients in this study were men which reflects their elevated risk for this disease (see section 2.3. The age within this group ranged from 66 to 85 with a median at 73 years. The body mass index varied between 27.73 and 37.04 with a median of 30.93. Eighty % of the patients had a positive smoking status. The pack years showed a wide range from 0 to 50 with a median at 20. Forty % had smoked in their past and 40% were current smokers. Twenty % suffered from chronic obstructive pulmonary disease. Concerning comorbidities associated with cardiovascular disease, 60% of the patients suffered from hypertension, 60% from hyperlipidemia, 60% from coronary artery disease, 20 % from diabetes, and 60% had experienced myocardial infarction or stroke.

Parameter	N	(%)	Median	Min-Max
Age (years)	5		72.86	65.72-84.88
Body Mass Index	5		30.93	27.73-37.04
Pack years	5		20	0-50
Time between blood analyses (months)	9		6.0	5.1-9.1
Time between CT analyses (months)	9		6.0	4.5-10.2
AAA progression				
slow	5	56		
fast	4	44		
Gender (male)	5	100		
Smoker Status				
never	1	20		
current	2	40		
past	2	40		
Hypertension	3	60		
Hyperlipidemia	3	60		
Coronary artery disease	3	60		
Myocardial infarction	2	40		
Stroke	1	20		
Diabetes mellitus	1	20		
COPD	1	20		

Table 7: Demographics of AAA patients included in monitoring analysis.
Abbreviations: COPD, chronic obstructive pulmonary disease. CT, computer tomography. AAA, abdominal aortic aneurysm.

5.1.2.2. Explorative Parameters

As described in the methods 4.1.3.1. - 4.1.3.4., DNA-histone complexes, citrullinated histone 3 protein, myeloperoxidase protein and MPO-histone complexes were measured by ELISA, as seen in Table 8. The maximum diameter of the aneurysm was determined via computed tomography angiography. CTA and blood measurements were conducted every six months. Based on 5 AAA patients, nine 6-month monitoring periods were performed.

Overall, the aortic diameter significantly increased in AAA monitoring patients over time. At the first measurement the median diameter was 53.9 mm (36.7 mm to 62.8 mm) while 6 months later the median diameter measured 56.5 mm (38.2 mm to 64.3 mm, p=0.007). In contrast, the concentration of MPO-histone protein complexes decreased significantly during the monitoring period. At the first time point a median of 15.5 RU (6.3 RU to 20.8 RU) and at the second time point a median of 12.2 RU (6.3 RU to 20.3 RU; p=0.008) was determined. The other explorative variables did not differ significantly between time points.

Parameter	Time point (1)	Time point (2)	Difference	p-value	N
	Median (min-max)	Median (min-max)			
AAA diameter (mm)	53.9 (36.7-62.8)	56.5 (38.2-64.3)	1.5 (0.7-6.4)	**0.007**	9
DNA–histone (RU)	11.8 (4.8-18.0)	11.8 (5.6-19.4)	0.3 (-6.1-7.7)	0.401	9
CitH3 (ng/ml)	32.8 (21.1-138.38)	45.3 (19.5-184.8)	1.7 (-22.9-18.1)	0.594	9
MPO-histone (RU)	15.5 (6.3-20.8)	12.2 (6.3-20.3)	-0.4 (-4.5-3.1)	**0.008**	9
MPO (ng/ml)	58.9 (9.3-235.3)	128.2 (9.3-249.3)	0.3(-66.4-78.0)	0.374	9

Table 8: Explorative parameters in AAA monitoring.
Abbreviations. MPO, myeloperoxidase. citH3, citrullinated histone 3. AAA, abdominal aortic aneurysm. RU, relative unites.

5.1.2.3. Laboratory parameters

Apart from comparing the explorative parameters for NETosis between the two time points, common laboratory parameters were of interest to detect potential co-morbidities associated with AAA progression.

There was no significant difference between the two time points with regard to levels of free hemoglobin, lymphocytes, erythrocytes, monocytes, leukocytes, neutrophils, platelets mean thrombocyte volume, pancreatic amylase, alpha amylase, c-reactive protein, high density lipoprotein, total cholesterol, triglycerides, albumin, urea, creatinine, D-dimer and activated partial thromboplastin time. However, at the later time point of investigation concentrations of 24-hydroxyvitamin D were elevated (p=0.051), while fibrinogen levels (p=0.051), low density lipoprotein levels (p=0.028), and the cholesterol/high density lipoprotein ratio (p=0.015) were lowered (Table 9).

At time point one 24-hydroxyvitamin D levels were at a median of 50.3 nmol/l (24.8 nmol/l to 101.0 nmol/l) whereas the samples at time point two displayed a median of 75.0 nmol/l (24.8 nmol/l to 115.0 nmol/l). Fibrinogen showed a median of 414.0 mg/dl (344.0 mg/dl to 648.0 mg/dl) at time point one while the follow-up samples had a median at 357.0 mg/dl (181.0 mg/dl to 421.0 mg/dl). Low density lipoprotein showed a median of 92.8 mg/dl (36.6 mg/dl to 181.0 mg/dl) at time point one while in the follow-up samples the median was at 74.4 mg/dl (36.6 mg/dl to 124.8 mg/dl). The cholesterol/high density lipoprotein ratio showed a median of 5.0 (3.5 to 7.3) at the first time point and 3.8 (3.0 to 5.1) at the second time point (Table 9).

Parameter	Time point (1)	Time point (2)	Difference	p-value	N
	Median (min-max)	Median (min-max)	Median (min-max)		
Low density lipoprotein (mg/dl)	92.8 (36.6-181.0)	74.4 (36.6-124.8)	-10.7 (-80.2-3.2)	**0.028**	9
Cholesterol/High density lipoprotein ratio	5.0 (3.5-7.3)	3.8 (3.0-5.1)	-1.1 (-2.2-0.3)	**0.015**	9
Erythrocytes (10^6/µl)	4.68 (4.22-7.58)	4.64 (4.28-6.92)	-0.18 (-2.91-0.42)	0.286	9
Platelets (10^3/µl)	146 (33-209)	179 (131-213)	17 (-22-100)	0.139	9
Leukocytes (10^3/µl)	7.7 (4.1-10.3)	7.7 (6.4-14.3)	0.5 (-1.3-4.5)	0.286	9
Neutrophils (10^3/µl)	4.6 (3.1-7.6)	5.7 (3.9-11.3)	0.2 (-0.7-4.1)	0.515	9
Lymphocytes (%)	23 (10.2-35.3)	23.0 (13.6-35.3)	-1.2 (-6.3-11.2)	0.998	9
Monocytes (%)	5.9 (3.6-14.2)	6.2 (4.0-11.2)	-0.1 (-4.3-3.9)	0.859	9
Neutrophils (%)	70.9 (60.2-79.6)	70.9 (60.2-79.3)	-0.2 (-8.7-8.4)	0.575	9
C-reactive protein (mg/dl)	0.48 (0.2-13.9)	0.22 (0.15-1.46)	-0.12 (-13.76-0.92)	0.477	9
Mean thrombocyte volume	10.4 (8.8-10.9)	10.5 (9.3-11.4)	0.1 (-0.2-0.5)	0.202	7
Free hemoglobin (mg/dl)	3.1 (1.8-4.3)	3.4 (1.6-15.0)	0.9 (-0.8-11.7)	0.123	8
Antithrombin III (%)	96 (91-116)	96 (87-113)	-2.5 (-3-2)	0.194	4
Activated partial thromboplastin time (s)	3.55 (30-37)	33.5 (31.7-41.1)	1.0 (-2.5-4.1)	0.440	9
Fibrinogen (mg/dl)	414.0 (344.0-648.0)	357.0 (181.0-421.0)	-49.0 (-434.0-13.0)	0.051	9
D-dimer (µg/ml)	1.32 (0.6-2.37)	1.47 (0.63-2.27)	-0.06 (-0.28-0.64)	1.000	4
Cholesterol total (mg/dl)	174.0 (107.0-270.0)	172.0 (91.0-215.0)	-24.0 (-124.0-40.0)	0.192	9
High density lipoprotein (mg/dl)	37.0 (25.0-48.0)	38.0 (18.0-63.0)	5.0 (-14.0-33.0)	0.262	9
Triglycerides (mg/dl)	241 (88-546)	215 (106-250)	-19 (-359-47)	0.123	9
Albumin (g/l)	45.5 (38.2-49.0)	45.5 (40.0-49.0)	-0.2 (-4.7-7.2)	0.944	9
Urea (mg/dl)	13.6 (11.7-26.7)	15.3 (11.4-28.5)	1.3 (-10.1-12.3)	0.722	9
Creatinine (mg/dl)	1.04 (0.66-1.64)	0.93 (0.66-1.87)	0.00 (-0.55-0.34)	1.000	9
Pancreatic amylase (u/l)	15.5 (15-30)	15.5 (14-21)	-1 (-9-1)	0.257	4
Alpha amylase (u/l)	33.0 (21-54)	33 (21-101)	0.0 (-21-60)	0.833	9
25-Hydroxyvitamin D (nmol/l)	50.3 (24.8-101.0)	75.0 (24.8-115.0)	9.4 (-4.7-64.7)	0.051	9

Table 9: Clinical parameters in AAA patient monitoring.

5.1.2.4. Prognostic Marker Evaluation for AAA Progression

It was then assessed whether any of the investigated parameters at time point 1 could predict aneurysm growth (i.e. the difference in maximal aortic diameter) over the next 6 months. The analysis of common laboratory parameters showed that baseline levels of erythrocytes and high density lipoprotein levels were significantly correlated with AAA growth (Table 10). In fact, the difference in AAA diameter (between time point 2 and 1) correlated positively with the number of erythrocytes (R=0.712, p=0.031; Fig. 16A) and negatively with high density lipoprotein blood concentrations (R=-0.681, p=0.043; Fig. 16B).

There were no significant correlations between any of the other routine laboratory parameters and AAA progression. However, blood leukocytes, albumin and creatinine showed coefficients (rho) higher than 0.4 which is generally qualified as moderate correlation. When patients and monitoring periods were grouped into slow (<2 mm/6 months) and fast (≥2 mm/6 months) aneurysm growth, only erythrocytes and albumin showed a trend towards higher levels at baseline in the fast progressors (Table 10).

Regarding the explorative neutrophil-related parameters a negative correlation between citH3 and AAA growth (R=-0.729, p=0.026*;* Fig. 16C) was found, and slow/fast progressors differed in their citH3 baseline values (p=0.050).

Parameter	N	Rho (correlation)	p-value (correlation)	p-value (slow/fast progression)
Erythrocytes (10^6/µl)	9	0.712	**0.031**	0.086
High density lipoprotein (mg/dl)	9	-0.681	**0.043**	0.268
Leukocytes (10^3/µl)	9	0.644	0.061	0.221
Albumin (g/l)	9	0.533	0.122	0.065
Creatinine (mg/dl)	9	-0.424	0.256	0.086
CitH3 (ng/ml)	9	-0.729	**0.026**	0.050
Mean thrombocyte volume	12	0.736	**0.006**	
Platelets (10^3/µl)	14	0.688	**0.007**	
Activated partial thromboplastin time (s)	14	0.578	**0.030**	
Low density lipoprotein (mg/dl)	14	-0.490	0.075	
DNA–histone (RU)	14	-0.499	0.069	

Table 10: Prognostic marker value of laboratory parameters for AAA progression.
Abbreviations. citH3, citrullinated histone 3. RU, relative unites.

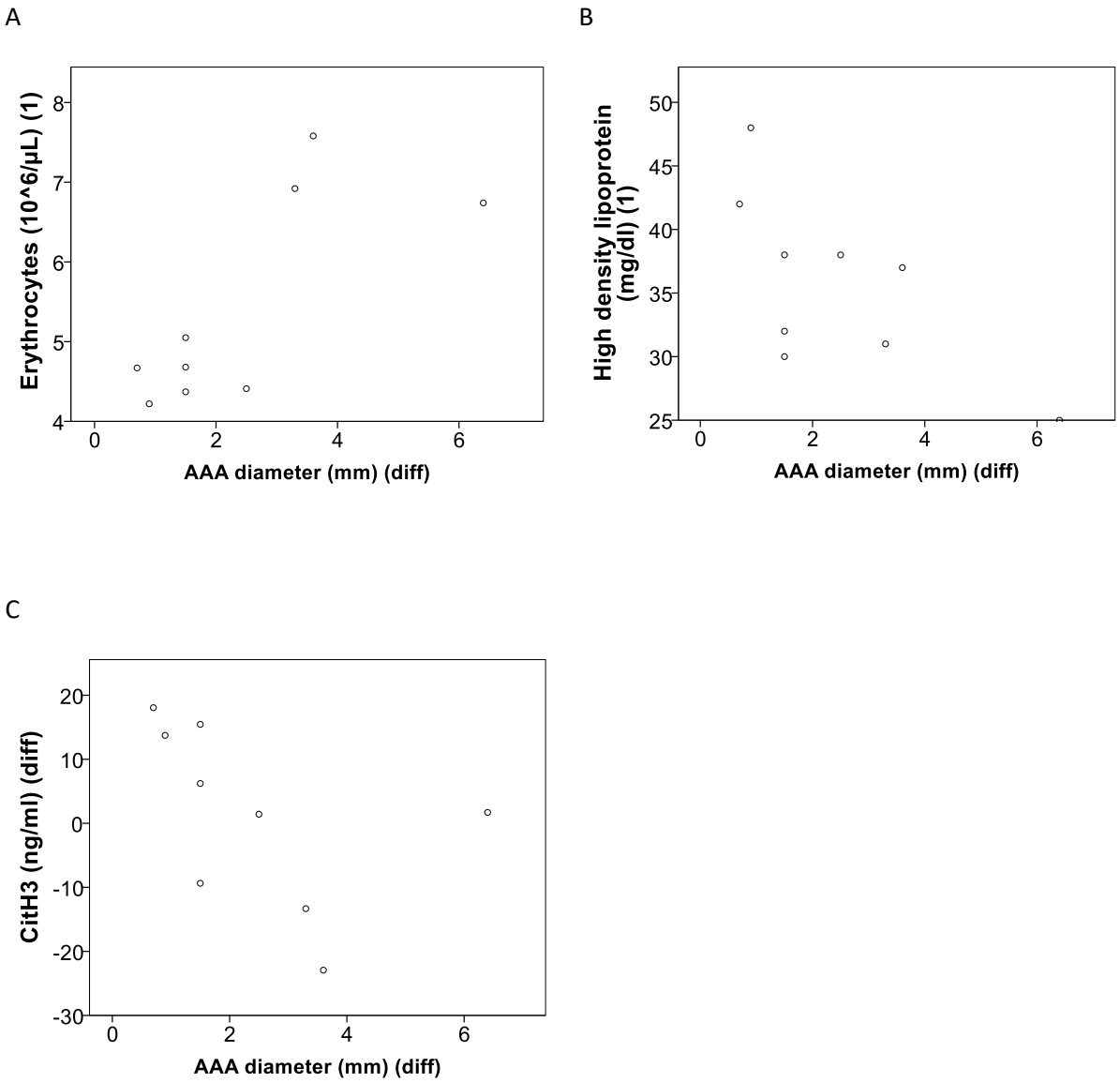

Figure 15: Correlations of blood parameters and AAA growth.
The scatter diagrams illustrate the correlation between A) erythrocytes at baseline and subsequent AAA diameter progression, B) high density lipoprotein and C) citH3 levels at time point 1 and AAA diameter progression over the next 6 months.
Abbreviations. citH3, citrullinated histone 3. AAA, abdominal aortic aneurysm.

Furthermore, we tested for correlations among all explorative and laboratory parameters and the AAA diameter in the collected data set, independent of the time point of investigation.

Analyses revealed significant positive correlations between maximal aortic diameter and the activated partial thromboplastin time (R=0.578, p=0.030, Fig. 17A), mean thrombocyte volume (R=0.736, p=0.006; Fig. 17B) and platelet counts (R=0.688, p=0.007; Fig. 17C). AAA diameter and blood levels of low density lipoprotein (R=-0.490, p=0.075) or DNA-histone complexes (R=-0.499, p=0.069) correlated negatively.

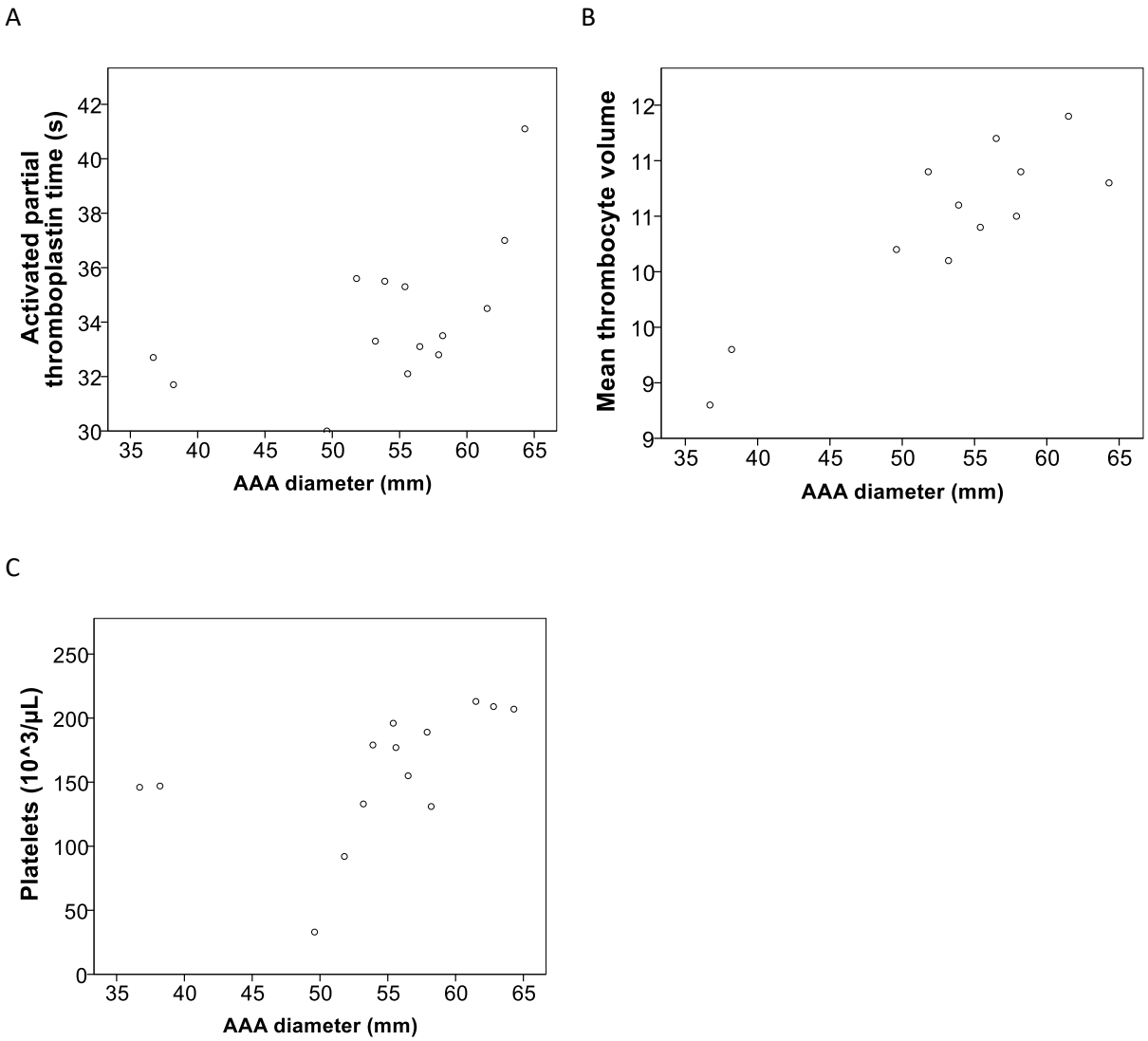

Figure 16: Correlation between AAA diameter and laboratory parameters (irrespective of time point of investigation).

The scatter diagrams illustrate the correlation of AAA diameter and A) activated thromboplastin time, B) mean thrombocyte volume and C) platelets.

Abbreviations. AAA, abdominal aortic aneurysm.

Next, the question was addressed whether there was a correlation between any of the explorative and laboratory parameter values established at the two time points (Table 11).

Significant correlations could be detected between neutrophil concentrations and D-dimer (R=-0.842, p=0.002), creatinine (R=0.576, p=0.031), urea (R=0.605, p=0.022), low density lipoprotein (R=-0.675, p=0.008) and mean thrombocyte volume (R=0.739, p=0.006). Analyses revealed also that citH3 levels correlated significantly with 25-hydroxyvitamin D (R=0.635, p=0.015), creatinine (R=-0.627, p=0.016), urea (R=-0.638, p=0.014) and free hemoglobin (R=0.687, p=0.010). In addition, a significant correlation was determined between MPO and 25-hydroxyvitamine D (R=-0.565, p=0.035), creatinine (R=0.640, p=0.014), urea (R=0.678, p=0.008), low density lipoprotein (R=-0.578, p=0.030) and mean thrombocyte volume (R=0.578, p=0.049). Furthermore, MPO-histone complexes correlated significantly with D-dimer (R=-0.673, p=0.033), 25-hydroxyvitamin D (R=-0.723 p=0.003), creatinine (R=0.625, p=0.017) and urea (R=0.532, p=0.050). Finally, analysis detected a significant correlation between DNA-histone complexes and creatinine (R=-0.819, p<0.001) and urea (R=-0.706, p=0.005).

Parameter 1	Parameter 2	Rho	p-value	N
Neutrophils (10^3/µl)				
	D-dimer (µg/ml)	-0.842	**0.002**	10
	Creatinine (mg/dl)	0.576	**0.031**	14
	Urea (mg/dl)	0.605	**0.022**	14
	Low density lipoprotein (mg/dl)	-0.675	**0.008**	14
	Mean thrombocyte volume	0.739	**0.006**	12
CitH3 (ng/ml)				
	25-Hydroxyvitamin D (nmol/l)	0.635	**0.015**	14
	Creatinine (mg/dl)	-0.627	**0.016**	14
	Urea (mg/dl)	-0.638	**0.014**	14
	Free hemoglobin (mg/dl)	0.687	**0.010**	13
MPO (ng/ml)				
	25-Hydroxyvitamin D (nmol/l)	-0.565	**0.035**	14
	Creatinine (mg/dl)	0.640	**0.014**	14
	Urea (mg/dl)	0.678	**0.008**	14
	Low density lipoprotein (mg/dl)	-0.578	**0.030**	14
	Mean thrombocyte volume	0.578	**0.049**	12
MPO-histone (RU)				
	D-dimer (µg/ml)	-0.673	**0.033**	10
	25-Hydroxyvitamin D (nmol/l)	-0.723	**0.003**	14
	Creatinine (mg/dl)	0.625	**0.017**	14
	Urea (mg/dl)	0.532	**0.050**	14
DNA–histone (RU)				
	Creatinine (mg/dl)	-0.819	**<0.001**	14
	Urea (mg/dl)	-0.706	**0.005**	14

Table 11: Correlations between explorative and clinical parameters in AAA monitoring.
Abbreviations. MPO, myeloperoxidase. citH3, citrullinated histone 3. RU, relative unites.

Regarding potential correlations among the neutrophil-related explorative parameters (Table 12) a significant association between citH3 and neutrophils (R=-0.609, p=0.003), MPO (R=-0.538, p=0.047) and MPO-histone complexes (R=-0.596, p=0.025) was detected. Furthermore, the analysis determined that MPO correlated significantly with neutrophil levels (R=0.723, p=0.003), MPO-histone complexes (R=0.864, p<0.000) and DNA-histone complexes (R=-0.726, p=0.003). Significant correlations were found also between blood concentrations of MPO-histone complexes and neutrophils (R=0.736, p=0.003) and DNA-histone complexes (R=-0.711, p=0.004). Finally, DNA-histone complexes and neutrophils (R=-0.640, p=0.014) and MPO-histone complexes (R=-0.711, p=0.004) were significantly associated with each other.

Parameter 1	Parameter 2	Rho	p-value	N
CitH3 (ng/ml)				
	Neutrophils (10^3/µl)	-0.609	**0.003**	14
	MPO (ng/ml)	-0.538	**0.047**	14
	MPO-histone (RU)	-0.596	**0.025**	14
MPO (ng/ml)				
	Neutrophils (10^3/µl)	0.723	**0.003**	14
	MPO-histone (RU)	0.864	**0.000**	14
	DNA–histone (RU)	-0.726	**0.003**	14
MPO-histone (RU)				
	Neutrophils (10^3/µl)	0.736	**0.003**	14
	DNA–histone (RU)	-0.711	**0.004**	14
DNA–histone (RU)				
	Neutrophils (10^3/µl)	-0.640	**0.014**	14
	MPO-histone (RU)	-0.711	**0.004**	14

Table 12: Correlations among explorative parameters in AAA monitoring.
Abbreviations. MPO, myeloperoxidase. citH3, citrullinated histone 3. RU, relative unites.

5.2. Animal Study

5.2.1. Optimization of DNA Release Assay

Since the aim of AAA mouse studies was to test the therapeutic potential of anti-NET therapy, a simple and reliable assay to screen NET formation in isolated mouse neutrophils was warranted. NET induction in mouse blood is accompanied by an increase in cell-free DNA which can be measured by fluorescent DNA dyes. First, the optimal conditions for the DNA release assay had to be established. For this purpose it was of utmost importance to determine an effective dose of the calcium ionophore A23187 to induce maximal DNA release from neutrophilic granulocytes in vitro.

Mouse blood was drawn from the vena cava and granulocytes were isolated with a commercial neutrophil enrichment kit. A23187 was applied at 0.25 µM, 0.5 µM, 1 µM, 2 µM and 4 µM and DNA release was measured by determining the relative fluorescence units (RFU) during a period of 165 min (Fig. 18). At 120 minutes moderate stimulation of DNA release could be observed at 0.25 µM (9.24 RFU), 0.5 µM (17.48 RFU), and 1 µM (12.49 RFU) A23187 when compared to the untreated control (10.68 RFU). However, A23187 showed a strong stimulatory effect at 2 µM (25.41 RFU at 120 minutes) and at 4 µM (27.20 RFU at 120 minutes).

It was also determined whether 2 mM of GSK484 had an impact on the basal DNA release and could block NET induction. Indeed, the addition of GSK484 reduced NET formation in response to 4 µM A23187 (to 9.27 RFU at 120 min).

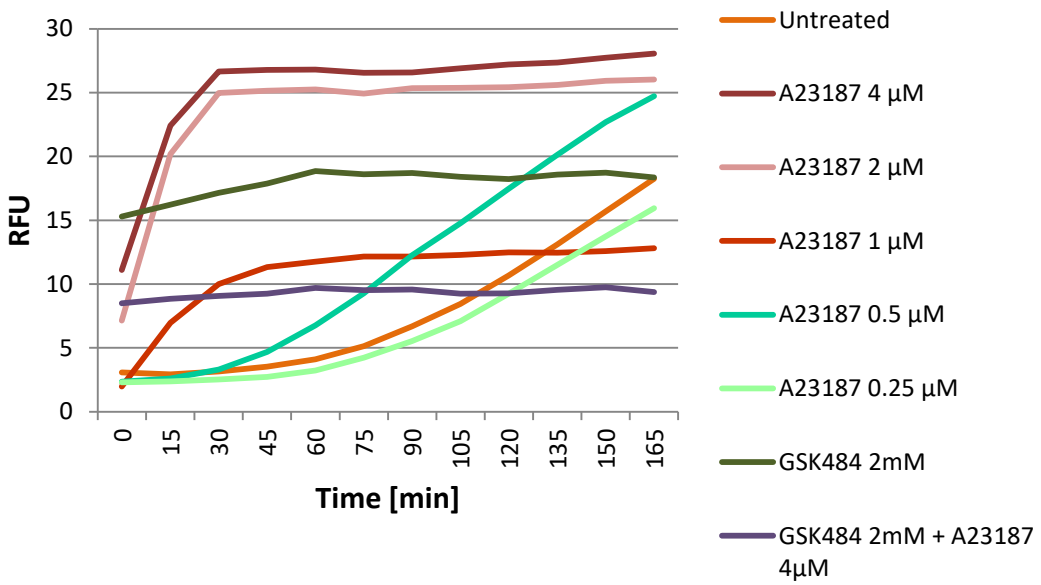

Figure 17: Dose-response to A23187 with regard to NET stimulatory effect on neutrophilic granulocytes.

Blood from five ApoE KO mice was drawn and pooled. Isolated neutrophils were pretreated with NET inhibitor GSK484 for 30 min (where indicated), then stimulated in vitro by A23187 at 0.25 µM, 0.5 µM, 1 µM, 2 µM and 4 µM for 165 minutes. DNA release by NETosis was monitored with Sytox Green incorporation and measurement of relative fluorescent units.

Abbreviations. RFU, relative fluorescent units.

Next, the minimal number of neutrophilic granulocytes per assay was determined, since experimental mouse blood and neutrophil counts are limited. At first, 50.000 or 100.000 cells were added to each 96-well. The cells were treated with 0 or 4 µM of A23187. The results of the DNA release assay showed that there was no considerable difference in background signal between the two cell concentrations in the untreated controls. When stimulated with A23187, the release of DNA was higher (57 RFU at 120 min) when applying 100.000 cells/well than with 50.000 cells/well (39 RFU). However, NET induction was clearly detectable with the lower cell concentration (Fig. 19). As a result, 50.000 cells per well were used for further experimentation.

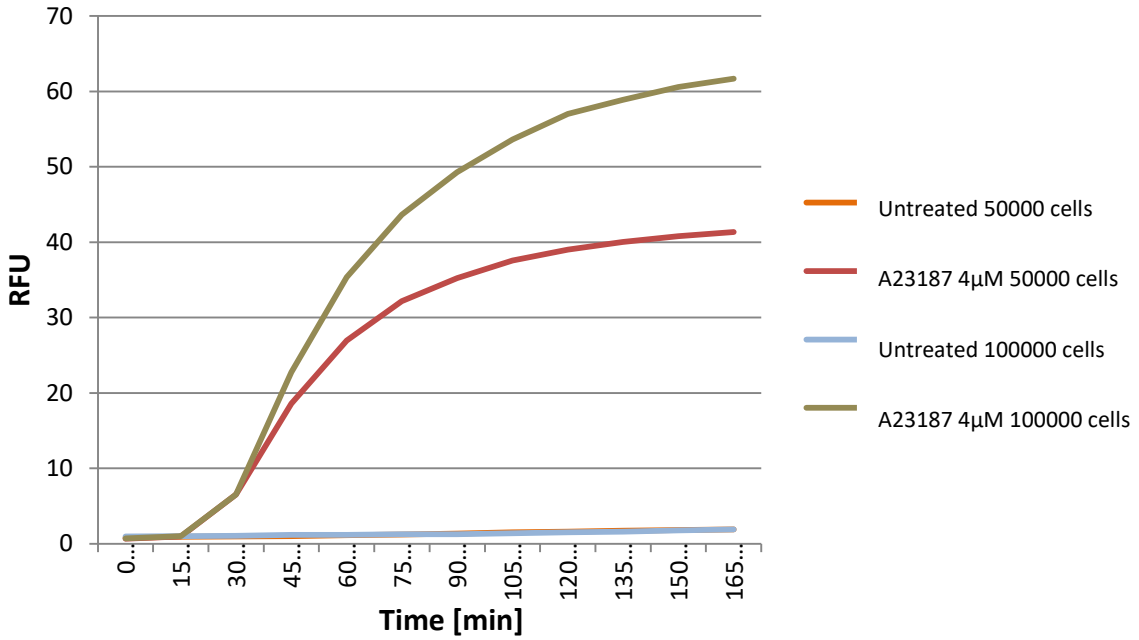

Figure 18: Determination of DNA release when using 50.000 or 100.000 neutrophilic granulocytes per assay.

Three ApoE KO mice were treated with a single intravenous application of 200 µl PBS-/- (as negative control for subsequently conducted in vivo GSK484 administration in toxicity assays). Twenty-four hours later about 800 µl blood were taken from the vena cava inferior for the isolation of neutrophils. The isolated neutrophils were pooled. Either 50.000 or 100.000 neutrophils per well were used. The cells were left untreated or stimulated with 4 µM of A23187 and the DNA release was measured.
Abbreviations. RFU, relative fluorescent units.

Next, it was tested whether ethanol (EtOH) or Hanks' balanced salt solution (HBSS) was the optimal solvent for the NET inhibitor GSK484. In addition, the optimal concentration of GSK484 had to be determined.

At 120 minutes the untreated neutrophilic granulocytes showed nearly no basal DNA release and an RFU value of only 1.62. The stimulatory effect of 4 µM of A23187 on DNA release (39.00 RFU) was as effective as a high dose of 133 µM A23187 (38.10 RFU), indicating saturation (Fig. 20B). This confirmed that 4 µM of A23187 was the optimal concentration to induce DNA release by mouse neutrophils in vitro.

The NET inhibitor GSK484 was initially dissolved in EtOH. Aliquots of the stock were applied to obtain final concentrations of 3.2 µM, 16 µM, 80 µM, 400 µM and 2 mM. After 120 min of neutrophil treatment with GSK484 at 2 mM, the spontaneous DNA release was at 15.62 RFU. To induce DNA release 4 µM of

A23187 were applied which raised the RFU close to 40. However, the combined treatment with 2 mM of GSK484 and A23187 lowered the RFU to 17.36, indicating that the inhibitory properties of GSK484 were strong enough to suppress the A23187-induced DNA release. Lower concentrations of GSK484 led to a considerably weaker inhibition of the basal DNA release, e.g., at 120 minutes the RFU was 31.90 at 3.2 µM of GSK484, 33.32 at 16 µM, and 22.88 at 80 µM (Fig. 20A).

It remains to be elucidated why neutrophil treatment with 400 µM GSK484 and 4 µM of A23187 led to a somewhat higher DNA release (40.25 RFU at 120 minutes) than sole stimulation with 4 µM of A23187 (39.00 RFU at 120 minutes).

Next GSK484 was diluted in HBSS (Fig. 20B) and applied to obtain final assay concentrations of 3.2 µM, 16 µM, 80 µM, 400 µM and 2 mM GSK484. When compared to data obtained with EtOH-diluted GSK484, a somewhat arbitrary effect of this compound on the DNA release was observed at 120 min, i.e., at 3.2 µM of GSK484 the RFU value was 26.91, at 16 µM 25.71 and at 80 µM 27.02. Importantly, it has to be noted that GSK484 precipitated in the HBSS stock.

To conclude, it was decided to use 2 mM of GSK484, dissolved in EtOH, due its strong inhibitory effect on the A23187-induced DNA release. However, ethanol is known to be cytotoxic. As a consequence an ethanol solvent control group was added to the experimental set-up to control for its potential impact.

A

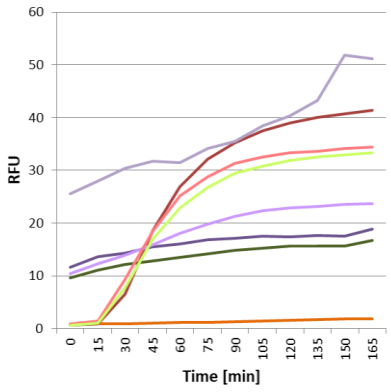

B

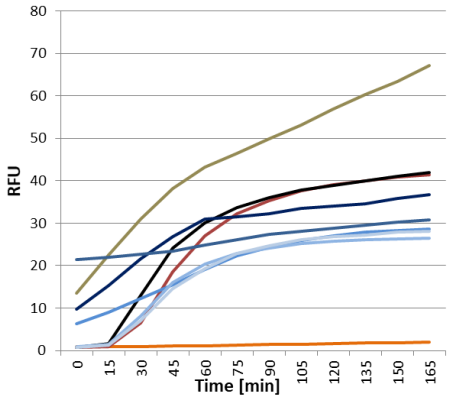

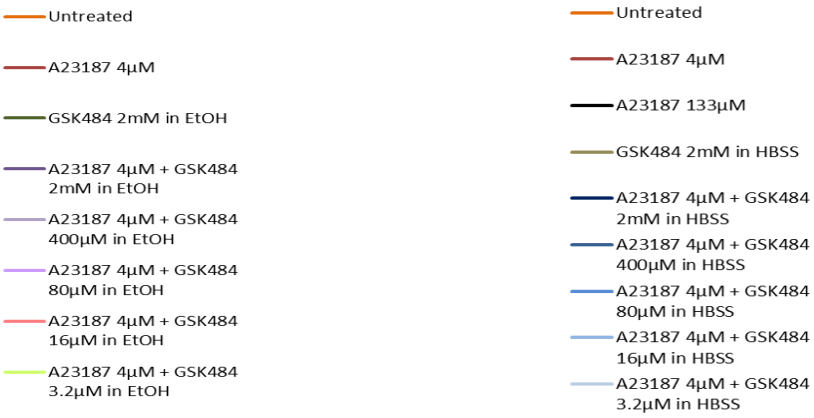

Figure 19: Dose-dependent inhibitory effects of GSK484 on A23187-induced DNA release by mouse neutrophils.

Three ApoE KO mice were treated with a single intravenous application of 200 µl PBS-/- (as negative control for subsequently conducted in vivo GSK484 administration in toxicity assays). Twenty-four hours later about 800 µl blood were drawn from the vena cava inferior for the isolation of neutrophils and isolated cells were pooled. Fifty thousand neutrophils were used per DNA release assay. In A) GSK484 was diluted in EtOH and in B) in HBSS prior to addition to assay wells. The cells were stimulated with 4 µM or 133 µM of A23187 (as indicated) and the DNA release was measured over 165 min.

Abbreviations. RFU, relative fluorescent units. EtOH, ethanol. HBSS, Hank's balanced salt solution.

5.2.2. GSK484 Toxicity and Dose Finding in Vivo

The experience gained by experiments in vitro (see section 5.2.1.), had to be adapted to in vivo conditions for subsequent application in AAA mouse models. In a first approach, 200 µl PBS-/- were injected into the vena jugularis externa of ApoE KO mice in order to establish a control group for a more accurate comparison. After 24 hours blood was taken and DNA release was assayed with isolated mouse neutrophils.

At 120 minutes the RFU of untreated controls was 0.9 and was raised to 39.8 by 4 µM A23187, indicating an approximately 40-fold stimulatory effect of A23187 (Fig. 21). Both, 2 mM of GSK484 and 2 mM of GSK484 plus 4 µM of A23187 led to RFU values around 13. This confirmed that neutrophilic granulocytes, obtained from PBS-treated animals, exhibited NET reactivity in vitro. Furthermore, in vitro

addition of GSK484 again suppressed DNA release effectively. However, it remained to be elucidated why GSK484 treatment alone caused the same level of DN

A release as the combination treatment with A23187.

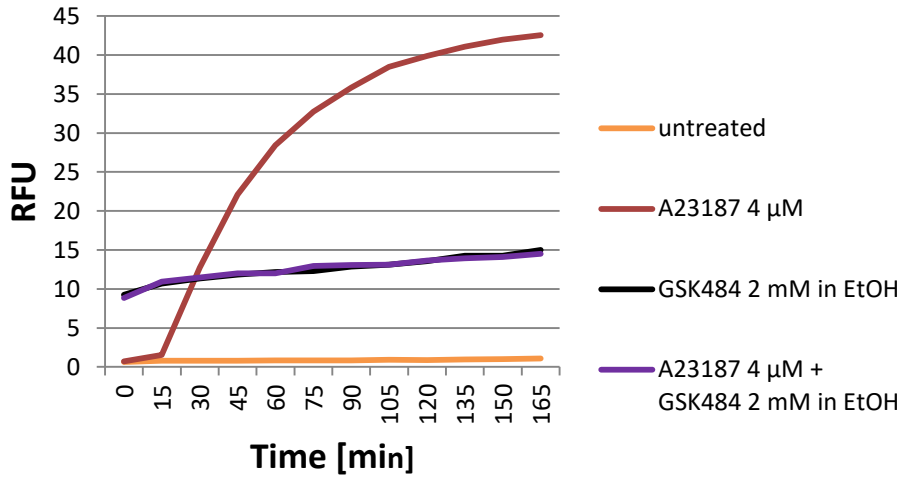

Figure 20: DNA release by neutrophils from PBS treated control mice.
Two-hundred µl PBS-/- were injected into the vena jugularis externa of three ApoE KO mice. Twenty-four hours later about 500 µl blood were drawn from the vena cava inferior for the isolation of neutrophilic granulocytes. Due to lack of neutrophils the blood of the mice was pooled. The experiment was repeated a second time with two ApoE KO mice and blood was pooled. Data from the second experiment are being shown. Each time 50.000 neutrophils per well were used. GSK484 was diluted in EtOH and DNA release was stimulated with 4 µM A23187 over a time course of 165 min. Abbreviations. RFU, relative fluorescent units. EtOH, ethanol.

Next, the optimal in vivo dose of GSK484 and possible adverse effects of this compound had to be determined. To start, the EtOH stock of GSK484 was diluted with 0.9% NaCl to reach 0.2 µg of GSK484 /g mouse body weight in a total volume of 200 µl which were injected into the vena jugularis externa of ApoE KO mice. The veterinarians Anne Kramer and Katharina Tillmann of the local animal experimentation facility were contacted to inspect the animals. Mice showed barely any side effects. They were more active than usual and showed signs of slight abdominal pain. After 24 hours blood was drawn, neutrophils isolated and the DNA release assay was performed.

At 120 minutes cells showed a basal RFU of 2.00, which was raised about 13-fold to 27.25 by 4 µM A23187 (Fig. 22). In comparison to the PBS-treated mice 40-fold stimulatory effect by 4 µM A23187) a reduction in DNA release was detectable (Fig. 21). Adding 2 mM of GSK484 in vitro further suppressed A23187-induced DNA release to 21.59 RFU at 120 minutes. Again, GSK484 exposure in vitro raised the background fluorescence of mouse neutrophils to 12.32 RFU at 120 minutes.

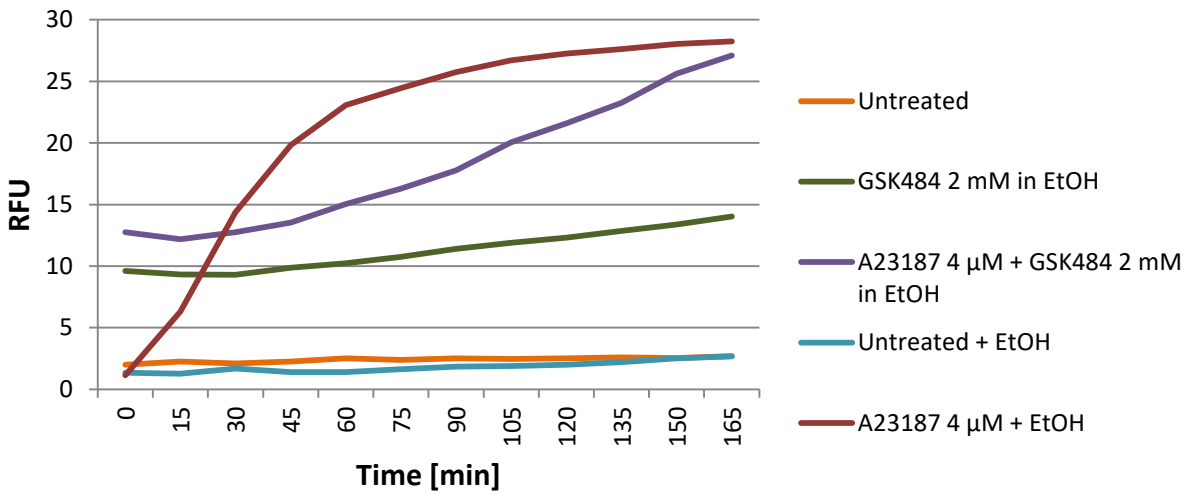

Figure 21: DNA release after in vivo application of GSK484 at 0.2 µg/g body weight.
Injection of GSK484 0.2 µg/g bodyweight was performed into the vena jugularis externa of three ApoE KO mice. 24 hours later about 500 µl blood were drawn from the vena cava inferior for the isolation of neutrophils. Fifty thousand (pooled) neutrophils were used per assay. GSK484 was diluted in EtOH for in vivo and in vitro application. DNA release was stimulated in vitro with 4 µM A23187 over a time course of 165 min.
Abbreviations. RFU, relative fluorescent units. EtOH, ethanol.

As next step, the dose was elevated to 2.0 µg of GSK484/g body weight in order to achieve a more prominent inhibitory effect on the DNA release by NET formation. In addition, the in vitro concentration of A23187 was reduced to 1 and 2 µM in order to lower the magnitude of NET induction in the isolated neutrophils and possibly facilitate the detection of anti-NET effects by in vivo applied GSK484.

Mice were inspected closely after GSK484 administration. Again no side effects, except for increased activity levels and mild abdominal pain, were noted. In the isolated neutrophilic granulocytes the basal RFU value of DNA release was 1.64 at 120 minutes (Fig. 23). A23187 induced NET formation dose-dependently: 25.82 RFU at 1 µM, 32.29 RFU at 2 µM, and 34.33 RFU at 4 µM, indicating a 21-fold elevation. In vitro application of 2 mM GSK484 alone resulted in a slightly higher DNA release (15.28 RFU) than the combination of 2 mM of GSK484 + 2 µM of A23187 (11.06 RFU). Surprisingly, 2.0 µg of GSK484/g body weight showed a weaker inhibitory effect on DNA release, induced by 4 µM of A23187 (21-fold elevated compared to untreated control) than 0.2 µg of GSK484/g body weight (13-fold elevated, compare Fig. 22).

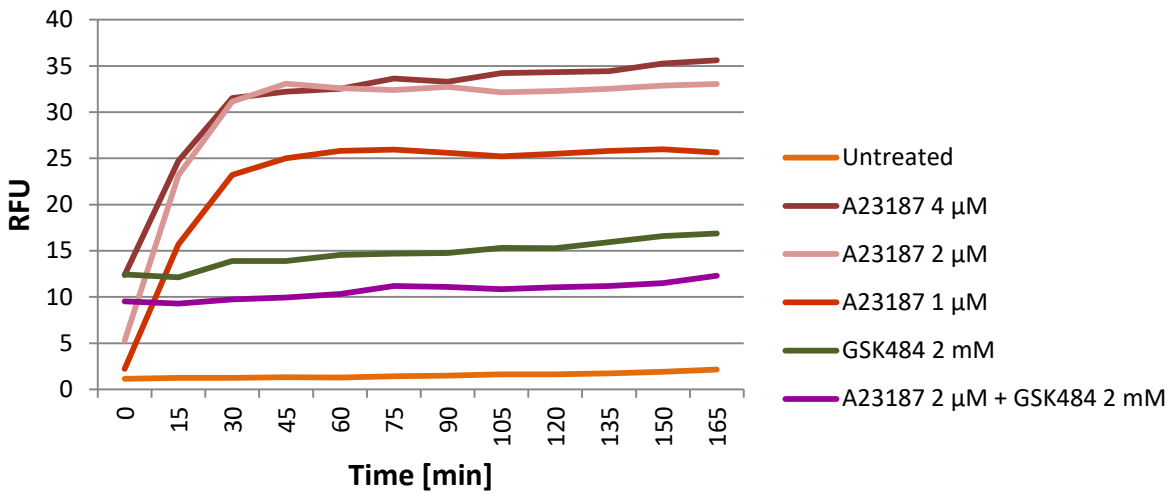

Figure 22: DNA release after in vivo application of GSK484 at 2 µg/g mouse weight.
Injection of 200 µl GSK484 at 2.0 µg/g body weight was performed into the vena jugularis externa of three ApoE KO mice. Twenty-four hours later about 500 µl blood were drawn from the vena cava inferior for the isolation of neutrophilic granulocytes. Mice were evaluated individually. GSK484 was diluted in EtOH for in vivo and in vitro application. DNA release was stimulated in vitro with 1, 2 or 4 µM A23187 over a time course of 165 min. The diagram shows the data of one individual animal.
Abbreviations. RFU, relative fluorescent units.

Finally the highest possible dose of GSK484 (based on solubility in EtOH) was tested in vivo and 20.0 µg of GSK484/g body weight were injected into the vena jugularis externa. The mice again showed barley any side effects. After 24 hours blood was drawn and DNA release was assayed in isolated neutrophilic granulocytes. Cells were only stimulated by 1.5 µM of A23187 due to the assumption that 4 µM was saturating and possibly too strong to detect the in vivo GSK484 inhibitory effects. At 120 minutes the RFU in the untreated cells was 3.4 and in the A23187 stimulated cells 19.9, indicating a 6-fold increased DNA release (Fig. 24). Surprisingly, in vitro addition of 2 mM of GSK484 alone led to a stronger DNA release (49.21 RFU) than 1.5 µM of A23187 or the combination of 2 mM of GSK484 with 1.5 µM of A23187 (RFU 31.01).

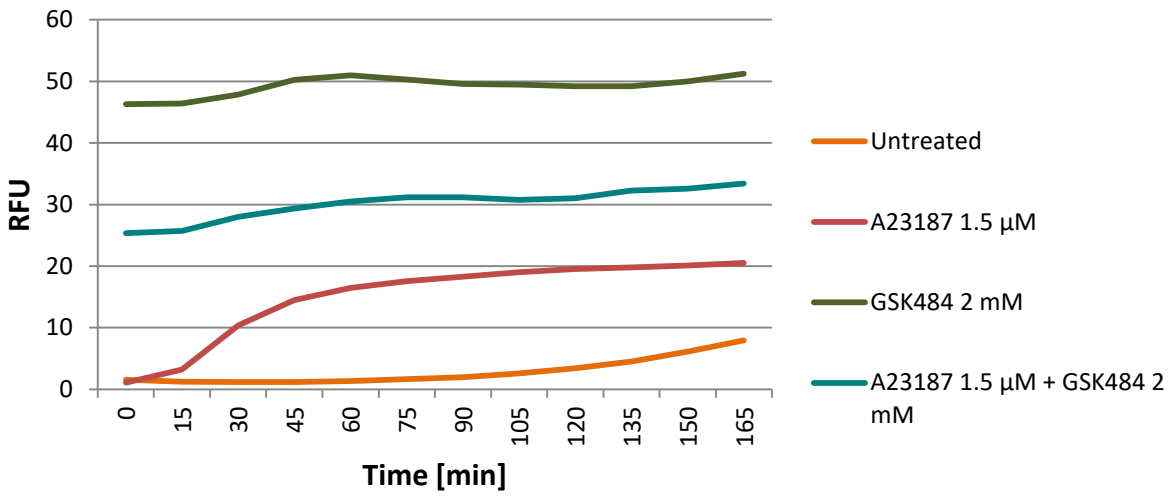

Figure 23: DNA release after in vivo application of GSK484 at 20 µg/g mouse weight. GSK484 was injected at 20.0 µg/g body weight in 200 µl solvent into the vena jugularis externa of three ApoE KO mice. Twenty-four hours later about 900 µl blood were drawn from the vena cava inferior for the isolation of neutrophils. Fifty thousand pooled neutrophilic granulocytes were used per in vitro DNA release assay. GSK484 was diluted in EtOH for application in vitro and in vivo. DNA release by isolated neutrophils was stimulated with 1.5 µM A23187 over a time course of 165 min. Abbreviations. RFU, relative fluorescent units.

At the time of experimentation, data on the pharmacokinetics of this compound in mice were lacking. Therefore, it was tested whether the time period of 24 hours was too long for the inhibitor to still show a sufficient pharmacological effect.

GSK484 was injected into the vena jugularis externa of three ApoE KO mice at a dose of 2.0 µg/g body weight. In addition, a new control group with saline injection (N=2) had to be generated. Blood samples were drawn already after 4 hours, mouse neutrophils were isolated. In the DNA release assay 2 µM of A23187 were applied (Fig. 25).

At 120 minutes the untreated neutrophilic granulocytes of the new control group showed a similar DNA release (RFU 4.57) as the GSK484-pretreated group (6.26 RFU). However, when 2 µM of A23187 were applied in vitro, a stronger stimulatory effect was observed in the cells isolated from GSK484-pretreated mice (27.57) than from control animals (22.63 RFU). Based on these results it was suspected that (the reversible PAD4 inhibitor) GSK484 may be washed out during the isolation of the neutrophilic granulocytes from mouse blood and hence be ineffective during in vitro experiments.

At 120 minutes the untreated cells of the GSK484-pretreated animals showed an RFU value of 6.26, which was raised to 27.57 RFU by 2 µM of A23187, indicating an about 4-fold increased DNA release. In vitro treatment of GSK484 was able to further lower the baseline RFU to 3.43. However, it remains unclear why a higher RFU of 37.19 was obtained by the combination of A23187 and GSK484 treatment as compared to A23187 alone.

A

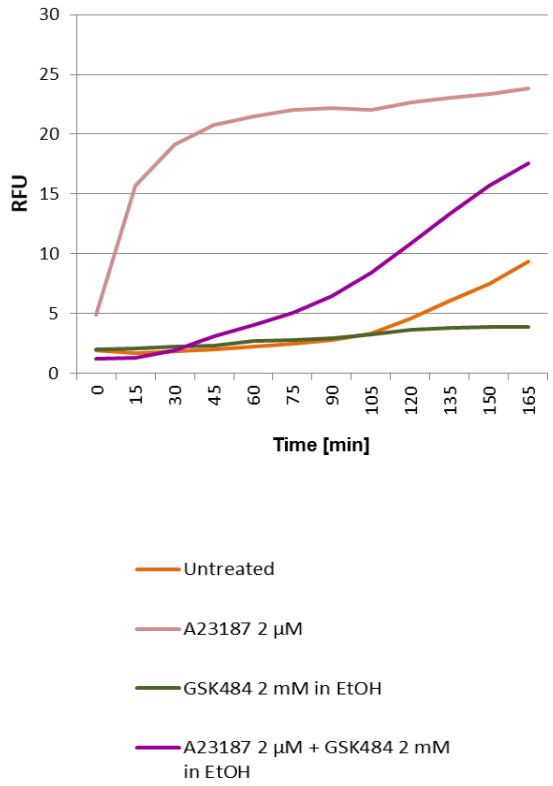

B

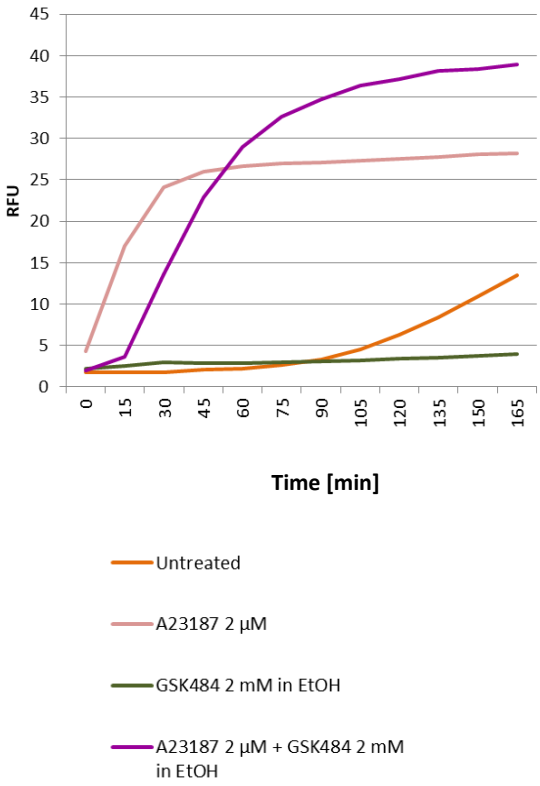

Figure 24: DNA release based on GSK484 injection at 2.0 µg/g mouse weight and neutrophil isolation after four hours.

A) 200 µl PBS-/- were injected into the vena jugularis externa of two ApoE KO mice, B) 2.0 µg GSK484/g body weight were injected into the vena jugularis externa of three ApoE KO mice. Four hours later about 600 µl of blood were drawn from the vena cava inferior for the isolation of neutrophils. Fifty thousand pooled neutrophils were used per assay. GSK484 was diluted in EtOH. DNA release by isolated neutrophils was stimulated with 2 µM A23187 over a time course of 165 min. Abbreviations. RFU, relative fluorescent units. EtOH, ethanol.

The following table (Table 13) gives an overview on the DNA release of neutrophilic granulocytes obtained from ApoE KO mice depending on the different treatments in vivo as well as in vitro.

	In vivo treatment					
	Control (N=2)*	**GSK 2.0** (N=4)*	**Control** (N=5)*	**GSK 0.2** (N=3)*	**GSK 2.0** (N=3)	**GSK 20.0** (N=3)*
In vitro treatment	**After 4 Hours**		**After 24 Hours**			
Untreated	4.57 (single measure ment)	5.43 ±2.08	1.53 ±0.35	2.23 ±0.36	1.97 ±0.54	3.40 ±1.17
A23187 1 µM					26.33 ±5.09	
A23187 1.5 µM						19.54 ±4.54
A23187 2 µM	22.63 (single measure ment)	28.13 ±4.74			23.79 ±12.11	
A23187 4 µM			39.25 ±7.65	27.25 (single measurement)	27.72 ±9.35	
A23187 133 µM			38.90 2.36			
GSK484 2 mM	3.66 (single measure ment)	3.77 ±1.93	14.93 ±2.14	12.32 ±1.94	9.90 ±6.10	49.21 ±4.65
GSK484 2 mM+ A23187 4 µM			15.51 ±2.26	21.60 ±18.10	10.63 ±3.47	
GSK484 2 mM+ A23187 1.5 µM						31.01 ±1.47
GSK484 2 mM+ A23187 2 µM	10.84 ±4.66	37.19 ±3.59				

Table 13: Overview on DNA release assay results.

ApoE KO mice were injected either with 200 µl PBS-/- or GSK484 at the following concentrations: 0.2, 2.0 µg/g or 20.0 µg GSK484/g body weight. Depending on the setting blood was taken after 4 or 24 hours. The isolation of neutrophilic granulocytes and the DNA release assay were performed as described in Methods. Means ± standard deviation were calculated for RFU values obtained at 120 minutes. Results obtained under the standard conditions of 4 µM A23187 and 2 mM GSK484 are highlighted in blue color.

* after neutrophil isolation cells of the individual mice were pooled prior to assay initiation

Abbreviations. GSK, GSK484.

In conclusion, it was decided not to proceed further with the isolation of neutrophilic granulocytes and DNA release assays to monitor in vivo effects on mouse neutrophils and their NETosis potential. It was assumed that the long isolation process of >6 hours, involving numerous washing steps, may lead to inactivation and removal of GSK484 from mouse blood and mouse neutrophils. In addition, the half-life of GSK484 in ApoE KO mice was unknown and it appeared possible that the experiments required too much time for the substance to show its full inhibitory effect. Furthermore, it remained to be elucidated why the combined treatment with A23187 and GSK484 led to paradox results in the in vitro DNA release assay. Hence, ex vivo testing of mouse blood for NETosis potential was switched to blood smears.

5.2.3. NET Formation in Blood Smears

For this assay, blood samples were drawn from ApoE KO mice with angiotensin II-induced AAA. To be more specific, animals received a subcutaneous osmotic pump releasing AngII over a time frame of 28 days which resulted in aneurysm formation. At day 14, expansion of the aortic diameter was verified by ultrasound and an intravenous catheter was inserted into the vena jugularis externa, connected to a subcutaneous mouse port for serial access. Mice were treated daily with a single injection of 200 µl PBS-/- (controls) or 200 µl of PBS containing 2.0 µg of GSK484/g body weight via the port chamber. On day 28 of the experiment the aortic diameter was again assessed by ultrasound and mice were euthanized to obtain blood from the vena cava inferior. Aliquots of blood were used immediately for in vitro NET induction by A23187 (50, 200 and 500 µM) over 2 hours. Blood smears were generated and stained to identify leukocytes by Hoechst-positive nuclei, neutrophilic granulocytes by Ly6G-positive immunostaining and NETs by Hoechst-positive fragmented nuclei (early stage) or DNA strings (late stage) with citH4 staining. Cells were counted under the confocal microscope in comparable field views.

Figure 26 shows representative confocal pictures of blood smears from one control mouse.
When no A23187 was added hardly any NETosis was observed. Stimulation with 50 µM of A23187 led to formation of small fragmented cells. Stimulation with 200 µM and 500 µM A23187 resulted in the formation of elongated NETs (strings), who appeared like string-like structure extending from the cell body.
Interestingly, only the stimulation with 500 µM A23187 resulted in prominent staining with anti-citrullinated histone H4 antibody.

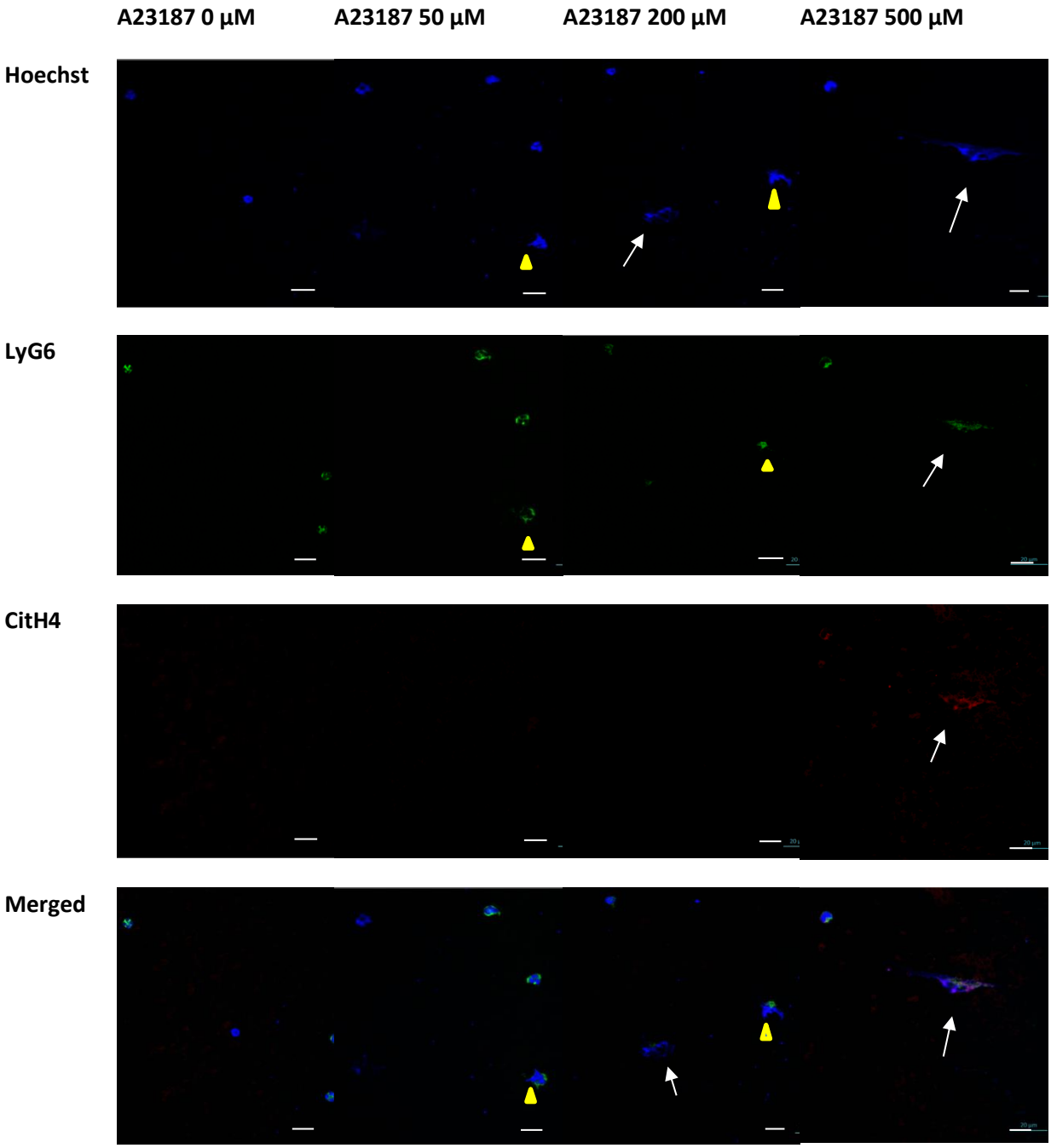

Figure 25: Confocal images of immunofluorescence-stained blood smears of a control treated AAA mouse.

Blood was drawn from a PBS-treated ApoE KO mouse with aneurysm induction by AngII. Blood aliquots were stimulated in vitro with 0, 50, 200 or 500 µM of A23187 for two hours to induce DNA release. Smears of the samples were triple-stained for DNA with Hoechst dye (in blue), for the neutrophil surface marker LyG6 (in green), and for citrullinated histone H4 (in red). Yellow rectangles indicate fragmented cells and white arrowheads point to formed NETs, appearing as string-like structures extending from the remnant cell body. Magnification: 63x using 1.4 Plan-Apochromat, oil, DIC; scale bar: 20 µM.

Abbreviations. citH4, citrullinated histone 4.

Figure 27 shows representative confocal pictures of blood smears from one ApoE KO mouse receiving daily injections of 2.0 µg of GSK484/g body weight. When no A23187 was added, NETosis was not observed. Stimulation with 50 µM of A23187 led to less formation of small fragmented cells in comparison to blood from the control-treated mouse (Fig. 26). Stimulation with 200 µM and 500 µM A23187 resulted in the formation of a few NETs. However, hardly any string-like structures were detected. In addition, A23187-stimulated cells from the GSK484 treated mouse did not reveal any immunoreactivity for citrullinated histone H4.

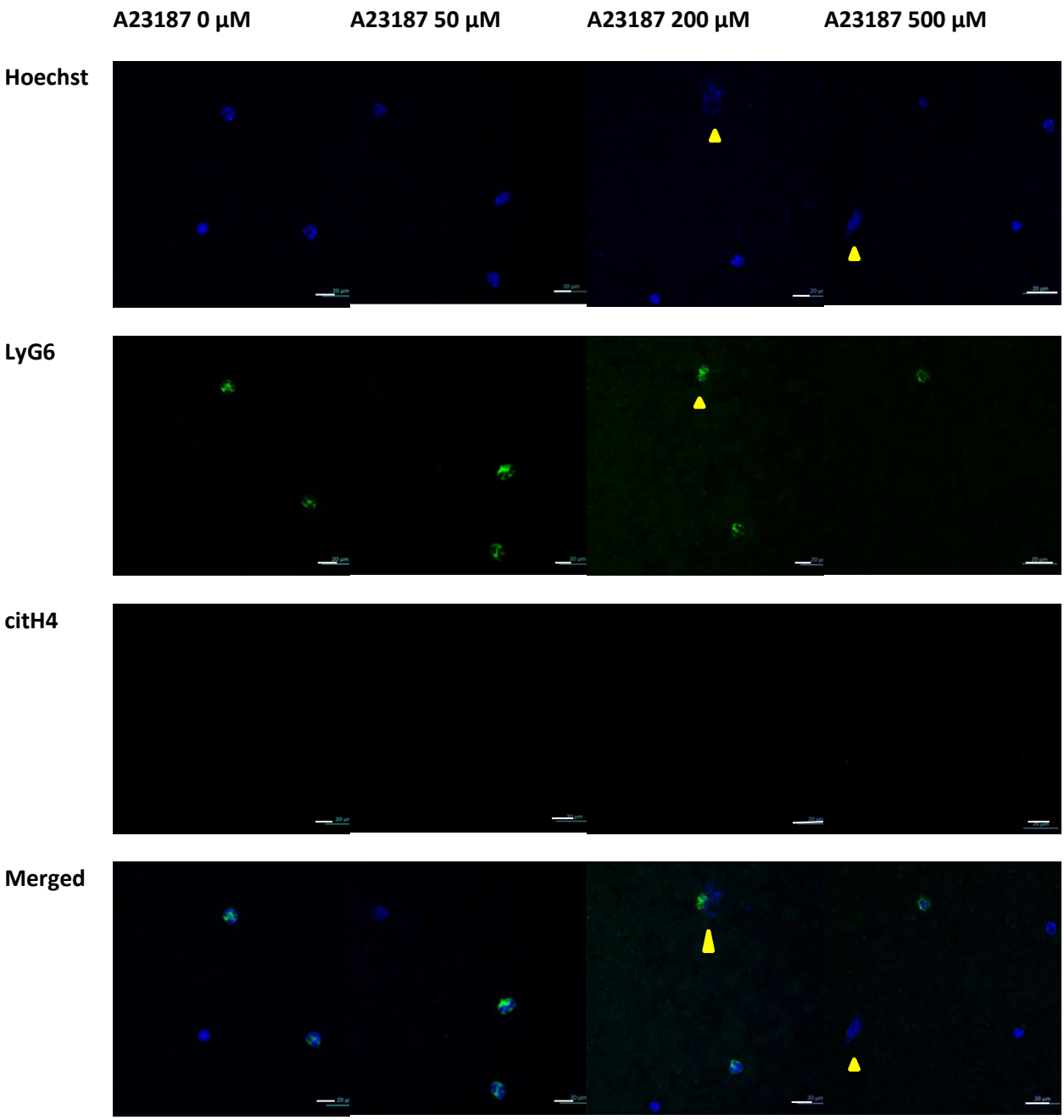

Figure 26: Confocal images of immunofluorescence-stained blood smears of an AAA mouse treated with 2.0 µg of GSK484/g body weight.

Blood was drawn from a GSK484-treated ApoE KO mouse with aneurysm induction by AngII. Aliquots were stimulated in vitro with 0, 50, 200 or 500 µM of A23187 for two hours to induce DNA release. Smears of the blood samples were triple-stained by Hoechst dye (in blue) and anti-LyG6 antibody (in green), and anti-citrullinated histone H4 antibody (in red). Yellow rectangles indicate fragmented cells and white arrowheads point to NETs, appearing as string-like structure extending from the remaining cell body. Magnification: 63x using 1.4 Plan-Apochromat, oil, DIC; scale bar: 20 µM.
Abbreviations. citH4, citrullinated histone 4.

As the next step, the occurrence of NETs in the blood smears was evaluated in quantitative terms, i.e., the percentages of NETs was determined in relation to intact white blood cells (WBC) and neutrophilic granulocytes without and with stimulation of DNA release by A23187. It is important to note that NET frequency could exceed 100% when NET counts were higher than counts of intact leukocytes or neutrophils (set to 100%).

Table 14 summarizes the relative frequency of NETs in blood smears from control-treated AAA mice (N=10). NETs occurred at 0.5% of WBC and at 3.5% of the population of neutrophilic granulocytes. Stimulation by A23187 caused a dose-dependent increase to 43% of WBC (at 500 µM) and 134% of the neutrophils (500 µM). At 50 µM of A23187 early stages of NETs were predominant, while 500 and 1000 µM of A23187 resulted mostly in the formation of DNA strings (not shown). Furthermore, it has to be noted that the higher the A23187 concentration, the fewer intact cells were countable. The highest dose of A23187 (1 mM) was only tested in control-treated AAA mice, gave aberrant results and was hence omitted from the standardized assay in further experiments.

When compared to control-treated AAA mice, GSK484 administration did not alter the basal frequency of NETs in the blood smears (Table 15). Treatment of mice with GSK484 reduced NETosis (in terms of mean NET frequency) of WBC stimulated by 50 µM or 200 µM of A23187, and led to a nearly significant (p=0.053) reduction at 500 µM (Fig. 28). In addition, GSK484 treatment reduced significantly (p=0.014) NETs of neutrophils, stimulated by 50 µM of A23187, and exerted a nearly significant effect (p=0.077) at 500 µM of A23187. In addition, the occurrence of late stages (strings) was reduced in all treatment groups (data not shown).

	% NETs of white blood cells					% NETs of neutrophils				
	CTRL	**A23187 50µM**	**A23187 200µM**	**A23187 500µM**	**A23187 1000µM**	**CTRL**	**A23187 50µM**	**A23187 200µM**	**A23187 500µM**	**A23187 1000µM**
mean	0.51	5.14	10.02	42.95	16.00	3.48	39.57	91.72	133.66	168.16
SD	0.42	2.85	10.40	21.58	11.44	3.46	30.66	114.46	69.62	84.88
Min	0.00	2.29	0.50	22.78	2.80	0.00	8.89	5.00	71.88	24.50
max	1.35	12.15	33.33	65.71	28.57	10.00	108.33	366.67	120.00	230.77

Table 14: Effect of A23187 on the relative frequency of NETs in blood smears of control-treated AAA mice. (N=10)
Abbreviations. CTRL, control. SD, standard deviation. NETs, neutrophil extracellular traps.

	% NETs of white blood cells				% NETs of neutrophils			
	GSK	**A23187 50µM**	**A23187 200µM**	**A23187 500µM**	**GSK**	**A23187 50µM**	**A23187 200µM**	**A23187 500µM**
mean	0.73	2.84	6.22	13.62	1.96	9.56	14.40	41.20
min	0.00	0.00	3.39	0.00	0.00	0.00	6.06	0.00
max	2.30	6.72	9.38	27.47	5.56	27.78	20.55	194.17
SD	0.94	3.00	2.33	12.23	2.27	11.76	6.30	49.27

Table 15: Effect of A23187 on the formation of NETs in AAA mice treated with GSK484 at 2.0 µg/g body weight. (N=5)
Abbreviations. GSK, GSK484. SD, standard deviation. NETs, neutrophil extracellular traps.

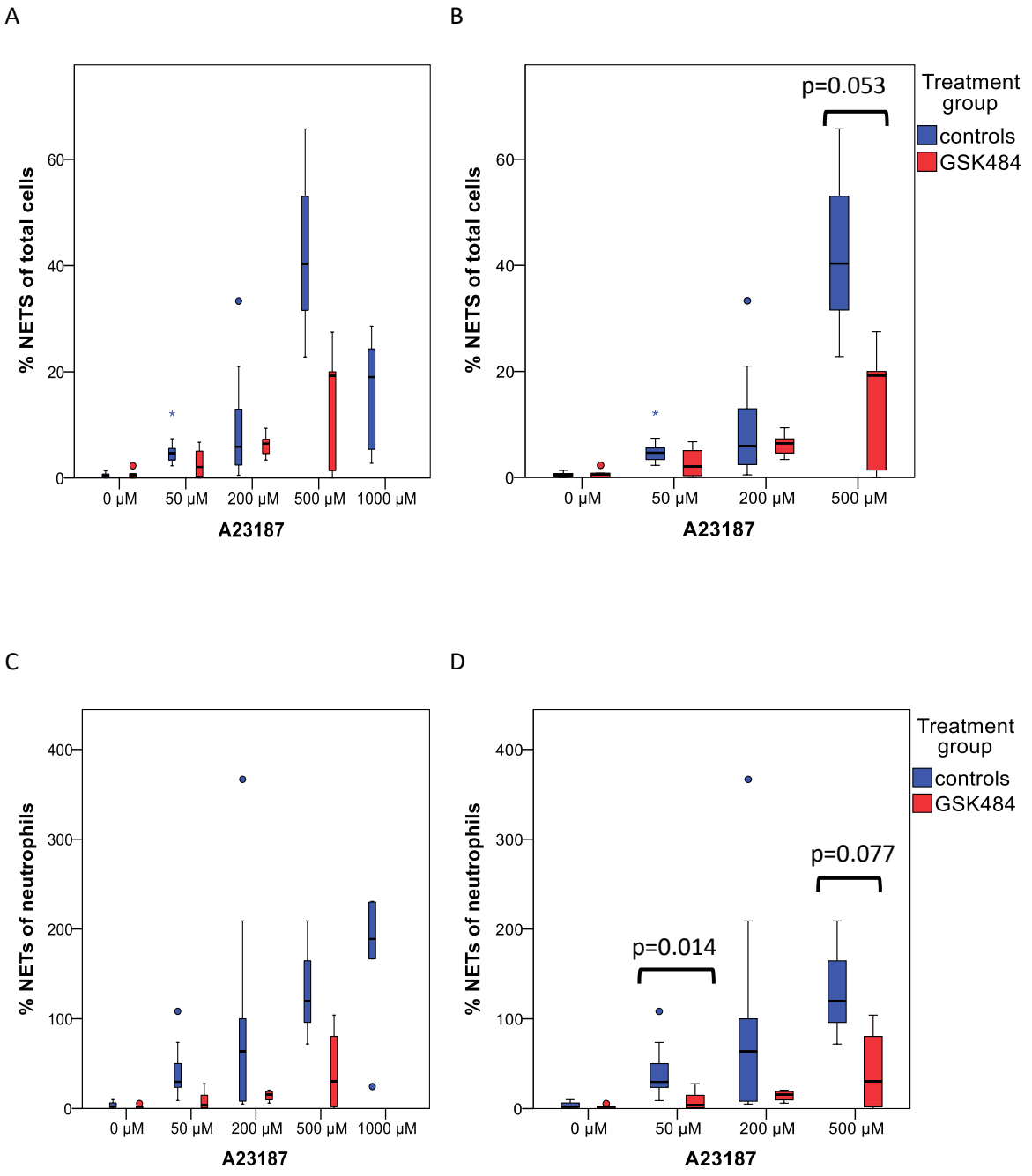

Figure 27: Dose-dependent effect of A23187 on NETosis in blood samples obtained from control or GSK484-treated AAA mice.

Blood samples obtained from control-treated mice (N=10; blue) and mice treated with 2.0 µg of GSK484/g body weight (N=5; red) were stimulated for 2 h with A23187 at increasing concentration. Blood smears were generated, immunofluorescence staining was performed and NET counts determined in relation to intact cells. Box blots A) and B) show the percentage of NETs in relation to total white blood cells, while C) and D) show the percentage of NETs of neutrophilic granulocytes.

Abbreviations. NETs, neutrophil extracellular traps.

5.2.4. AAA Formation in Mice

Seventeen ApoE KO mice were randomly assigned to two groups. The aorta was screened by ultrasound and no signs of AAA formation were obtained before start of treatment (Tables 16 and 17). As described previously, angiotensin II was applied via mini-pumps over a period of 14 days to generate the AAA in the suprarenal region. Five animals died of aneurysm rupture within this period. The area of AAA at its maximal diameter was determined by ultrasound at regular intervals, as described in the Methods. At day 14 post start of angiotensin II treatment there was no significant difference in area or diameter of any AAA region between the two treatment groups (Table 18).

On day 14 portal chambers were implanted, which caused the loss of 3 animals. Then, treatment was randomly started with either PBS (for control) or 2.0 µg of GSK484/g body weight for further 14 days. On day 28 ultrasound screening was again performed to evaluate a potential therapeutic effect of GK484 treatment. However, none of the recorded parameters of aorta dimensions revealed a significant difference between the control mice and those which had been subjected to anti-NET therapy (Tables 16, 17, 18 and Figures 29 and 30).

Parameter	Baseline Mean (min-max)	SD	N	Day 14 Mean (min-max)	SD	N	Day 28 Mean (min-max)	SD	N
Mean suprarenal area (mm3)	0.909 (0.761-1.066)	0.12	5	1.107 (0.874-1.321)	0.19	5	1.590 (1.364-1.746)	0.17	4
Mean suprarenal diameter (mm)	1.095 (1.004-1.162)	0.07	5	1.198 (0.991-1.297)	0.14	4	1.486 (1.286-1.777)	0.21	4
Mean infrarenal diameter (mm), long axis view	0.912 (0.792-1.067)	0.11	5	1.093 (0.734-1.508)	0.28	5	1.045 (1.000-1.101)	0.05	4
Max suprarenal diameter (mm), long axis view	1.080 (0.891-1.274)	0.15	5	1.585 (1.160-2.174)	0.37	5	1.647 (1.137-2.684)	0.61	5

Table 16: Measurement of aorta by ultrasound in control AAA mice treated with saline.
Baseline ultrasound measurements were performed on day 0 before start of angiotensin II treatment. The second ultrasound was conducted on day 14, when daily treatment with 200 µl PBS per animal was started. On day 28 the final ultrasound was performed. Data are expressed as mean and standard deviation. For further information see Methods.

Table 17 shows an overview of aorta ultrasound measurements recorded of mice treated with GSK484 at 2.0 µg/g body weight.

Parameter	Baseline Mean (min-max)	SD	N	Day 14 Mean (min-max)	SD	N	Day 28 Mean (min-max)	SD	N
Mean suprarenal area (mm3)	0.843 (0.752-0.967)	0.11	5	1.427 (0.857-2.081)	0.46	5	1.939 (0.921-3.160)	0.87	5
Mean suprarenal diameter (mm)	1.037 (0.986-1.104)	0.05	5	1.246 (1.015-1.452)	0.20	5	1.568 (1.095-2.210)	0.43	5
Mean infrarenal diameter (mm), long axis view	0.894 (0.834-0.933)	0.04	5	1.047 (0.983-1.306)	0.15	5	1.107 (0.958-1.459)	0.21	5
Max suprarenal diameter (mm), long axis view	0.999 (0.783-1.317)	0.22	5	1.409 (1.045-1.648)	0.23	5	1.694 (1.430-1.973)	0.26	5

Table 17: Measurement of aorta by ultrasound in AAA mice treated daily with 2.0 µg of GSK484/g body weight.

Baseline ultrasound measurements were performed on day 0 before start of angiotensin II treatment. The second ultrasound was conducted on day 14, when daily treatments with 2.0 µg of GSK484/g body weight were started. On day 28 the final ultrasound was performed. Data are expressed as mean and standard deviation.

Parameter	Baseline p-value	N (C)	(G)	Day 14 p-value	N (C)	(G)	Day 28 p-value	N (C)	G)
Mean suprarenal area (mm3)	0.347	5	5	0.251	5	5	0.462	4	5
Mean suprarenal diameter(mm)	0.175	5	5	0.462	4	5	0.806	4	5
Mean infrarenal diameter(mm), long axis view	0.917	5	5	0.347	5	5	0.712	4	5
Max suprarenal diameter(mm), long axis view	0.465	5	5	0.465	5	5	0.347	5	5

Table 18: Statistical analysis of data obtained by ultrasound measurements of the aorta in control mice (C) and GSK484 (G) treated mice.

Statistical analysis was conducted with the Mann-Whitney-U-Test.

Figure 29 illustrates the data distribution and Table 18 shows the statistical analyses of aorta ultrasound measurements.

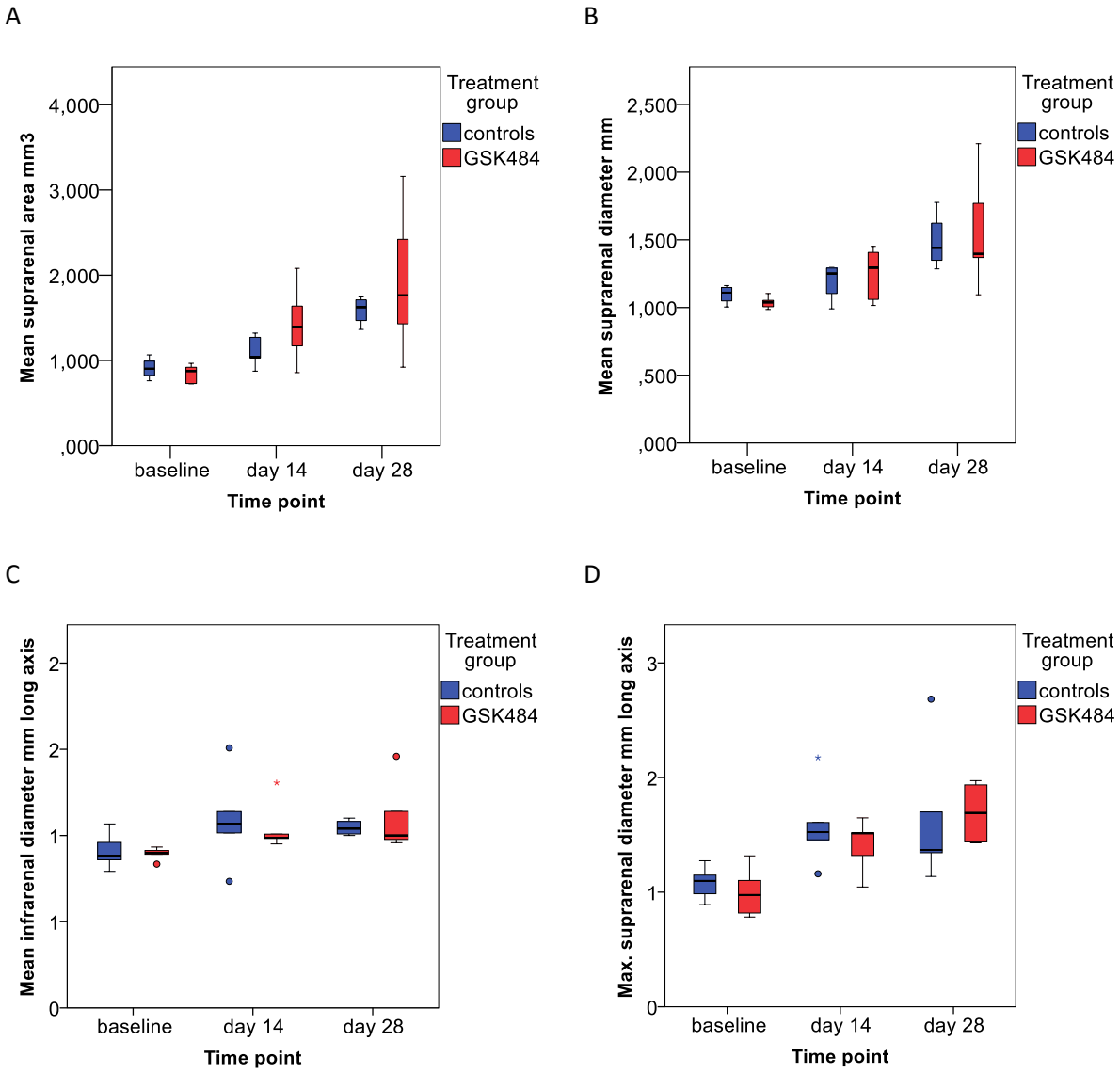

Figure 28: Ultrasound measurements of AAA mice treated with GSK484 or saline for negative control.

The boxplots illustrate the measurements that were conducted at the following regions of the abdominal aorta: A) mean suprarenal area (mm^3) in short axis view, B) mean suprarenal diameter (mm) in short axis view, C) mean infrarenal diameter (mm) in long axis view, and D) mean suprarenal diameter (mm) in long axis view.

Figure 30 shows representative ultrasound images of AAA formation. The baseline ultrasound of the abdominal aorta in short axis view is given in A (diameter = 0.761 mm). On day 14 an increase in diameter is seen in short (B) (0.956 mm) and in long axis view (C) (1.642 mm).

A

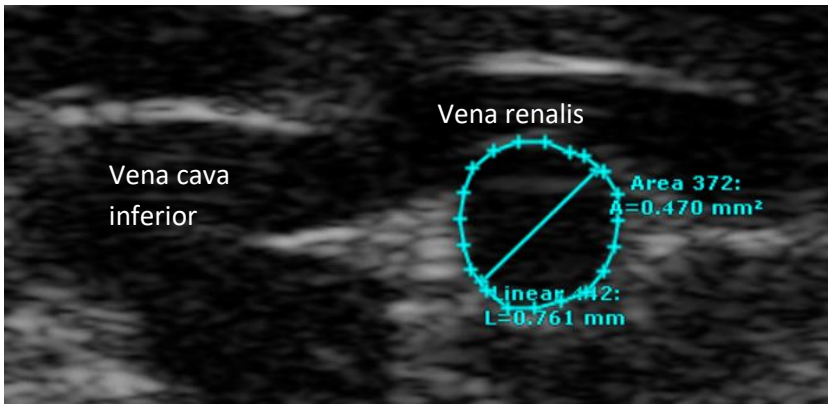

B

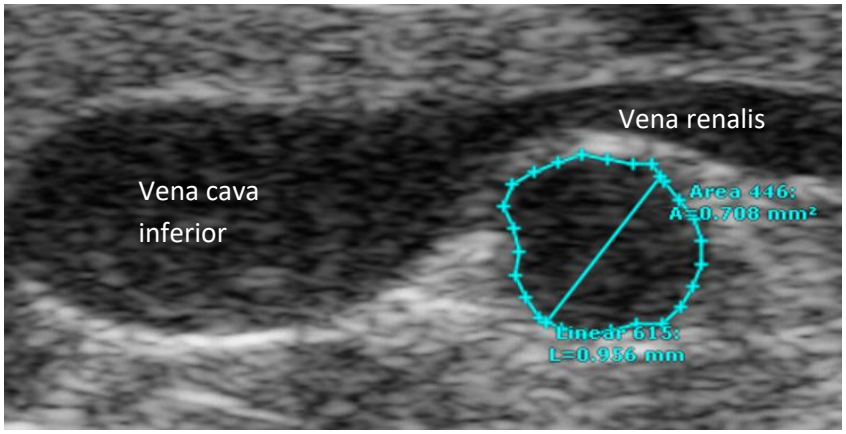

C

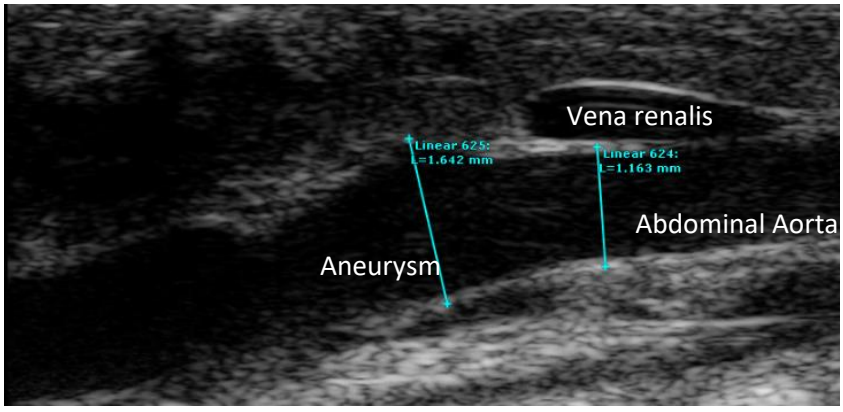

Figure 29: Ultrasound images of the abdominal aorta of a control-treated AAA mouse.
Assessment of the diameter and area of the abdominal aorta using (A) short axis B mode at baseline, (B) short axis B mode and (C) long axis B mode 14 days after angiotensin II pump implantation. The diameter and area were measured during systole. Tracing was performed using the built-in Vevo 2100 software. Measurements were conducted from the outer aortic wall on one side to the outer aortic wall on the opposite side.

6. Discussion

The first aim of this study was to determine levels of NETosis markers in peripheral blood of AAA patients during monitoring and pre- and post-surgery. It was hypothesized that NET marker levels in the pre-surgery phase would be associated with aneurysm progression, might hence predict AAA growth and should drop after surgical repair. In addition, the selective PAD4 inhibitor GSK484 was tested as potential pharmaceutical treatment option in an experimental model of AAA formation.

A few studies have addressed NETosis in patients with various diseases like systemic lupus erythematosus [167], chronic granulomatous disease [168] and vasculitis [169]. However, the role of NETs in the development and progression of AAA is less characterized. NETs are able to recruit platelets and neutrophils to the endothelium. This supported the hypothesis, that they may take part in the pathogenesis of thrombosis and the activation of the extrinsic and intrinsic coagulation pathways which has subsequently been confirmed [170, 171]. Also chronic bacterial infections may sustain a basal NETosis activity in the body which may trigger AAA formation, e.g., NETs may play a part in AAA development in conjunction with periodontitis [144]. However, up to date parameters indicating NETosis have not yet been investigated specifically in the context of AAA progression and repair which was the main subject of this study.

Demographics

Concerning the patient demographics in the present study on aneurysm progression and repair, 100% of all AAA patients were men, which reflects their elevated risk for this disease [11]. Several cardiovascular comorbidities have been linked to AAA formation [13, 14]. In our collective of cases, being investigated in the pre- and post-surgery phase, 85.7% suffered from hypertension, 100% from hyperlipidemia, 28.6% had experienced coronary artery disease and myocardial infarction and 28.6% were treated for diabetes mellitus type II. In the monitoring study the pattern of co-morbidities was similar, i.e., 60% showed hypertension, hyperlipidemia and diseased coronary arteries, 40% myocardial infarction and 20% diabetes mellitus type II. It has been reported that an increase in the diastolic blood pressure per 10 mm Hg is associated with an AAA expansion rate of 0.02 cm per year [20]. A different study did not confirm the correlation between hypertension and progression of the aortic diameter, but found a positive correlation between hypertension and the risk of rupture [23]. Interestingly, diabetes mellitus type II was found to be associated with a reduced risk of AAA formation. Recently it was reported that the oral antidiabetic metformin may exert a protective effect possibly by limiting inflammation and stimulating the production of extracellular matrix in the arterial wall [26].

In our collective more than 80% of the patients were cigarette smokers. Smoking of tobacco products is known to be a central risk factor in the formation and progression of AAA [11, 191]. The odds for developing an AAA are correlating positively with the number of daily cigarettes and of overall pack years, e.g., men smoking more than 25 cigarettes per day have a 15-fold risk of developing an AAA when compared to non-smokers [19, 192]. Furthermore, current tobacco smoking results in a 0.05 cm increase in aneurysm growth per year [20] and the risk of rupturing is increased twofold [12]. Even after quitting the risk remains elevated which indicates that the adverse effects of tobacco smoking are largely irreversible [19]. Recently Tulgar et al. reported that the neutrophil-to-lymphocyte ratio increases with each pack year, indicating stimulation of the innate immune system and a pro-inflammatory state [192]. In fact, tobacco promotes AAA formation through triggering inflammation, which is based on the elevated release of cytokines, like TNFα and IL-1ß, from macrophages [22]. Nicotine also stimulates

MMP expression, which triggers proteolysis and apoptosis of SMCs [21, 22]. In our study 42.9% of the patients in the pre- and post-surgery group and 20% in the monitoring group suffered from chronic obstructive pulmonary disease. This disease is associated with smoking, elevated serum TNFα levels and an increased chemotaxis of circulating neutrophils towards IL-8 and leukotriene B4, indicating a systemic influence of smoking on neutrophil migration and activation [193].

Laboratory parameters

Hemostasis and fibrin destruction continuously occur at the site of the ILT. This may result in elevated levels of coagulation and fibrinolysis factors in the blood of AAA patients originating from the tissue of the ILT [89]. Most reports focused on fibrinogen, the fibrin degradation product D-dimer and on the thrombin-antithrombin III complex. In the present study D-dimer did not increase significantly in AAA patients during the monitoring period and there were also no changes in D-dimer levels in the pre- or post-surgery phase. However, a significant negative correlation between D-dimer and MPO-histone complexes ($p=0.033$) and neutrophils ($p=0.002$) was observed. These results indicate that D-dimer might not be associated with pro-inflammatory processes occurring in the AAA. Fibrinogen, however, tended to decrease throughout the monitoring period ($p=0.051$) almost reaching statistical significance.

The findings of this study disagree partly with previous reports, e.g., in a meta-analysis fibrinogen, the fibrinogen degradation product D-dimer, and the thrombin-antithrombin III complex prevailed as diagnostic markers by correlating with the size of the AAA and of the ILT [91]. In 2011 Golledge et al. proposed that plasma D-dimer may be a diagnostic and prognostic parameter for AAA progression [92]. Additional studies confirmed [194, 195] that D-dimer values correlate with the volume of the ILT as well as AAA diameter and have a high diagnostic value for the presence and prognostic value for the progression of the disease. It was assumed that elevated plasma levels may be a result of the constant remodeling of fibrin in the ILT. As a consequence, elevated D-dimer levels are proposed to be associated with the destruction of the media in AAA which is promoted further by the ILT. It was also observed that fibrinogen levels were elevated years before an AAA had formed. This shows that deregulated hemostasis and fibrinolysis are involved in AAA pathogenesis at an early stage [93]. To conclude, our study did not confirm previous findings, which may be largely due to the low number of patients investigated.

In 2018 Kubota et al. observed that elevated lipoprotein(a) blood levels were a risk factor for AAA development [196]. Further studies showed that increases in lipoprotein(a) may be due to gene polymorphisms of the lipoprotein receptor related protein 5 (LRP5) [197] and that a decreased expression of LRP5 in peripheral blood cells occurs in AAA patients. LRP5 encodes a transmembrane low-density lipoprotein receptor that binds and internalizes ligands in the process of receptor-mediated endocytosis and that may be involved in the regulation of lipoprotein(a) concentrations in blood. However, it remains to be investigated whether lipoprotein(a) may serve actually as prognostic marker for AAA. In the present study lipoprotein(a) levels significantly decreased ($p=0.034$) after surgery, which indicates again a putative significance of this protein in the pathogenesis of AAA. A weak negative correlation with the explorative parameter MPO was detected as well ($p=0.032$, $Rho=-0.572$). The significance of these findings remains to be elucidated in a larger collective of AAA patients.

It has been observed that erythrocytes get trapped in the fibrin mesh of the ILT which leads to increased hemolysis [198]. Our study confirmed these observations, i.e., post-operative levels of erythrocytes were increased significantly ($p=0.018$), whereas free hemoglobin levels were decreased ($p=0.028$).

Furthermore, the percentage of lymphocytes dropped in the post-surgery phase (p=0.028) presumably due to repair of the locus of chronic inflammation by EVAR or OSR. Furthermore, in the pre- and post-surgery cohort a positive correlation was evident between the percentage of lymphocytes and DNA-histone complexes (p=0.056, Rho=0.521). This finding supports the hypothesis that neutrophils may be activated in the chronic inflammatory process of AAA and form NETs.

It should further be noted that according to international recommendations [13], the AAA patients of the present study were treated with lipid-lowering drugs, e.g. statins and/or vitamin D. This regimen led to a significant decrease during the monitoring period in low density lipoprotein (p=0.028) and the cholesterol/high density lipoprotein ratio (p=0.015) and an increase in 25-hydroxyvitamin D levels (p=0.051).

Explorative parameters

AAA shows many characteristics of a chronic inflammatory disease and may serve as a site of neutrophil accumulation and formation of NETs. Furthermore, chronic inflammation at other sites in the body may sustain a basal NETosis activity and trigger AAA formation, such as the elevated risk for AAA in patients suffering from chronic periodontitis [144]. In this study by Delbosc et al., markers for NETs, like citrullinated histones and cell-free DNA (cfDNA), were elevated in the luminal part of the ILT and the adventitia of the AAA wall. In addition, the plasma of AAA patients contained more cell-free DNA and DNA-myeloperoxidase (MPO) complexes when compared to healthy controls. Likewise, in an experimental AAA model cfDNA and DNA-MPO complexes were elevated in the plasma [144]. Recently, further studies confirmed that NETs may indeed contribute to the pathogenesis of AAA irrespective of bacterial infections [175, 199, 200].

The formation of NETs involves activation of neutrophilic granulocytes. Ninety-five % of PMNs express MPO to generate ROS [56, 57]. In AAA patients, however, circulating PMNs show more MPO but less catalase activity than PMNs of healthy individuals, which indicates a gross imbalance towards a pro-oxidative state [58]. These observations led to the idea that not only NETosis but also increased oxidative stress by activated neutrophilic granulocytes may be a main factor in the pathogenesis of AAA [58].

It is not fully established that NETosis is causally involved in AAA formation. The present study showed that circulating DNA-histone complexes (p=0.018), citH3 (p=0.043) and MPO (p=0.028) were decreased significantly after surgery. It remains unclear why MPO-histone complexes were not significantly altered. A positive correlation was shown between DNA-histone complexes and citH3 (p=0.003, Rho=0.732), DNA-histone complexes and MPO (p=0.017, Rho=0.626) and citH3 and MPO (p<0.001, Rho=0.868). These findings support the notion that all three parameters originate from the same source, namely activated neutrophils, and reinforce our hypothesis that NETs take an essential part in the pathogenesis of AAA.

In a next step, patients suffering from AAA were subjected to a monitoring program, including computed tomography angiography of the abdominal aorta and analyses of serum and plasma samples every 6 months, to evaluate which parameter may predict disease progression. Within the observation period the median diameter of the AAA increased significantly (p=0.007) from 53.9 mm to 56.5 mm. A non-significant tendency towards increasing MPO (p=0.374) and citH3 (p=0.594) could be observed. It appears possible that a longer observation period is necessary to obtain clear results. The reasons for

the significant decrease in MPO-histone complexes (p=0.008) in the monitored patients remains to be elucidated.

When baseline levels at the beginning of the monitoring period were compared with the change in AAA diameter over the next 6 months, the number of erythrocytes correlated positively with AAA progression (p=0.031, Rho=0.712). This finding challenges the assumption that red blood cells in circulation are reduced, as they get trapped in the fibrin mesh of the ILT [198] and hence increase in the post-operative phase after aneurysm repair (p=0.018). However, higher erythrocyte counts may also be due to increased loss at the ILT site and subsequent erythropoiesis, in which case they would reflect a more active thrombus resulting in faster media destruction. HDL is known to have a cardiovascular protective effect. A meta-analysis showed that patients with AAA showed significantly lower HDL levels than healthy controls [201]. The present study supports and extends these findings, i.e. HDL levels correlated negatively with the expansion of the AAA diameter (p=0.043, Rho=-0.681). In contrast to our expectations, citH3 levels were associated negatively with disease progression (p=0.026, Rho=-0.729). This finding contradicts our hypothesis that NETs promote the progression of AAA. Therefore, one has to take into consideration the possibility that NETosis may also antagonize the formation and progression of AAA. In 2016 Bilyy et al. observed that NETs protected healthy pancreatic tissue against the formation of necrosis by forming a barrier [202]. Furthermore, in patients suffering from gout, aggregated NETs degraded pro-inflammatory cytokines and chemokines resulting in a decreased recruitment and activation of neutrophils [61]. These findings indicate that NETs may exert protective effects in several inflammatory diseases.

To conclude, none of the explorative parameters evaluated at baseline showed the potential to predict disease progression, i.e. correlated positively with aneurysm growth. In contrast, the NET marker citH3 correlated negatively. However, the significant decrease in DNA-histone complexes, citH3 and MPO post-surgery is strong evidence that NETosis indeed plays an essential role in the pathogenesis of AAA. Therefore, the formation of NETs may serve as target for pharmaceutical treatment.

At the moment there is no selective pharmaceutical treatment option for AAA patients. Medication may slow down disease progression by reducing comorbidities but the only curative treatment is still surgical intervention [56]. The present study applied a rodent model to evaluate whether NETosis may serve as therapeutic AAA target. There are a number of different AAA animal models, like the elastase perfused rat model, the elastase perfused mouse model and the angiotensin II infused mouse model. However, not all of them mimic the risk factors of the disease and some do not even develop a thrombus [182-185]. For this study the angiotensin II infused mouse model was used due to the fact that it mimics several human risk factors. Mice homozygous for the ApoE mutation develop hyperlipidemia. The treatment with angiotensin II leads to hypertension. The mice are of male gender. All these risk factors in combination play an important part during the pathogenesis of AAA. It also has been observed that angiotensin II infusion leads to an increased infiltration of macrophages resulting in a dilatation of the wall [186, 187]. In addition, this model generates an atherosclerotic lesion, luminal dilatation, medial degeneration, inflammation and intramural thrombus development. However, it has to be noted that the aneurysm forms suprarenal and the thrombus develops intramural, whereas in humans most aneurysm are located infrarenal and the thrombus forms in the luminal part of the aorta [188].

Activation of protein kinase C (PKC) seems to play a key role in NET formation [203], i.e., PKCζ may activate PAD4 [155, 156], which is able to citrullinate the arginine of histones leading to a weakening of the electrostatic binding between histones and DNA [179]. Accordingly, it has been observed that PAD4

deficient mice are unable to form NETs [180]. In 2018 Meher et al. showed that treatment with a broad-spectrum inhibitor of protein citrullination (Cl-amidine) attenuated AAA formation in an elastase-induced AAA mouse model [204]. However, it was not determined whether this type of treatment was able to stop progression of an already established AAA.

In the present study male ApoE KO mice received angiotensin II infusion via an osmotic pump. Ultrasound imaging showed that on day 14 of the treatment mice had developed an aortic dilatation, expanding from a mean baseline value of about 1 mm to 1.5 mm maximal suprarenal aortic diameter after two weeks. From day 14 on mice were treated daily with either PBS-/- (controls) or the selective PAD4 inhibitor GSK484 via an intravenous port system. GSK484 was tolerated well by the animals, as established by escalation of single doses. None of the animals died due to toxicity. Hence, a treatment dose of 2.0 µg GSK484 per g mouse weight was chosen.

On day 28, blood samples were taken from animals in order to verify an inhibitory effect of GSK484 on the NETosis potential, quantified by the DNA release assay. As outlined in section 5.2.2 the results of this assay were inconclusive and difficult to reproduce. Thus, it was decided not to apply the neutrophil isolation and DNA release detection technique due to the assumption that the long isolation process of >6 hours, involving many washing steps, may not only wash out but also reverse the effect of GSK484, since it was described as selective but reversible PAD4 inhibitor. In future experiments, it would be useful to determine not only the pharmacokinetic profile of GSK484 in the living animal but also the stability of the compound in ex-vivo/in-vitro approaches in order to improve the evaluation of the therapeutic efficacy of this compound.

As alternative and rapid approach to determine NETosis, aliquots of mouse blood samples were stimulated in vitro for 2 hours, then smeared and fixed and subsequently subjected to immunostaining and evaluation by confocal microscopy as outlined in section 4.2.10. To evaluate the reliability of this technique, setup experiments had to be performed. Isolated blood cells of control animals were stimulated in vitro with 0 µM, 50 µM, 200 µM, 500 µM and 1000 µM A23187, which increased NETosis dose-dependently, as determined by the above mentioned approach. Next, blood samples of GSK484-treated animals were compared to those obtained from their untreated counterparts. There was a difference (of borderline significance) in the occurrence of NETs within the white blood cells between controls (42.95% NETs) and GSK484-treated mice (13.62% NETs) when cells were stimulated in vitro with 500 µM of A23187 ($p=0.053$). Furthermore, the frequency of NETosis in relation to intact neutrophils obtained with 50 µM of A23187 showed a significantly different ($p=0.014$) percentage of NETs in controls (39.57%) and GSK484-treated mouse blood (9.56%). In the control group the higher concentrations of A23187 resulted in the formation of DNA strings whereas the GSK484 treated cells showed rather early stages of NETosis in form of fragmented cells. These observations led to the interpretation that GSK484 may inhibit NETosis when stimulated with lower concentrations of A23187 but may only delay the process when higher concentrations of A23187 are applied. Furthermore, these results indicate that the NETosis capacity was indeed reduced in the GSK484-treated animals, which led us to evaluate its effect on AAA progression as determined by ultrasound investigation of the suprarenal aortic diameter. In contrast to our hypothesis, the GSK484 treated group showed no significant difference in aneurysm expansion from day 14 to day 28, despite apparently reduced NETosis capacity. While the results are limited by the low number of animals investigated, they may also indicate that NET formation is not substantially involved in the progression of established disease but rather in the initiation/formation of aneurysms as indicated by previous reports [175, 204].

NETosis may be involved not only in the formation of AAA but also in other pathophysiological processes. It has been published recently that subcutaneous GSK484 application reduced neuropathic pain in a rodent model [205]. Another study showed that GSK484 was able to treat cancer-associated kidney failure in an experimental model [206]. Furthermore, it has been observed that GSK484 is able to reduce angiogenesis induced by NET formation [207, 208].This is indication that death of neutrophils is occurring in many different diseases, thus stressing the fact that inhibitors of NETosis may have a broad therapeutic value. Thus, even though GSK484 had no significant effect on AAA progression in the applied mouse model, potential beneficial "side effects" on e.g. kidney disease associated with aneurysms may warrant further investigation.

The present study has a number of strengths and weaknesses. Strengths include the novelty of using NETosis markers as laboratory parameters in AAA patients in the monitoring stage as well as in the pre- and post-surgery period. Secondly, it was demonstrated that intravenous treatment with PAD4 inhibitor GSK484 reduced the NETosis capacity in ApoE KO mice. This suggests that NETosis inhibition by GSK484 may be tested in various disease settings involving NET formation. Third, a surgical approach of port implantation into the vena jugularis externa has been established in young mice. This new technique may be of considerable experimental value for repeated intravenous application of test compounds.

On the other hand, the present work exhibits also several limitations. Designed as explorative study, the number of patients and animals investigated was rather small. Therefore, the results can hardly be compared to more comprehensive AAA studies [92]. Although the present work gives some indication that NETosis parameters correlate negatively with AAA progression in humans, this finding has to be confirmed in a larger collective of patients. Second, counting NETs under the confocal microscope has to be discussed when addressing weaknesses. Immunofluorescence staining is a recognized technology in visualizing NETs [190] repeatedly counting the NETs yielded comparable results, which points towards consistency of the data acquired. However, the analysis has to be performed separately for each single blood smear which harbors a distinct potential of error. Thus, a standardized counting protocol performed by the same individual and re-evaluation of blinded samples by a second person should guarantee the reproducibility of the results. Third, none of the AAA mouse models covers all aspects of the human disease. It was shown recently that in one knock-out mouse strain two different AAA models showed opposite effects [199, 200, 209]. Therefore, the effectiveness of GSK484 to inhibit aneurysm progression should be tested in additional AAA models, e.g. in mice with elastase-induced AAA.

7. References

1. Takayama, T. and D. Yamanouchi, *Aneurysmal disease: the abdominal aorta.* Surg Clin North Am, 2013. **93**(4): p. 877-91, viii.
2. Vega de Ceniga, M., et al., *Growth rate and associated factors in small abdominal aortic aneurysms.* Eur J Vasc Endovasc Surg, 2006. **31**(3): p. 231-6.
3. Nordon, I.M., et al., *Pathophysiology and epidemiology of abdominal aortic aneurysms.* Nat Rev Cardiol, 2011. **8**(2): p. 92-102.
4. Gianfagna, F., et al., *Prevalence of abdominal aortic aneurysms and its relation with cardiovascular risk stratification: protocol of the Risk of Cardiovascular diseases and abdominal aortic Aneurysm in Varese (RoCAV) population based study.* BMC Cardiovasc Disord, 2016. **16**(1): p. 243.
5. Paraskevas, K.I., *Abdominal aortic aneurysms in women.* Lancet, 2017. **390**(10103): p. 1643.
6. Makrygiannis, G., et al., *Sex differences in abdominal aortic aneurysm: the role of sex hormones.* Ann Vasc Surg, 2014. **28**(8): p. 1946-58.
7. Brown, P.M., D.T. Zelt, and B. Sobolev, *The risk of rupture in untreated aneurysms: the impact of size, gender, and expansion rate.* J Vasc Surg, 2003. **37**(2): p. 280-4.
8. Vardulaki, K.A., *Incidence among men of asymptomatic aortic abdominal aneurysms: estimates from 500 screen detected cases.* J. Med. Screen., 1999. **6**: p. 50-54.
9. Howard, D.P., et al., *Population-Based Study of Incidence of Acute Abdominal Aortic Aneurysms With Projected Impact of Screening Strategy.* J Am Heart Assoc, 2015. **4**(8): p. e001926.
10. Ashton, H.A., et al., *The Multicentre Aneurysm Screening Study (MASS) into the effect of abdominal aortic aneurysm screening on mortality in men: a randomised controlled trial.* Lancet, 2002. **360**(9345): p. 1531-9.
11. Schooling, C.M., *Smoking, sex, risk factors and abdominal aortic aneurysm: is it all down to testosterone?* J Epidemiol Community Health, 2015. **69**(5): p. 495.
12. Sweeting, M.J., et al., *Meta-analysis of individual patient data to examine factors affecting growth and rupture of small abdominal aortic aneurysms.* Br J Surg, 2012. **99**(5): p. 655-65.
13. Moll, F.L., et al., *Management of abdominal aortic aneurysms clinical practice guidelines of the European society for vascular surgery.* Eur J Vasc Endovasc Surg, 2011. **41 Suppl 1**: p. S1-s58.
14. Chaikof, E.L., et al., *SVS practice guidelines for the care of patients with an abdominal aortic aneurysm: executive summary.* J Vasc Surg, 2009. **50**(4): p. 880-96.
15. Halushka, M.K., *Single gene disorders of the aortic wall.* Cardiovasc Pathol, 2012. **21**(4): p. 240-4.
16. Kent, K.C., et al., *Analysis of risk factors for abdominal aortic aneurysm in a cohort of more than 3 million individuals.* J Vasc Surg, 2010. **52**(3): p. 539-48.
17. Jahangir, E., et al., *Smoking, sex, risk factors and abdominal aortic aneurysms: a prospective study of 18 782 persons aged above 65 years in the Southern Community Cohort Study.* J Epidemiol Community Health, 2015. **69**(5): p. 481-8.
18. Aune, D., et al., *Tobacco smoking and the risk of abdominal aortic aneurysm: a systematic review and meta-analysis of prospective studies.* Sci Rep, 2018. **8**(1): p. 14786.
19. Wong, D.R., W.C. Willett, and E.B. Rimm, *Smoking, hypertension, alcohol consumption, and risk of abdominal aortic aneurysm in men.* Am J Epidemiol, 2007. **165**(7): p. 838-45.
20. Bhak, R.H., et al., *Factors associated with small abdominal aortic aneurysm expansion rate.* JAMA Surg, 2015. **150**(1): p. 44-50.
21. Li, Z.Z. and Q.Y. Dai, *Pathogenesis of abdominal aortic aneurysms: role of nicotine and nicotinic acetylcholine receptors.* Mediators Inflamm, 2012. **2012**: p. 103120.
22. Lau, P.P., et al., *Nicotine induces proinflammatory responses in macrophages and the aorta leading to acceleration of atherosclerosis in low-density lipoprotein receptor(-/-) mice.* Arterioscler Thromb Vasc Biol, 2006. **26**(1): p. 143-9.

23. Brown, L.C. and J.T. Powell, *Risk factors for aneurysm rupture in patients kept under ultrasound surveillance. UK Small Aneurysm Trial Participants.* Ann Surg, 1999. **230**(3): p. 289-96; discussion 296-7.
24. Aggarwal, S., et al., *Abdominal aortic aneurysm: A comprehensive review.* Exp Clin Cardiol, 2011. **16**(1): p. 11-5.
25. Shantikumar, S., et al., *Diabetes and the abdominal aortic aneurysm.* Eur J Vasc Endovasc Surg, 2010. **39**(2): p. 200-7.
26. Fujimura, N., et al., *Metformin treatment status and abdominal aortic aneurysm disease progression.* J Vasc Surg, 2016. **64**(1): p. 46-54 e8.
27. Welsch, U., *Lehrbuch Histologie*. Vol. 2. 2006, Munich: Elsevier. 237-241.
28. Rodella, L.F., et al., *Abdominal aortic aneurysm and histological, clinical, radiological correlation.* Acta Histochem, 2016. **118**(3): p. 256-62.
29. Michel, J.B., et al., *Novel aspects of the pathogenesis of aneurysms of the abdominal aorta in humans.* Cardiovasc Res, 2011. **90**(1): p. 18-27.
30. Shimizu, K., R.N. Mitchell, and P. Libby, *Inflammation and cellular immune responses in abdominal aortic aneurysms.* Arterioscler Thromb Vasc Biol, 2006. **26**(5): p. 987-94.
31. Henderson, E.L., et al., *Death of smooth muscle cells and expression of mediators of apoptosis by T lymphocytes in human abdominal aortic aneurysms.* Circulation, 1999. **99**(1): p. 96-104.
32. Hellenthal, F.A., et al., *Histological features of human abdominal aortic aneurysm are not related to clinical characteristics.* Cardiovasc Pathol, 2009. **18**(5): p. 286-93.
33. Sano, M., et al., *Lymphangiogenesis and angiogenesis in abdominal aortic aneurysm.* PLoS One, 2014. **9**(3): p. e89830.
34. Paik, D.C., et al., *Ongoing angiogenesis in blood vessels of the abdominal aortic aneurysm.* Exp Mol Med, 2004. **36**(6): p. 524-33.
35. Wang, D.H., et al., *Mechanical properties and microstructure of intraluminal thrombus from abdominal aortic aneurysm.* J Biomech Eng, 2001. **123**(6): p. 536-9.
36. Adolph, R., et al., *Cellular content and permeability of intraluminal thrombus in abdominal aortic aneurysm.* J Vasc Surg, 1997. **25**(5): p. 916-26.
37. O'Leary, S.A., et al., *The biaxial mechanical behaviour of abdominal aortic aneurysm intraluminal thrombus: classification of morphology and the determination of layer and region specific properties.* J Biomech, 2014. **47**(6): p. 1430-7.
38. Dale, M.A., M.K. Ruhlman, and B.T. Baxter, *Inflammatory cell phenotypes in AAAs: their role and potential as targets for therapy.* Arterioscler Thromb Vasc Biol, 2015. **35**(8): p. 1746-55.
39. Jiang, X., et al., *Fate of the mammalian cardiac neural crest.* Development, 2000. **127**(8): p. 1607-16.
40. Airhart, N., et al., *Smooth muscle cells from abdominal aortic aneurysms are unique and can independently and synergistically degrade insoluble elastin.* J Vasc Surg, 2014. **60**(4): p. 1033-41; discussion 1041-2.
41. Kadoglou, N.P. and C.D. Liapis, *Matrix metalloproteinases: contribution to pathogenesis, diagnosis, surveillance and treatment of abdominal aortic aneurysms.* Curr Med Res Opin, 2004. **20**(4): p. 419-32.
42. Khan, J.A., et al., *Intraluminal thrombus has a selective influence on matrix metalloproteinases and their inhibitors (tissue inhibitors of matrix metalloproteinases) in the wall of abdominal aortic aneurysms.* Ann Vasc Surg, 2012. **26**(3): p. 322-9.
43. Cheung, C., et al., *Generation of human vascular smooth muscle subtypes provides insight into embryological origin-dependent disease susceptibility.* Nat Biotechnol, 2012. **30**(2): p. 165-73.
44. Ailawadi, G., et al., *Smooth muscle phenotypic modulation is an early event in aortic aneurysms.* J Thorac Cardiovasc Surg, 2009. **138**(6): p. 1392-9.
45. Bown, M.J., et al., *Abdominal aortic aneurysm is associated with a variant in low-density lipoprotein receptor-related protein 1.* Am J Hum Genet, 2011. **89**(5): p. 619-27.
46. Muratoglu, S.C., et al., *LRP1 protects the vasculature by regulating levels of connective tissue growth factor and HtrA1.* Arterioscler Thromb Vasc Biol, 2013. **33**(9): p. 2137-46.

47. Davis, F.M., et al., *Smooth muscle cell deletion of low-density lipoprotein receptor-related protein 1 augments angiotensin II-induced superior mesenteric arterial and ascending aortic aneurysms.* Arterioscler Thromb Vasc Biol, 2015. **35**(1): p. 155-62.
48. Lopez-Candales, A., et al., *Decreased vascular smooth muscle cell density in medial degeneration of human abdominal aortic aneurysms.* Am J Pathol, 1997. **150**(3): p. 993-1007.
49. Boussel, L., et al., *Aneurysm growth occurs at region of low wall shear stress: patient-specific correlation of hemodynamics and growth in a longitudinal study.* Stroke, 2008. **39**(11): p. 2997-3002.
50. Kanai, A.J., et al., *Shear stress induces ATP-independent transient nitric oxide release from vascular endothelial cells, measured directly with a porphyrinic microsensor.* Circ Res, 1995. **77**(2): p. 284-93.
51. Rajagopalan, S., et al., *Reactive oxygen species produced by macrophage-derived foam cells regulate the activity of vascular matrix metalloproteinases in vitro. Implications for atherosclerotic plaque stability.* J Clin Invest, 1996. **98**(11): p. 2572-9.
52. Tronc, F., et al., *Role of matrix metalloproteinases in blood flow-induced arterial enlargement: interaction with NO.* Arterioscler Thromb Vasc Biol, 2000. **20**(12): p. E120-6.
53. Page-McCaw, A., A.J. Ewald, and Z. Werb, *Matrix metalloproteinases and the regulation of tissue remodelling.* Nat Rev Mol Cell Biol, 2007. **8**(3): p. 221-33.
54. Pickering, J.G., et al., *Coordinated effects of fibroblast growth factor-2 on expression of fibrillar collagens, matrix metalloproteinases, and tissue inhibitors of matrix metalloproteinases by human vascular smooth muscle cells. Evidence for repressed collagen production and activated degradative capacity.* Arterioscler Thromb Vasc Biol, 1997. **17**(3): p. 475-82.
55. Malek, A.M., et al., *Fluid shear stress differentially modulates expression of genes encoding basic fibroblast growth factor and platelet-derived growth factor B chain in vascular endothelium.* J Clin Invest, 1993. **92**(4): p. 2013-21.
56. Piechota-Polanczyk, A., et al., *The Abdominal Aortic Aneurysm and Intraluminal Thrombus: Current Concepts of Development and Treatment.* Front Cardiovasc Med, 2015. **2**: p. 19.
57. Eiserich, J.P., et al., *Myeloperoxidase, a leukocyte-derived vascular NO oxidase.* Science, 2002. **296**(5577): p. 2391-4.
58. Ramos-Mozo, P., et al., *Proteomic analysis of polymorphonuclear neutrophils identifies catalase as a novel biomarker of abdominal aortic aneurysm: potential implication of oxidative stress in abdominal aortic aneurysm progression.* Arterioscler Thromb Vasc Biol, 2011. **31**(12): p. 3011-9.
59. Eliason, J.L., et al., *Neutrophil depletion inhibits experimental abdominal aortic aneurysm formation.* Circulation, 2005. **112**(2): p. 232-40.
60. Middleton, R.K., et al., *The pro-inflammatory and chemotactic cytokine microenvironment of the abdominal aortic aneurysm wall: a protein array study.* J Vasc Surg, 2007. **45**(3): p. 574-80.
61. Schauer, C., et al., *Aggregated neutrophil extracellular traps limit inflammation by degrading cytokines and chemokines.* Nat Med, 2014. **20**(5): p. 511-7.
62. Houard, X., et al., *Differential inflammatory activity across human abdominal aortic aneurysms reveals neutrophil-derived leukotriene B4 as a major chemotactic factor released from the intraluminal thrombus.* FASEB J, 2009. **23**(5): p. 1376-83.
63. Pagano, M.B., et al., *Complement-dependent neutrophil recruitment is critical for the development of elastase-induced abdominal aortic aneurysm.* Circulation, 2009. **119**(13): p. 1805-13.
64. Dutertre, C.A., et al., *Deciphering the stromal and hematopoietic cell network of the adventitia from non-aneurysmal and aneurysmal human aorta.* PLoS One, 2014. **9**(2): p. e89983.
65. Rao, J., et al., *Distinct macrophage phenotype and collagen organization within the intraluminal thrombus of abdominal aortic aneurysm.* J Vasc Surg, 2015. **62**(3): p. 585-93.
66. Satoh, H., et al., *Expression and localization of tumour necrosis factor-alpha and its converting enzyme in human abdominal aortic aneurysm.* Clin Sci (Lond), 2004. **106**(3): p. 301-6.

67. Koch, A.E., et al., *Enhanced production of the chemotactic cytokines interleukin-8 and monocyte chemoattractant protein-1 in human abdominal aortic aneurysms.* Am J Pathol, 1993. **142**(5): p. 1423-31.
68. Arango Duque, G. and A. Descoteaux, *Macrophage cytokines: involvement in immunity and infectious diseases.* Front Immunol, 2014. **5**: p. 491.
69. Juvonen, J., et al., *Elevated circulating levels of inflammatory cytokines in patients with abdominal aortic aneurysm.* Arterioscler Thromb Vasc Biol, 1997. **17**(11): p. 2843-7.
70. Anzai, A., et al., *Adventitial CXCL1/G-CSF expression in response to acute aortic dissection triggers local neutrophil recruitment and activation leading to aortic rupture.* Circ Res, 2015. **116**(4): p. 612-23.
71. Tieu, B.C., et al., *An adventitial IL-6/MCP1 amplification loop accelerates macrophage-mediated vascular inflammation leading to aortic dissection in mice.* J Clin Invest, 2009. **119**(12): p. 3637-51.
72. Raffort, J., et al., *Monocytes and macrophages in abdominal aortic aneurysm.* Nat Rev Cardiol, 2017.
73. Werb, Z., M.J. Banda, and P.A. Jones, *Degradation of connective tissue matrices by macrophages. I. Proteolysis of elastin, glycoproteins, and collagen by proteinases isolated from macrophages.* J Exp Med, 1980. **152**(5): p. 1340-57.
74. Didangelos, A., et al., *Extracellular matrix composition and remodeling in human abdominal aortic aneurysms: a proteomics approach.* Mol Cell Proteomics, 2011. **10**(8): p. M111 008128.
75. Lv, B.J., et al., *Plasma levels of cathepsins L, K, and V and risks of abdominal aortic aneurysms: a randomized population-based study.* Atherosclerosis, 2013. **230**(1): p. 100-5.
76. Sun, J., et al., *Cathepsin K deficiency reduces elastase perfusion-induced abdominal aortic aneurysms in mice.* Arterioscler Thromb Vasc Biol, 2012. **32**(1): p. 15-23.
77. Rabkin, S.W., *The Role Matrix Metalloproteinases in the Production of Aortic Aneurysm.* Prog Mol Biol Transl Sci, 2017. **147**: p. 239-265.
78. Knox, J.B., et al., *Evidence for altered balance between matrix metalloproteinases and their inhibitors in human aortic diseases.* Circulation, 1997. **95**(1): p. 205-12.
79. Eskandari, M.K., et al., *Enhanced abdominal aortic aneurysm in TIMP-1-deficient mice.* J Surg Res, 2005. **123**(2): p. 289-93.
80. Thubrikar, M.J., et al., *Effect of thrombus on abdominal aortic aneurysm wall dilation and stress.* J Cardiovasc Surg (Torino), 2003. **44**(1): p. 67-77.
81. Meyer, C.A., C. Guivier-Curien, and J.E. Moore, Jr., *Trans-thrombus blood pressure effects in abdominal aortic aneurysms.* J Biomech Eng, 2010. **132**(7): p. 071005.
82. Vorp, D.A., et al., *Association of intraluminal thrombus in abdominal aortic aneurysm with local hypoxia and wall weakening.* J Vasc Surg, 2001. **34**(2): p. 291-9.
83. Kazi, M., et al., *Influence of intraluminal thrombus on structural and cellular composition of abdominal aortic aneurysm wall.* J Vasc Surg, 2003. **38**(6): p. 1283-92.
84. Sakalihasan, N., et al., *Activated forms of MMP2 and MMP9 in abdominal aortic aneurysms.* J Vasc Surg, 1996. **24**(1): p. 127-33.
85. Folkesson, M., et al., *Presence of NGAL/MMP-9 complexes in human abdominal aortic aneurysms.* Thromb Haemost, 2007. **98**(2): p. 427-33.
86. Fontaine, V., et al., *Role of leukocyte elastase in preventing cellular re-colonization of the mural thrombus.* Am J Pathol, 2004. **164**(6): p. 2077-87.
87. Defawe, O.D., et al., *Gradient of proteolytic enzymes, their inhibitors and matrix proteins expression in a ruptured abdominal aortic aneurysm.* Eur J Clin Invest, 2004. **34**(7): p. 513-4.
88. Choke, E., et al., *Increased angiogenesis at the site of abdominal aortic aneurysm rupture.* Ann N Y Acad Sci, 2006. **1085**: p. 315-9.
89. Davies, R.S., et al., *Coagulation, fibrinolysis, and platelet activation in patients undergoing open and endovascular repair of abdominal aortic aneurysm.* J Vasc Surg, 2011. **54**(3): p. 865-78.

90. Siennicka, A., et al., *Haemostatic factors and intraluminal thrombus thickness in abdominal aortic aneurysm. Is secondary fibrinolysis relevant?* J Physiol Pharmacol, 2013. **64**(3): p. 321-30.
91. Sidloff, D.A., et al., *A systematic review and meta-analysis of the association between markers of hemostasis and abdominal aortic aneurysm presence and size.* J Vasc Surg, 2014. **59**(2): p. 528-535.e4.
92. Golledge, J., et al., *Evaluation of the diagnostic and prognostic value of plasma D-dimer for abdominal aortic aneurysm.* Eur Heart J, 2011. **32**(3): p. 354-64.
93. Lindblad, B., G. Borner, and A. Gottsater, *Factors associated with development of large abdominal aortic aneurysm in middle-aged men.* Eur J Vasc Endovasc Surg, 2005. **30**(4): p. 346-52.
94. Vega de Ceniga, M., et al., *Analysis of expansion patterns in 4-4.9 cm abdominal aortic aneurysms.* Ann Vasc Surg, 2008. **22**(1): p. 37-44.
95. Thompson, S.G., et al., *Systematic review and meta-analysis of the growth and rupture rates of small abdominal aortic aneurysms: implications for surveillance intervals and their cost-effectiveness.* Health Technol Assess, 2013. **17**(41): p. 1-118.
96. Khosla, S., et al., *Meta-analysis of peak wall stress in ruptured, symptomatic and intact abdominal aortic aneurysms.* Br J Surg, 2014. **101**(11): p. 1350-7; discussion 1357.
97. Qadura, M., et al., *Mortality and reintervention following elective abdominal aortic aneurysm repair.* J Vasc Surg, 2013. **57**(6): p. 1676-83, 1683 e1.
98. Teufelsbauer, H., et al., *Endovascular stent grafting versus open surgical operation in patients with infrarenal aortic aneurysms: a propensity score-adjusted analysis.* Circulation, 2002. **106**(7): p. 782-7.
99. Setacci, F., et al., *Abdominal aortic aneurysm.* J Cardiovasc Surg (Torino), 2016. **57**(1): p. 72-85.
100. Thompson, R.W., et al., *Disseminated intravascular coagulation caused by abdominal aortic aneurysm.* J Vasc Surg, 1986. **4**(2): p. 184-6.
101. de Maistre, E., et al., *High incidence of venous thrombosis after surgery for abdominal aortic aneurysm.* J Vasc Surg, 2009. **49**(3): p. 596-601.
102. Paravastu, S.C., et al., *Endovascular repair of abdominal aortic aneurysm.* Cochrane Database Syst Rev, 2014(1): p. CD004178.
103. Weiss, N., R.N. Rodionov, and A. Mahlmann, *Medical management of abdominal aortic aneurysms.* Vasa, 2014. **43**(6): p. 415-21.
104. Periard, D., et al., *Reduction of small infrarenal abdominal aortic aneurysm expansion rate by statins.* Vasa, 2012. **41**(1): p. 35-42.
105. Takagi, H., et al., *Effects of statin therapy on abdominal aortic aneurysm growth: a meta-analysis and meta-regression of observational comparative studies.* Eur J Vasc Endovasc Surg, 2012. **44**(3): p. 287-92.
106. Salata, K., et al., *Statins Reduce Abdominal Aortic Aneurysm Growth, Rupture, and Perioperative Mortality: A Systematic Review and Meta-Analysis.* J Am Heart Assoc, 2018. **7**(19): p. e008657.
107. Piechota-Polanczyk, A., et al., *Simvastatin decreases free radicals formation in the human abdominal aortic aneurysm wall via NF-kappaB.* Eur J Vasc Endovasc Surg, 2012. **44**(2): p. 133-7.
108. Ortego, M., et al., *Atorvastatin reduces NF-kappaB activation and chemokine expression in vascular smooth muscle cells and mononuclear cells.* Atherosclerosis, 1999. **147**(2): p. 253-61.
109. Rezaie-Majd, A., et al., *Simvastatin reduces expression of cytokines interleukin-6, interleukin-8, and monocyte chemoattractant protein-1 in circulating monocytes from hypercholesterolemic patients.* Arterioscler Thromb Vasc Biol, 2002. **22**(7): p. 1194-9.
110. Steinmetz, E.F., et al., *Treatment with simvastatin suppresses the development of experimental abdominal aortic aneurysms in normal and hypercholesterolemic mice.* Ann Surg, 2005. **241**(1): p. 92-101.

111. Evans, J., et al., *Simvastatin attenuates the activity of matrix metalloprotease-9 in aneurysmal aortic tissue.* Eur J Vasc Endovasc Surg, 2007. **34**(3): p. 302-3.
112. Kaber, G., et al., *Antagonism of the antithrombotic and anti-atherosclerotic actions of aspirin by rofecoxib in the cholesterol-fed rabbit.* Br J Pharmacol, 2011. **164**(2b): p. 561-9.
113. Antithrombotic Trialists, C., et al., *Aspirin in the primary and secondary prevention of vascular disease: collaborative meta-analysis of individual participant data from randomised trials.* Lancet, 2009. **373**(9678): p. 1849-60.
114. Eldrup, N., et al., *Long-term incidence of myocardial infarct, stroke, and mortality in patients operated on for abdominal aortic aneurysms.* J Vasc Surg, 2012. **55**(2): p. 311-7.
115. Chen, C.Y., et al., *Long-term outcome of patients with aortic aneurysms taking low-dose aspirin: a population-based cohort study.* J Investig Med, 2013. **61**(6): p. 1004-12.
116. Abdul-Hussien, H., et al., *Doxycycline therapy for abdominal aneurysm: Improved proteolytic balance through reduced neutrophil content.* J Vasc Surg, 2009. **49**(3): p. 741-9.
117. Curci, J.A., et al., *Preoperative treatment with doxycycline reduces aortic wall expression and activation of matrix metalloproteinases in patients with abdominal aortic aneurysms.* J Vasc Surg, 2000. **31**(2): p. 325-42.
118. Curci, J.A., et al., *Pharmacologic suppression of experimental abdominal aortic aneurysms: acomparison of doxycycline and four chemically modified tetracyclines.* J Vasc Surg, 1998. **28**(6): p. 1082-93.
119. Lindeman, J.H., et al., *Clinical trial of doxycycline for matrix metalloproteinase-9 inhibition in patients with an abdominal aneurysm: doxycycline selectively depletes aortic wall neutrophils and cytotoxic T cells.* Circulation, 2009. **119**(16): p. 2209-16.
120. Rughani, G., L. Robertson, and M. Clarke, *Medical treatment for small abdominal aortic aneurysms.* Cochrane Database Syst Rev, 2012(9): p. Cd009536.
121. Wanhainen, A., K. Mani, and J. Golledge, *Surrogate Markers of Abdominal Aortic Aneurysm Progression.* Arterioscler Thromb Vasc Biol, 2016. **36**(2): p. 236-44.
122. Gurtelschmid, M., M. Bjorck, and A. Wanhainen, *Comparison of three ultrasound methods of measuring the diameter of the abdominal aorta.* Br J Surg, 2014. **101**(6): p. 633-6.
123. Kauffmann, C., et al., *Measurements and detection of abdominal aortic aneurysm growth: Accuracy and reproducibility of a segmentation software.* Eur J Radiol, 2012. **81**(8): p. 1688-94.
124. Parr, A., et al., *Thrombus volume is associated with cardiovascular events and aneurysm growth in patients who have abdominal aortic aneurysms.* J Vasc Surg, 2011. **53**(1): p. 28-35.
125. Nambi, P., et al., *Non-contrast computed tomography is comparable to contrast-enhanced computed tomography for aortic volume analysis after endovascular abdominal aortic aneurysm repair.* Eur J Vasc Endovasc Surg, 2011. **41**(4): p. 460-6.
126. Parr, A., et al., *Comparison of volume and diameter measurement in assessing small abdominal aortic aneurysm expansion examined using computed tomographic angiography.* Eur J Radiol, 2011. **79**(1): p. 42-7.
127. Kitagawa, A., et al., *The role of diameter versus volume as the best prognostic measurement of abdominal aortic aneurysms.* J Vasc Surg, 2013. **58**(1): p. 258-65.
128. Sakalihasan, N., et al., *Positron emission tomography (PET) evaluation of abdominal aortic aneurysm (AAA).* Eur J Vasc Endovasc Surg, 2002. **23**(5): p. 431-6.
129. Tegler, G., et al., *Inflammation in the walls of asymptomatic abdominal aortic aneurysms is not associated with increased metabolic activity detectable by 18-fluorodeoxglucose positron-emission tomography.* J Vasc Surg, 2012. **56**(3): p. 802-7.
130. Sadat, U., et al., *Ultrasmall superparamagnetic iron oxide-enhanced magnetic resonance imaging of abdominal aortic aneurysms--a feasibility study.* Eur J Vasc Endovasc Surg, 2011. **41**(2): p. 167-74.
131. Richards, J.M., et al., *Abdominal aortic aneurysm growth predicted by uptake of ultrasmall superparamagnetic particles of iron oxide: a pilot study.* Circ Cardiovasc Imaging, 2011. **4**(3): p. 274-81.

132. Satta, J., et al., *Aminoterminal propeptide of type III procollagen in the follow-up of patients with abdominal aortic aneurysms.* J Vasc Surg, 1997. **25**(5): p. 909-15.
133. Stather, P.W., et al., *Meta-analysis and meta-regression analysis of biomarkers for abdominal aortic aneurysm.* Br J Surg, 2014. **101**(11): p. 1358-72.
134. Zhang, W., et al., *Plasma microRNAs serve as potential biomarkers for abdominal aortic aneurysm.* Clin Biochem, 2015. **48**(15): p. 988-92.
135. Ramos-Mozo, P., et al., *Increased plasma levels of NGAL, a marker of neutrophil activation, in patients with abdominal aortic aneurysm.* Atherosclerosis, 2012. **220**(2): p. 552-6.
136. McCracken, J.M. and L.A. Allen, *Regulation of human neutrophil apoptosis and lifespan in health and disease.* J Cell Death, 2014. **7**: p. 15-23.
137. Delves, P.J. and I.M. Roitt, *The immune system. First of two parts.* N Engl J Med, 2000. **343**(1): p. 37-49.
138. Schmidt, R.F., *Physiologie des Menschen*. 2010, Springer: Heidelberg. p. 489-491.
139. Brinkmann, V. and A. Zychlinsky, *Beneficial suicide: why neutrophils die to make NETs.* Nat Rev Microbiol, 2007. **5**(8): p. 577-82.
140. Maletto, B.A., et al., *Presence of neutrophil-bearing antigen in lymphoid organs of immune mice.* Blood, 2006. **108**(9): p. 3094-102.
141. Woodfin, A., et al., *The junctional adhesion molecule JAM-C regulates polarized transendothelial migration of neutrophils in vivo.* Nat Immunol, 2011. **12**(8): p. 761-9.
142. Hannawa, K.K., et al., *L-selectin-mediated neutrophil recruitment in experimental rodent aneurysm formation.* Circulation, 2005. **112**(2): p. 241-7.
143. Brinkmann, V., et al., *Neutrophil extracellular traps kill bacteria.* Science, 2004. **303**(5663): p. 1532-5.
144. Delbosc, S., et al., *Porphyromonas gingivalis participates in pathogenesis of human abdominal aortic aneurysm by neutrophil activation. Proof of concept in rats.* PLoS One, 2011. **6**(4): p. e18679.
145. Obermayer, A., et al., *New aspects on the structure of neutrophil extracellular traps from chronic obstructive pulmonary disease and in vitro generation.* PLoS One, 2014. **9**(5): p. e97784.
146. Urban, C.F., et al., *Neutrophil extracellular traps contain calprotectin, a cytosolic protein complex involved in host defense against Candida albicans.* PLoS Pathog, 2009. **5**(10): p. e1000639.
147. Papayannopoulos, V., et al., *Neutrophil elastase and myeloperoxidase regulate the formation of neutrophil extracellular traps.* J Cell Biol, 2010. **191**(3): p. 677-91.
148. Andrews, R.K., J.F. Arthur, and E.E. Gardiner, *Neutrophil extracellular traps (NETs) and the role of platelets in infection.* Thromb Haemost, 2014. **112**(4): p. 659-65.
149. von Kockritz-Blickwede, M. and V. Nizet, *Innate immunity turned inside-out: antimicrobial defense by phagocyte extracellular traps.* J Mol Med (Berl), 2009. **87**(8): p. 775-83.
150. Fuchs, T.A., et al., *Novel cell death program leads to neutrophil extracellular traps.* J Cell Biol, 2007. **176**(2): p. 231-41.
151. Yousefi, S., et al., *Viable neutrophils release mitochondrial DNA to form neutrophil extracellular traps.* Cell Death Differ, 2009. **16**(11): p. 1438-44.
152. Farrera, C. and B. Fadeel, *Macrophage clearance of neutrophil extracellular traps is a silent process.* J Immunol, 2013. **191**(5): p. 2647-56.
153. Steinberg, B.E. and S. Grinstein, *Unconventional roles of the NADPH oxidase: signaling, ion homeostasis, and cell death.* Sci STKE, 2007. **2007**(379): p. pe11.
154. Hermosilla, C., et al., *The intriguing host innate immune response: novel anti-parasitic defence by neutrophil extracellular traps.* Parasitology, 2014. **141**(11): p. 1489-98.
155. Neeli, I. and M. Radic, *Opposition between PKC isoforms regulates histone deimination and neutrophil extracellular chromatin release.* Front Immunol, 2013. **4**: p. 38.
156. Dabrowska, D., et al., *New Aspects of the Biology of Neutrophil Extracellular Traps.* Scand J Immunol, 2016. **84**(6): p. 317-322.

157. Matoszka, N., et al., *[NET and NETosis--new phenomenon in immunology].* Postepy Hig Med Dosw (Online), 2012. **66**: p. 437-45.
158. Hakkim, A., et al., *Activation of the Raf-MEK-ERK pathway is required for neutrophil extracellular trap formation.* Nat Chem Biol, 2011. **7**(2): p. 75-7.
159. Behnen, M., et al., *Immobilized immune complexes induce neutrophil extracellular trap release by human neutrophil granulocytes via FcgammaRIIIB and Mac-1.* J Immunol, 2014. **193**(4): p. 1954-65.
160. Itakura, A. and O.J. McCarty, *Pivotal role for the mTOR pathway in the formation of neutrophil extracellular traps via regulation of autophagy.* Am J Physiol Cell Physiol, 2013. **305**(3): p. C348-54.
161. McInturff, A.M., et al., *Mammalian target of rapamycin regulates neutrophil extracellular trap formation via induction of hypoxia-inducible factor 1 alpha.* Blood, 2012. **120**(15): p. 3118-25.
162. Remijsen, Q., et al., *Neutrophil extracellular trap cell death requires both autophagy and superoxide generation.* Cell Res, 2011. **21**(2): p. 290-304.
163. Douda, D.N., et al., *SK3 channel and mitochondrial ROS mediate NADPH oxidase-independent NETosis induced by calcium influx.* Proc Natl Acad Sci U S A, 2015. **112**(9): p. 2817-22.
164. Jorch, S.K. and P. Kubes, *An emerging role for neutrophil extracellular traps in noninfectious disease.* Nat Med, 2017. **23**(3): p. 279-287.
165. Pilsczek, F.H., et al., *A novel mechanism of rapid nuclear neutrophil extracellular trap formation in response to Staphylococcus aureus.* J Immunol, 2010. **185**(12): p. 7413-25.
166. Boilard, E. and P.R. Fortin, *Connective tissue diseases: Mitochondria drive NETosis and inflammation in SLE.* Nat Rev Rheumatol, 2016. **12**(4): p. 195-6.
167. Hakkim, A., et al., *Impairment of neutrophil extracellular trap degradation is associated with lupus nephritis.* Proc Natl Acad Sci U S A, 2010. **107**(21): p. 9813-8.
168. Bianchi, M., et al., *Restoration of anti-Aspergillus defense by neutrophil extracellular traps in human chronic granulomatous disease after gene therapy is calprotectin-dependent.* J Allergy Clin Immunol, 2011. **127**(5): p. 1243-52 e7.
169. Kessenbrock, K., et al., *Netting neutrophils in autoimmune small-vessel vasculitis.* Nat Med, 2009. **15**(6): p. 623-5.
170. Kimball, A.S., et al., *The Emerging Role of NETs in Venous Thrombosis and Immunothrombosis.* Front Immunol, 2016. **7**: p. 236.
171. Engelmann, B. and S. Massberg, *Thrombosis as an intravascular effector of innate immunity.* Nat Rev Immunol, 2013. **13**(1): p. 34-45.
172. Halverson, T.W., et al., *DNA is an antimicrobial component of neutrophil extracellular traps.* PLoS Pathog, 2015. **11**(1): p. e1004593.
173. Belaaouaj, A., *Neutrophil elastase-mediated killing of bacteria: lessons from targeted mutagenesis.* Microbes Infect, 2002. **4**(12): p. 1259-64.
174. Buchanan, J.T., et al., *DNase expression allows the pathogen group A Streptococcus to escape killing in neutrophil extracellular traps.* Curr Biol, 2006. **16**(4): p. 396-400.
175. Yan, H., et al., *Neutrophil Proteases Promote Experimental Abdominal Aortic Aneurysm via Extracellular Trap Release and Plasmacytoid Dendritic Cell Activation.* Arterioscler Thromb Vasc Biol, 2016. **36**(8): p. 1660-9.
176. Jones, J.E., et al., *Protein arginine deiminase 4 (PAD4): Current understanding and future therapeutic potential.* Curr Opin Drug Discov Devel, 2009. **12**(5): p. 616-27.
177. Lewis, H.D., et al., *Inhibition of PAD4 activity is sufficient to disrupt mouse and human NET formation.* Nat Chem Biol, 2015. **11**(3): p. 189-91.
178. Knuckley, B., et al., *Substrate specificity and kinetic studies of PADs 1, 3, and 4 identify potent and selective inhibitors of protein arginine deiminase 3.* Biochemistry, 2010. **49**(23): p. 4852-63.
179. Sorensen, O.E. and N. Borregaard, *Neutrophil extracellular traps - the dark side of neutrophils.* J Clin Invest, 2016. **126**(5): p. 1612-20.

180. Li, P., et al., *PAD4 is essential for antibacterial innate immunity mediated by neutrophil extracellular traps.* J Exp Med, 2010. **207**(9): p. 1853-62.
181. Thalin, C., et al., *Validation of an enzyme-linked immunosorbent assay for the quantification of citrullinated histone H3 as a marker for neutrophil extracellular traps in human plasma.* Immunol Res, 2017. **65**(3): p. 706-712.
182. Tsui, J.C., *Experimental models of abdominal aortic aneurysms.* Open Cardiovasc Med J, 2010. **4**: p. 221-30.
183. Manning, M.W., et al., *Abdominal aortic aneurysms: fresh insights from a novel animal model of the disease.* Vasc Med, 2002. **7**(1): p. 45-54.
184. Anidjar, S., et al., *Elastase-induced experimental aneurysms in rats.* Circulation, 1990. **82**(3): p. 973-81.
185. Yamaguchi, T., et al., *Morphologic changes in the aorta during elastase infusion in the rat aneurysm model.* J Surg Res, 2001. **95**(2): p. 161-6.
186. Rateri, D.L., et al., *Prolonged infusion of angiotensin II in apoE(-/-) mice promotes macrophage recruitment with continued expansion of abdominal aortic aneurysm.* Am J Pathol, 2011. **179**(3): p. 1542-8.
187. Qin, Z., et al., *Angiotensin II-induced TLR4 mediated abdominal aortic aneurysm in apolipoprotein E knockout mice is dependent on STAT3.* J Mol Cell Cardiol, 2015. **87**: p. 160-70.
188. Lu, H., et al., *Subcutaneous Angiotensin II Infusion using Osmotic Pumps Induces Aortic Aneurysms in Mice.* J Vis Exp, 2015(103).
189. ; Available from: http://www.velaz.cz/en/product/osmoticke-pumpy/
190. Hirose, T., et al., *Presence of neutrophil extracellular traps and citrullinated histone H3 in the bloodstream of critically ill patients.* PLoS One, 2014. **9**(11): p. e111755.
191. Lederle, F.A., D.B. Nelson, and A.M. Joseph, *Smokers' relative risk for aortic aneurysm compared with other smoking-related diseases: a systematic review.* J Vasc Surg, 2003. **38**(2): p. 329-34.
192. Tulgar, Y.K., et al., *The effect of smoking on neutrophil/lymphocyte and platelet/lymphocyte ratio and platelet indices: a retrospective study.* Eur Rev Med Pharmacol Sci, 2016. **20**(14): p. 3112-8.
193. Blidberg, K., et al., *Increased neutrophil migration in smokers with or without chronic obstructive pulmonary disease.* Respirology, 2012. **17**(5): p. 854-60.
194. Parry, D.J., et al., *Haemostatic and fibrinolytic factors in men with a small abdominal aortic aneurysm.* Br J Surg, 2009. **96**(8): p. 870-7.
195. Wallinder, J., D. Bergqvist, and A.E. Henriksson, *Haemostatic markers in patients with abdominal aortic aneurysm and the impact of aneurysm size.* Thromb Res, 2009. **124**(4): p. 423-6.
196. Kubota, Y., et al., *Lipoprotein(a) and abdominal aortic aneurysm risk: The Atherosclerosis Risk in Communities study.* Atherosclerosis, 2018. **268**: p. 63-67.
197. Galora, S., et al., *Low-density lipoprotein receptor-related protein 5 gene polymorphisms and genetic susceptibility to abdominal aortic aneurysm.* J Vasc Surg, 2013. **58**(4): p. 1062-8.e1.
198. Wilson, J.S., et al., *Biochemomechanics of intraluminal thrombus in abdominal aortic aneurysms.* J Biomech Eng, 2013. **135**(2): p. 021011.
199. Busch, A., et al., *Extra- and Intraluminal Elastase Induce Morphologically Distinct Abdominal Aortic Aneurysms in Mice and Thus Represent Specific Subtypes of Human Disease.* J Vasc Res, 2016. **53**(1-2): p. 49-57.
200. Krishna, S.M., et al., *High serum thrombospondin-1 concentration is associated with slower abdominal aortic aneurysm growth and deficiency of thrombospondin-1 promotes angiotensin II induced aortic aneurysm in mice.* Clin Sci (Lond), 2017. **131**(12): p. 1261-1281.
201. Takagi, H., et al., *Serum high-density and low-density lipoprotein cholesterol is associated with abdominal aortic aneurysm presence: a systematic review and meta-analysis.* Int Angiol, 2010. **29**(4): p. 371-5.

202. Bilyy, R., et al., *Neutrophil Extracellular Traps Form a Barrier between Necrotic and Viable Areas in Acute Abdominal Inflammation.* Front Immunol, 2016. **7**: p. 424.
203. Helgadottir, A., et al., *The same sequence variant on 9p21 associates with myocardial infarction, abdominal aortic aneurysm and intracranial aneurysm.* Nat Genet, 2008. **40**(2): p. 217-24.
204. Meher, A.K., et al., *Novel Role of IL (Interleukin)-1beta in Neutrophil Extracellular Trap Formation and Abdominal Aortic Aneurysms.* Arterioscler Thromb Vasc Biol, 2018. **38**(4): p. 843-853.
205. Tran, H., *Critical Role of Protein Arginine Deiminase 4 in Mast Cell Extracellular Trap Formation Leading to Neuropathic Pain in Sickle Mice*, in *59th Annual Meeting of the American Society of Hematology*. 2017, Blood: Atlanta, GA, U.S.A. p. 439.
206. Cedervall, J., et al., *Pharmacological targeting of peptidylarginine deiminase 4 prevents cancer-associated kidney injury in mice.* Oncoimmunology, 2017. **6**(8): p. e1320009.
207. Lavoie, S.S., et al., *Synthesis of Human Neutrophil Extracellular Traps Contributes to Angiopoietin-Mediated In Vitro Proinflammatory and Proangiogenic Activities.* J Immunol, 2018. **200**(11): p. 3801-3813.
208. Aldabbous, L., et al., *Neutrophil Extracellular Traps Promote Angiogenesis: Evidence From Vascular Pathology in Pulmonary Hypertension.* Arterioscler Thromb Vasc Biol, 2016. **36**(10): p. 2078-87.
209. Liu, Z., et al., *Thrombospondin-1 (TSP1) contributes to the development of vascular inflammation by regulating monocytic cell motility in mouse models of abdominal aortic aneurysm.* Circ Res, 2015. **117**(2): p. 129-41.

8. List of Abbreviations

AAA	Abdominal Aortic Aneurysm
A23	A23187
ACE	Inhibitor angiotensin converting enzyme
Ang II	Angiotensin II
BMI	body mass index
citH3	citrullinated histone 3 protein
CRP	C-reactive protein
CT	Computer tomography
CTAD	citrate, theophylline, adenosine, dipyridamole
DPBS +/+	Dulbecco's phosphate buffered saline (+) Cacl2, (+) MgCl2
DPI	Diphenyleneiodonium
ECM	extracellular matrix
ELISA	Enzyme-linked immunosorbent assay
EVAR	endovascular aortic repair
FACS	fluorescence-activated cell scanning
FDG	18-fluorodeoxyglucose
GSK	GSK484
HBSS	Hanks' balanced salt solution
HDL	high density lipoprotein HDL cholesterol
Il	Interleukin
iICs	Immobilized Immune Complexes
ILT	intraluminal thrombus
LDL	low density lipoprotein cholesterol
LPS	Lipopolysaccharide
LRP1	low density lipoprotein receptor protein 1
LRP5	lipoprotein receptor related protein 5
MHC	major histocompatibility complex
MMP	matrix metalloproteinase
MPO	Myeloperoxidase
MRI	magnetic resonance imaging
mTOR	mammalian Target of Rapamycin
NADPH	nicotinamide adenine dinucleotide phosphate
NET	neutrophil extracellular trap
NO	nitric oxide
OSR	open surgical repair
PAD	protein arginine deiminases
PBS -/-	phosphate buffered saline (-) Cacl2, (-) MgCl2
PKC	protein kinase C
PMA	phorbol myristate acetate
PMN	polymorphonuclear cells
RFU	relative flourescent units
RNS	nitrogen species
ROS	reactive oxygen species
RT	room temperature
RU	relative units
SMC	smooth muscle cells
TNF	tumor necrosis factor

TRL	toll like receptor
VSMC	vascular smooth muscle cells
WBC	White blood cells

9. List of Figures and Tables

9.1. Figures

9.2. Tables

10. Acknowledgement

First, I would like to thank my thesis advisors Prof. Dr. med. Ulrich Hoffmann Department of Angiology, Faculty of Medicine Ludwig-Maximilians-University of Munich and ao. Univ.-Prof. Dr. Christine Brostjan of the Department of Surgery, Surgical Research Laboratories at the Medical University of Vienna. They supported me whenever I had a question about my research, my statistics or my writing. They always offered technical and professional advice.

I would also like to thank Dr. Branislav Zagrapan and Dr. Wolf Eilenberg, who were supervising the clinical and animal study. They guided me through the laboratory work and supported establishing of the operative methods. They always gave input whenever I was stuck. Without their passionate participation this study could not have been successfully conducted.

A very special gratitude goes out to Luca Martelanz my fellow lab partner, who I have worked closely throughout the animal study. I also want to thank Johannes Klopf, my fellow lab partner and co-worker throughout the clinical study. They were always reliable, motivated and made often long hours in the lab very enjoyable.

In addition, I want to thank my fellow co-workers MSc. Katharina Seif and MSc. Hubert Hayden of the research group. Their support and encouragement provided a perfect basis for a pleasant working atmosphere in the lab. They always offered help whenever anything went wrong and provided input.

I want to thank all patients who provided their blood and made this study possible.

Finally, I am immensely grateful especially to my parents, who never fail to encourage me to pursuit my dreams and never give up. They constantly support me in every aspect of my life. They especially offered unfailing support and continuous encouragement throughout my years of university. This accomplishment would not have been possible without them.

11. Eidesstattliche Versicherung

Ich, Marie Therese Grasl, erkläre hiermit an Eides statt, dass ich die vorliegende Dissertation mit dem Titel

“The Potential Role of Neutrophil Extracellular Traps (NETs) as Biomarker and Therapeutic Target in Abdominal Aortic Aneurysms”

selbständig verfasst, mich außer der angegebenen keiner weiteren Hilfsmittel bedient und alle Erkenntnisse, die aus dem Schrifttum ganz oder annähernd übernommen sind, als solche kenntlich gemacht und nach ihrer Herkunft unter Bezeichnung der Fundstelle einzeln nachgewiesen habe.

Ich erkläre des Weiteren, dass die hier vorgelegte Dissertation nicht in gleicher oder in ähnlicher Form bei einer anderen Stelle zur Erlangung eines akademischen Grades eingereicht wurde.

Wien, den 18.10.2021	Marie Therese Grasl
_____	_____
Ort, Datum	Unterschrift Doktorandin